



A specialized 3D printer for the production of diaphysial bone grafts.

A Report Submitted in Partial Fulfillment of the Requirements for GENE  
404

Shubh Jagani, 20470615

Matt Jones, 20474981

Kyla Gardner, 20490354

Josh Bradshaw, 20479758

Isaac Hunter, 20480938

Alex Upenieks, 20487426

Faculty of Engineering  
Department of Systems Design Engineering

April 1, 2017

Course Instructor: Oscar Nespoli

## **Abstract**

Professor Willett's biomedical materials research lab requires an improved 3D printing process for making bone grafts out of curable biomaterial. The manufacturing process is required to have greater precision, and produce stronger parts than those made by a conventional 3D printer. Team SkelePrint has decided to address this problem by creating a lathe-type 3D printer in which the biomaterial is deposited onto a rotating mandrel. This printer deposits the ink in helical arcs to build up concentric cylindrical layers. This layering strategy yields stronger bone grafts than those created on a Cartesian printer. The printer was created from standard industrial automation components. Novel components on the printer include the biomaterial extrusion system, and the rotational axis assembly. This report outlines the design and validation of the printers mechanisms, control system and toolpath generation software.

# Contents

<b>1</b>	<b>Need Analysis</b>	<b>1</b>
1.1	Background on Professor Willett's Bone Graft Project . . . . .	1
1.2	Background on Prior Work in Professor Willett's lab . . . . .	3
1.3	Design Specifications . . . . .	5
	Discussion of Functional Requirements . . . . .	5
	Discussion of Non-Functional Requirements . . . . .	6
	Discussion of Constraint Requirements . . . . .	6
1.4	Concept Generation . . . . .	6
	Digital Laser Projection Printing . . . . .	6
	Five Axis Mandrel Printing . . . . .	7
	Three Axis Additive Lathe . . . . .	8
	Mandrel Printing using an Existing 3D Printer . . . . .	9
1.5	Concept Selection . . . . .	10
<b>2</b>	<b>Mechanical Design</b>	<b>11</b>
2.1	Mechanical Design Summary . . . . .	11
2.2	Rotational Axis . . . . .	11
	Angular Resolution . . . . .	11
	Print Bed Mechanism . . . . .	12
	Alignment with the Axial axis . . . . .	15
2.3	Linear Actuators . . . . .	16
	Belt Drive . . . . .	16
	Lead Screws . . . . .	17
	Ball Screw . . . . .	18
2.4	Axial Axis . . . . .	19
2.5	Radial Axis . . . . .	22
2.6	Motor Selection . . . . .	25
	Stepper Motors vs Servo Motors . . . . .	25

Stepper Motor Application Notes . . . . .	26
2.7 Motor Sizing . . . . .	26
2.8 Frame . . . . .	27
2.9 A Note on Measurement Convention and Tooling . . . . .	30
<b>3 Extrusion System</b>	<b>32</b>
<b>4 Controls Design Summary</b>	<b>34</b>
4.1 Review of Open-Source CNC Firmware Packages . . . . .	34
RAMPS . . . . .	35
Mach3 . . . . .	35
GRBL . . . . .	35
4.2 Choice of CNC Software Package . . . . .	35
4.3 Closed Loop Control . . . . .	37
Controller System Specifications . . . . .	38
PID Controller Tuning . . . . .	38
Quantifying Encoder Noise . . . . .	40
4.4 Extruder Controller . . . . .	40
4.5 Tool Path Generator . . . . .	44
Core Algorithm . . . . .	44
User Interface Design . . . . .	45
Tool Path Visualizer . . . . .	46
<b>5 Preliminary Experimentation Summary</b>	<b>49</b>
5.1 Additive Lathe Prototype I . . . . .	49
5.2 Additive Lathe Prototype I Testing Results . . . . .	50
5.3 Controls Testing Apparatus . . . . .	53
5.4 Extrusion Testing Apparatus . . . . .	55
<b>6 Design Verification Summary</b>	<b>58</b>
6.1 Mathematical Modelling and Analysis . . . . .	58
6.2 Prototyping and Testing . . . . .	59

6.3 Verification of Design Specifications . . . . .	60
Precision and Error Budget . . . . .	60
Closed Loop Control . . . . .	62
Safety . . . . .	62
<b>7 Design Project Management Summary</b>	<b>63</b>
<b>8 Next Steps</b>	<b>64</b>
8.1 Mechanical Design . . . . .	64
8.2 Electronics Design . . . . .	64
8.3 Control System Design . . . . .	65
8.4 Software Design . . . . .	65
8.5 Extrusion System Design . . . . .	65
8.6 Biomaterial Properties Testing . . . . .	65
<b>Appendix A: Engineering Data</b>	<b>67</b>
Design Specifications . . . . .	68
Motor Sizing Calculations . . . . .	74
Print weight . . . . .	76
Tool Path Generator Algorithm . . . . .	76
Feed Rate and Tangential Velocity Calculations . . . . .	78
Code . . . . .	79
Belt Length Calculation . . . . .	79
Extruder Pressure Requirement Calculation . . . . .	81
Slic3r Software Breakdown . . . . .	82
Video Demonstrations . . . . .	83
<b>Appendix B: Project Management Data</b>	<b>86</b>
Project Schedule and Work Breakdown Structure . . . . .	86
Organizational Structure and Roles . . . . .	90
Risk Register . . . . .	91
Project Budget and Current Expenses . . . . .	95

Bill of Materials . . . . .	98
<b>Appendix C: Knowledge Application</b>	<b>101</b>
<b>Appendix D: Troubleshooting</b>	<b>103</b>
Known Problems with the Printer . . . . .	103
Mechanical Problems . . . . .	103
Firmware Problems . . . . .	104
Electrical Problems . . . . .	104
General Warnings and Advice . . . . .	105
Electrical Troubleshooting . . . . .	106
Firmware Troubleshooting . . . . .	106
Controls System Troubleshooting . . . . .	106
Problems with the Mechaduino Motor Drivers . . . . .	106
One or more axis is unresponsive upon startup . . . . .	107
Motors turn erratically, missing their setpoint . . . . .	107
Motors make a rattling noise or vibrate violently, but stay in one place . . . . .	108
Motors jerk upon startup . . . . .	108
Mechanism Troubleshooting . . . . .	108
Wiring Diagrams . . . . .	109

# List of Figures

1	Anatomical diagram of a long bone cross section. Figure from the Wikimedia foundation.	2
2	A Hyrel 30M printer by Hyrel 3D used in Willet lab. Figure from [5].	3
3	Displacement style extruder used by the Willett lab in a Hyrel 30M printer by Hyrel 3D. Figure from [5].	4
4	Preliminary cylinder printing (left) and a femur model based off a rabbit bone (right).	4
5	Schematic diagram of a digital laser projection printer. Figure from [6].	7
6	Five axis 3D printer, created by 5AxisMaker. Figure from [7].	8
7	Three axis additive lathe printer created by a design team at Imperial College London. Figure from [8].	9
8	SkelePrint definition of axis names.	10
9	Timing belt implementation used on a previous lathe type 3D printer. Figure from [8].	12
10	CAD of the rotational axis transmission.	13
11	Turning between centers concept drawing	13
12	CAD model of the turning between centers technique used in our final prototype.	14
13	Mechanical design of the rotational assembly	15
14	Zen Toolworks 3D printer timing belt. Figure from [9].	17
15	A stepper motor with a lead screw integrated directly into its armature. Figure from [10].	18
16	Cutaway view of a ballnut, illustrating the tight coupling between the ball bearings and the screw threads. Figure from [11].	19
17	Ball screw assembly from ISEL Automation. Figure from [13].	20
18	CAD model of ball screw assembly in our final prototype.	21
19	Mechanical design of the axial assembly	22
20	CAD model of the radial axis assembly in our final prototype.	23
21	Mechanical design of the radial assembly	25

22	CAD model of the frame assembly in our final prototype. . . . .	29
23	Mechanical design of the overall printer . . . . .	30
24	Schematic diagram of pneumatic extrusion system. . . . .	32
25	Controls system diagram. . . . .	34
26	Controls system diagram. . . . .	36
27	Mechaduino controller block diagram . . . . .	37
28	System response of radial axis . . . . .	39
29	System response of axial axis . . . . .	39
30	System response of rotational axis . . . . .	40
31	Typical solenoid current draw when powered by a PWM driver. Taken from the Texas Instruments DRV101 Datasheet. Figure from [15]. . . . .	41
32	Texas Instruments reference design for a solenoid controller. . . . .	42
33	Solenoid controller schematic. . . . .	43
34	PCB Layout for the Solenoid Driver. . . . .	43
35	Graphical user interface for SkelePrint Tool Path Generator and generated G Code file. . . . .	46
36	Plots produced by MATLAB visualization code. . . . .	47
37	Additive Lathe Prototype 1 setup. . . . .	49
38	Results of first lab session with Additive Lathe Prototype 1. . . . .	51
39	Results of second lab session with Additive Lathe Prototype 1. . . . .	51
40	Result of first print using the biomaterial instead of plastic. Image taken as soon as print completed. . . . .	52
41	Result of first print using the biomaterial instead of plastic. Image taken as after print finished drying. . . . .	53
42	System diagram of LEGO prototype. . . . .	54
43	Controls testing LEGO prototype. . . . .	54
44	Typical regulator outlet pressure vs. flow curve. Figure from [17]. . . . .	55
45	Example of a test print completed using a new iteration of the Willett Lab ink. . . . .	57
46	Full scale error budget in $\mu m$ . . . . .	61
47	System level diagram of our printer design. . . . .	68

48	Ballscrew free body diagram from Oriental Motor [19] . . . . .	74
49	Print and mandrel radii . . . . .	76
50	Pitch and diameter of the windings. . . . .	77
51	Start locations of multi-flute coils. . . . .	77
52	Schematic diagram of the pulley reduction assembly to measure required timing belt length. . . . .	80
53	Matlab code for calculating the required belt length based on the pulley radius, and the vertical and horizontal distance between the pulleys. . . . .	81
54	YouTube Video of low fidelity prototype demonstration. . . . .	84
55	YouTube Video of extrusion demonstration. . . . .	84
56	YouTube Video of final prototype demonstration. . . . .	85
57	Comparison chart for planned work hours (blue) vs actual work hours (red) across the entire project. . . . .	86
58	Organizational chart of Team SkelePrint. . . . .	90
59	GRBL Pinout Diagram . . . . .	110
60	Mechaduino Wiring Diagram . . . . .	111
61	Mechaduino PCB Drawing. . . . .	112
62	Mechaduino Wiring Diagram . . . . .	112

# 1

## Need Analysis

### 1.1 Background on Professor Willett's Bone Graft Project

In orthopedic surgery, bone grafts are used to replace portions of bone which have been resected to halt the spread of cancer or infection [1]. Grafts are implanted in place of missing bone segments to mechanically stabilize the bone and restore the load bearing function. None of the bone grafts currently used in clinical practice are sufficient for replacing large sections of long bones [2]. Under long term cyclic loading, the metal scaffolding used to connect the bone graft to the living bone often erodes or breaks the living bone, and failure results in approximately 20-40% of implantations.

For the past year, Professor Willett and his research team have been developing better bone grafts for cases in which portions of a long bone's diaphysis (mid-section or shaft) must be replaced. To address the problem, they have developed a biocompatible material, which will be manufactured into bone grafts. Previous *in vivo* studies with current bone graft materials have shown that these materials are able to support bone growth and regeneration [3], which is one goal of Professor Willett's biomaterial. When implanted, the living bone will grow into the graft, forming strong connections that will out-last the current metal scaffolding approach [2].

The main obstacle that the research team faces in the bone graft development process is that their current samples are insufficiently strong. These samples were created on a conventional 3D printer. Conventional 3D printers are not adequate for producing bone grafts because they deposit material in flat layers, and the gap between the layers is a plane of weakness.

To improve the mechanical properties of the bone grafts, an improved manufacturing pro-

cess that allows the researchers to control the internal microstructure of the bone graft must be created. Their goal is to form the biomaterial into a stronger composite matrix. There are many possible internal geometries that could potentially improve the overall strength of the graft. As a starting point, Willett wishes to mimic the microstructure of human cortical bone in the bone graft manufacturing process.

The idea for developing the microstructure of the bone graft is inspired by the strength and fracture toughness of human cortical bone. On the microscopic level, human cortical bone is made up of concentric cylindrical structures called lamellae that form in a geometry similar to the rings of a tree trunk [4].

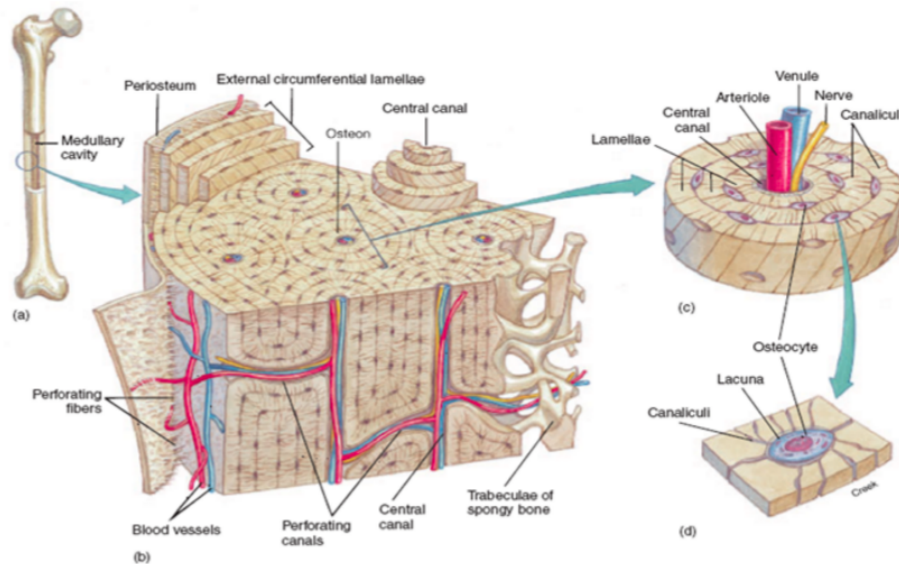


Figure 1: Anatomical diagram of a long bone cross section. Figure from the Wikimedia foundation.

The layered lamellae of long bones have a grain structure that is analogous to plywood. Fibers of consecutively layered lamellae run oblique to one another, alternating between each layer . This alternating structure gives cortical bone its strength in bending, and improves its fracture toughness. The main objective of this project is to develop a manufacturing process which can replicate this microstructure to improve the mechanical properties of the resulting bone grafts.

## 1.2 Background on Prior Work in Professor Willett's lab

Before the start of this project, the research team began work on 3D printing the biomaterial. The lab acquired a Cartesian 3D printer (Hyrel 30M by Hyrel 3D shown in Figure 2). To extrude the biomaterial, a displacement type extruder was used (#EMO-25 by Hyrel 3D shown in Figure 3).

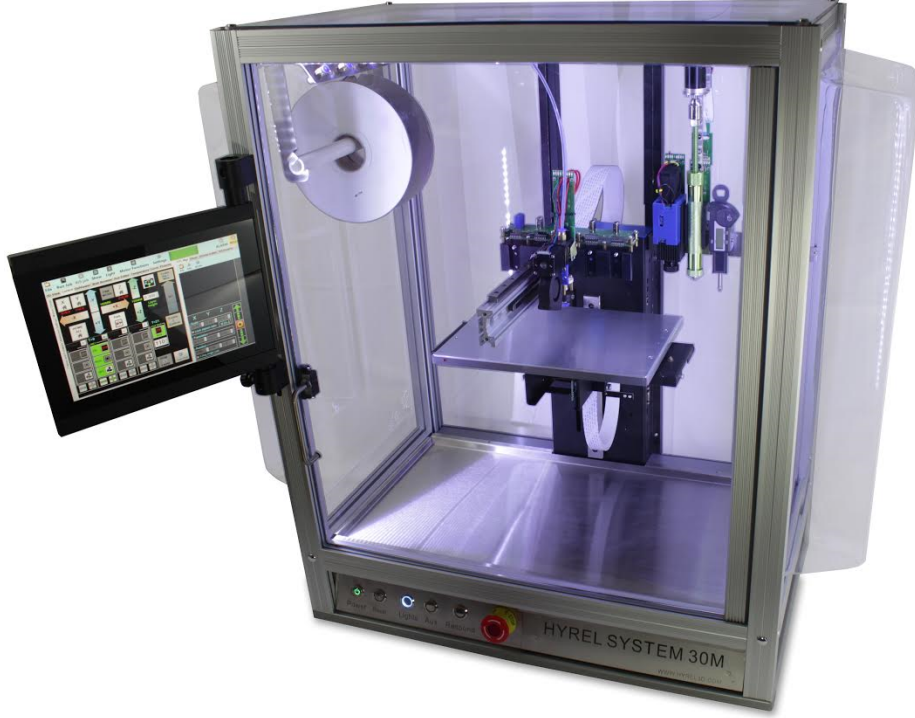


Figure 2: A Hyrel 30M printer by Hyrel 3D used in Willet lab. Figure from [5].

This system worked reasonably well as a proof of concept solution. The extruder deposited the ink in arcs approximately 0.5mm in diameter. The research team successfully printed several test parts. Figure 4 shows the first attempt at printing cylinders (left) and a rabbit femur (right) using a Cartesian 3D printer.

The main problem that the research team encountered while testing this system is that the feed rate of the displacement type extruder was inaccurate and unstable. The displacement



Figure 3: Displacement style extruder used by the Willett lab in a Hyrel 30M printer by Hyrel 3D. Figure from [5].

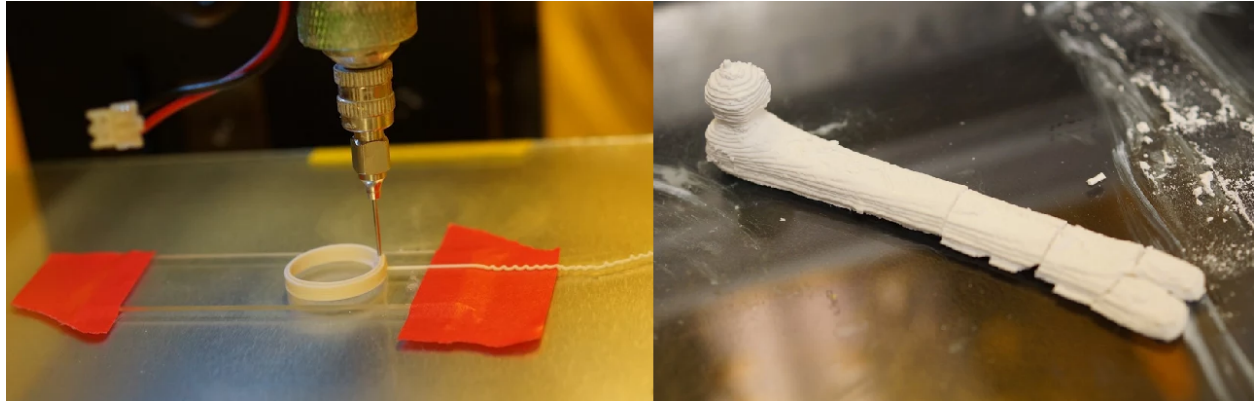


Figure 4: Preliminary cylinder printing (left) and a femur model based off a rabbit bone (right).

extruder works like a syringe pump. A stepper motor driven lead screw pushes the plunger of a high pressure stainless-steel syringe until pressure inside the syringe exceeds the biomaterial shear yield point. At this pressure, the biomaterial begins to extrude through the nozzle.

This system fails to function as a consistent extrusion mechanism because it is impossible to precisely control the pressure inside the syringe using only open-loop displacement control.

The biomaterial is a solid and slightly compressible, so the relationship between displacement and flow rate is difficult to model. The system frequently experienced glitches such as run-on extrusion after the motor was stopped. The extruder would also occasionally splurt at the beginning of the extrusion, pushing gobs of ink through the needle before steady flow began.

The research team also conducted preliminary curing tests. They tried using a UV lamp and a ring of UV band LEDs to cure the ink. Unfortunately, both of these approaches were far too slow to be viable for printing. The team recently acquired a high power precisely controlled UV laser, which works better.

### 1.3 Design Specifications

The design specifications were determined through conversing with Professor Willett and his research team, analyzing patents and other state-of-art printers, and by examining the scientific literature on additive manufacturing.

#### Discussion of Functional Requirements

The functional requirements are based on the intended use of the printer. The research team will use it for printing mechanical test samples. This means that the printer must manufacture parts precisely and in a repeatable manner. In accordance with this, the printer's accuracy and full scale error requirements have been defined to be much more stringent than typical 3D printing systems.

Our team has defined a full scale error budget of 100 and 150 microns for the axial and radial axis respectively. The error budget for the rotational axis is defined in terms of extrusion arc length ( $l = r\theta$ ). The rotational error budget is 200 microns at a  $35mm$  radius. The accuracy specifications will be designed for and verified using dynamics models of the printers actuators.

The error budgets for the axial and radial axis will be challenging to achieve, because the stack up tolerances of the printer's components and actuator error will all detract from the error budget. We have chosen the axial axis to be the reference for the printer's alignment. All other components are aligned with this rail.

## **Discussion of Non-Functional Requirements**

The non-functional requirements deal with safety considerations, and the requirements of regulatory bodies. Most of these are self-explanatory.

There are notable omissions from the non-functional requirements. There are no requirements directly related to ink chemistry, or the ink's material properties. There are also no requirements related to the eventual medical application of the prints, because this research project is still in its preliminary stages, and this printer will not be used to produce medical implants for use in humans.

Professor Willett acknowledges that the changing chemistry of the ink is problematic from a design perspective. However he is a capable engineer. The shared expectation is that the research team will modify or replace the printer's modular extrusion system to accommodate future changes in the ink.

The non-functional requirements also address the printers service life and maintenance. Most components of the printer will never require any maintenance beyond cleaning and lubrication, but the plastic parts will require periodic replacement.

## **Discussion of Constraint Requirements**

The constraint requirements outline the requirements necessary to make the printer suitable for use in the laboratory. The size of the printer is constrained, because bench space in the lab is limited.

The printer is also subject to the university's policies for electrically powered equipment, which dictate that the power supply must be certified by the CSA or Underwriters laboratories, and the printer's enclosure must be electrically grounded.

### **1.4 Concept Generation**

#### **Digital Laser Projection Printing**

Digital laser projection printing is the current state of the art additive manufacturing method in terms of strength and spatial resolution. In digital laser projection printing, a laser

projector selectively cures UV resin to form each layer [6]. Next, the printed part is lowered into the resin vat by a table mechanism and the layer creation process is repeated. This process is displayed in Figure 5. Digital laser projection produces minimal anisotropy in the part, because there are no voids in or between the layers.

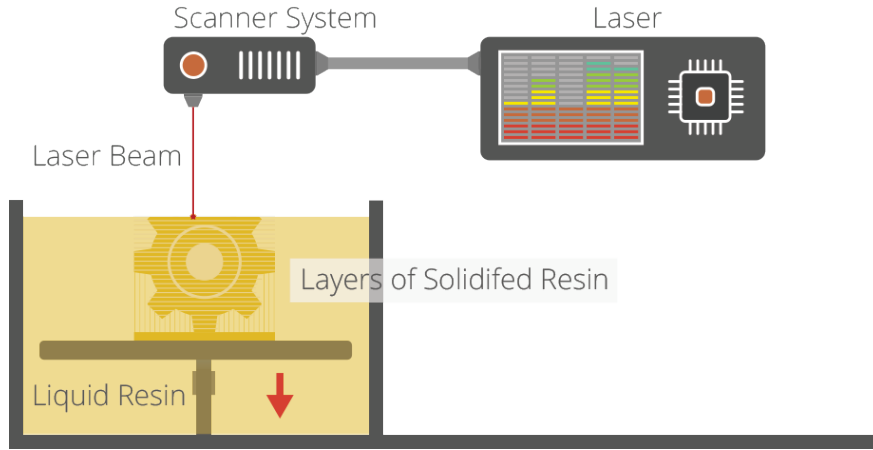


Figure 5: Schematic diagram of a digital laser projection printer. Figure from [6].

Digital laser projection was discarded as a design concept after experimentation with the inks. It was determined that the biomaterial could not be thinned sufficiently for it to flow properly.

### Five Axis Mandrel Printing

The next printing method considered was five axis printing. In five axis printing, the extruder is mounted on a serial robotic arm with five axes of freedom.

This design would make it possible to print the bone graft in a vertical orientation, without using a mandrel or any support material. It would also give professor Willett's team the flexibility to create other types of bone grafts other than grafts for the shafts of cortical bone.

Precedent for this design comes from companies such as 5axismaker, who have successfully created commercially viable 5 axis 3D printers like the one shown in Figure 6.

The principle disadvantage of this design concept is that it is inherently more difficult to create a high precision 5 axis robot arm. In a five axis robot arm, each segment (or axis) is mounted onto the previous one in series. This means that any inaccuracies in the each axis



Figure 6: Five axis 3D printer, created by 5AxisMaker. Figure from [7].

caused by manufacturing error, actuator error or control error will summate through vector addition.

### Three Axis Additive Lathe

Finally, a three axis additive lathe was considered as a printing method. In this method there is a cylindrical print bed, called a mandrel, that spins rotationally and an extruder deposits material additively onto this mandrel. The extruder can move along the mandrel from end to end, which is called axial movement and it can also move away from the mandrel to allow for multiple layers of the material to be added to the mandrel. An example of this is a printer designed by a group of Mechanical Engineering students at Imperial College London shown in Figure 7.

The advantage of this design is that cylindrical long bone geometries can be created with high precision, and that the control of this robot is straight forward. The principle disadvantage of this design is that it requires that the parts be printed on a mandrel. The

obvious consequence of this is that all parts must be hollow. Another disadvantage is that a process for releasing the print without damaging the part must be developed. The final disadvantage is that the parts must be approximately straight, which limits the types of bone grafts that can be produced.

### Mandrel Printing using an Existing 3D Printer

It is possible to do mandrel printing by modifying an existing 3D printer. Simply retrofitting a high precision mandrel into the printer and modifying that printer's control system is sufficient to allow virtually any 3D printer to do additive lathe style printing.

The advantage of this design is simplicity. The amount of new hardware required to implement this design is minimal. This allows the implementation to be completed quickly, and makes this technique more accessible to other research groups.

The disadvantage of retrofitting an existing 3D printer is that the overall print accuracy is limited by the resolution of that printer. Commercially available 3D printers are plagued by poor positional accuracy and repeatability. Most manufacturers do not specify or test these values.

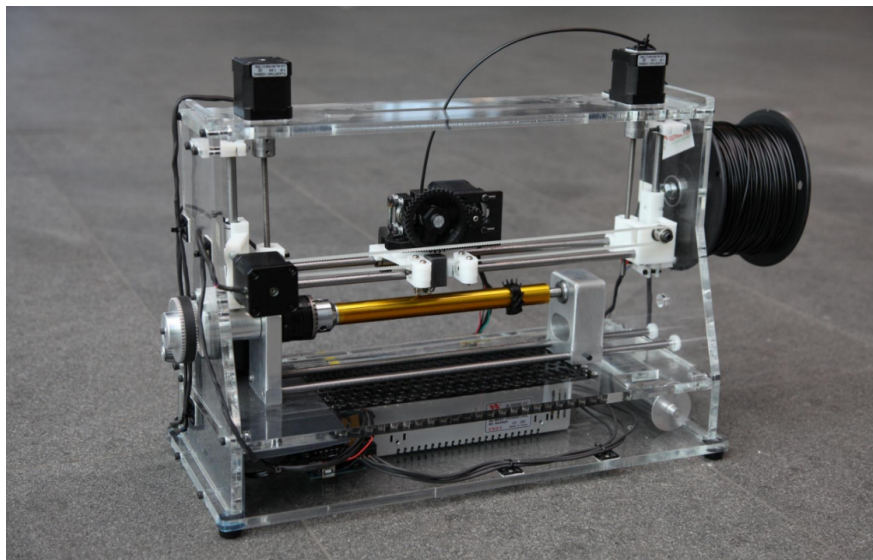


Figure 7: Three axis additive lathe printer created by a design team at Imperial College London. Figure from [8].

## 1.5 Concept Selection

Our team has selected the three axis additive lathe concept. This design is less flexible and scalable than the five axis printer. However, the three axis additive lathe will meet the lab's current needs for bone graft sample manufacturing.

The three axis design is far simpler, so there is less inherent technical risk in the design process. Limiting the printer to only three axis of motion made it easier to meet professor Willett's stringent accuracy and repeatability requirements.

The three axes we have chosen are visualized in Figure 8. The axis that rotates the printer is the rotational axis. The axis that moves the extruder along the length of the mandrel, traditionally known as the x-axis, is the axial axis. The axis that increases the distance of the extruder from the mandrel, traditionally known as the z-axis, is the radial axis.

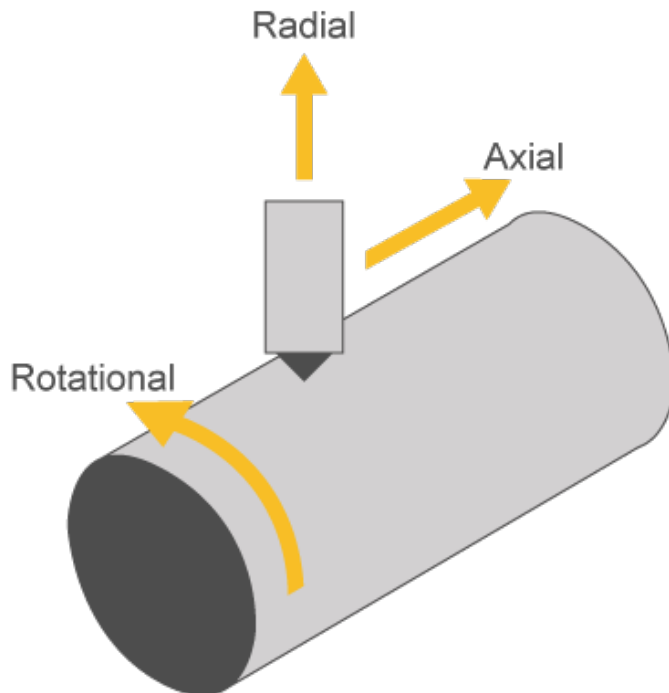


Figure 8: SkelePrint definition of axis names.

# 2

## Mechanical Design

### 2.1 Mechanical Design Summary

The mechanical design components of the printer included determining the appropriate motors for each axis of the printer, designing the three axes, the mechanics of the print bed mechanism, and the frame.

### 2.2 Rotational Axis

The most important specifications for the rotational axis is the angular resolution, ease of removal of the print, and alignment with the axial axis.

#### Angular Resolution

The rotation of the print bed must be controlled such that at the maximum printing radius, the minimum discrete rotation results in an arc length of less than 200 microns per step.

Given that the maximum print radius is 35mm (30mm print radius and a 5mm mandrel radius), the required reduction is:

$$\theta = \frac{0.2}{35} \times \frac{180}{\pi} = 0.33 \text{ degrees} \quad (1)$$

Thus the minimum reduction required to achieve the angular resolution is 2.72:1. We opted to use a timing belt for the reduction, because timing belt drives exhibit considerably less backlash than a geared reduction.

We opted to implement the timing belt reduction using a 26 tooth pulley and a 72 tooth pulley, making a 2.77:1 reduction. The pulleys chosen were MR2 (GT) High Torque Timing Pulleys from Misumi USA. These pulleys were chosen because they are lightweight and they can mount directly onto the shaft of our chosen stepper motor. For the timing belt itself, we chose MR2 (GT) High Torque Timing Belt also from Misumi USA. This material is

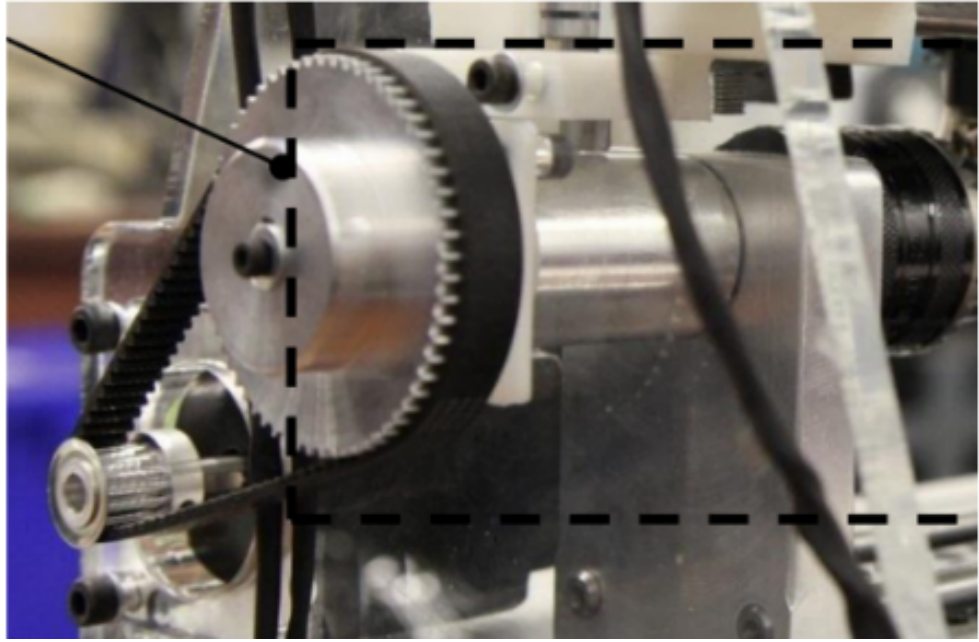


Figure 9: Timing belt implementation used on a previous lathe type 3D printer. Figure from [8].

sufficiently compliant, and resistant to stretching. The belt length calculation in Appendix A resulted in a required belt length of 241.1 mm. The first belt ordered was 242 mm, which was closest to the calculated length that we could order. Later we opted to order a slightly shorter belt to reduce slack.

The 26 tooth pulley connects directly to the motor shaft, while the 72 tooth pulley connects directly to the dead center drive shaft. The print bed drive shaft is supported by a bearing within a bearing housing. The design of this transmission system for the rotational axis can be seen in Figure 10.

### Print Bed Mechanism

The print bed design must enable the user to remove the print and interchange the mandrel. The design for the print bed holder is inspired by a machining technique called "turning between centers". Turning between centers involves holding the part between two pointed "centers" using friction, the setup can be seen in Figure 11. The drive end is called a dead center, and it applies the torque on the cylinder. The end on the other side is called a live center. The live center is mounted in "free-end" comprised of ball bearings, and ideally

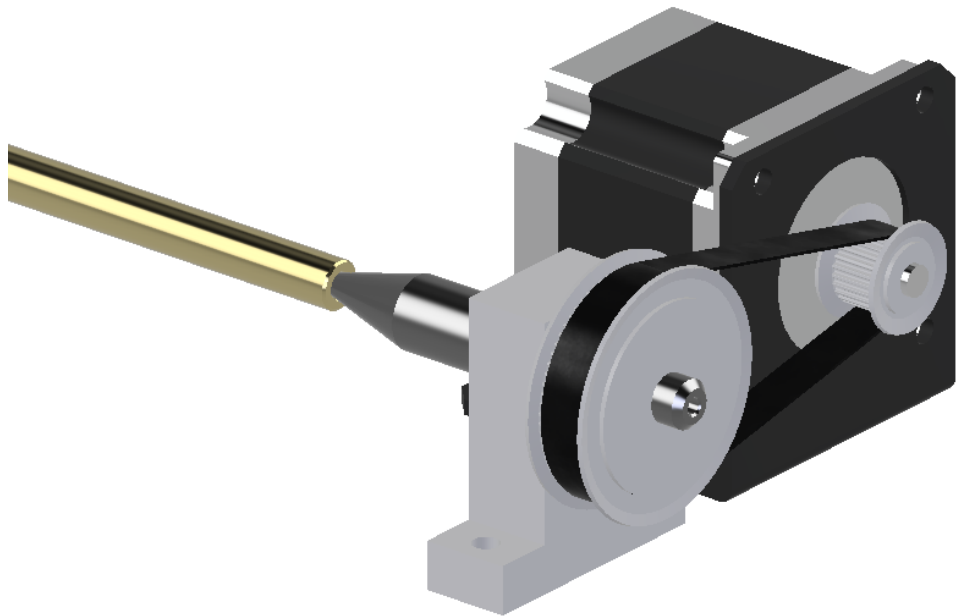


Figure 10: CAD of the rotational axis transmission.

should apply zero torque to the cylinder.

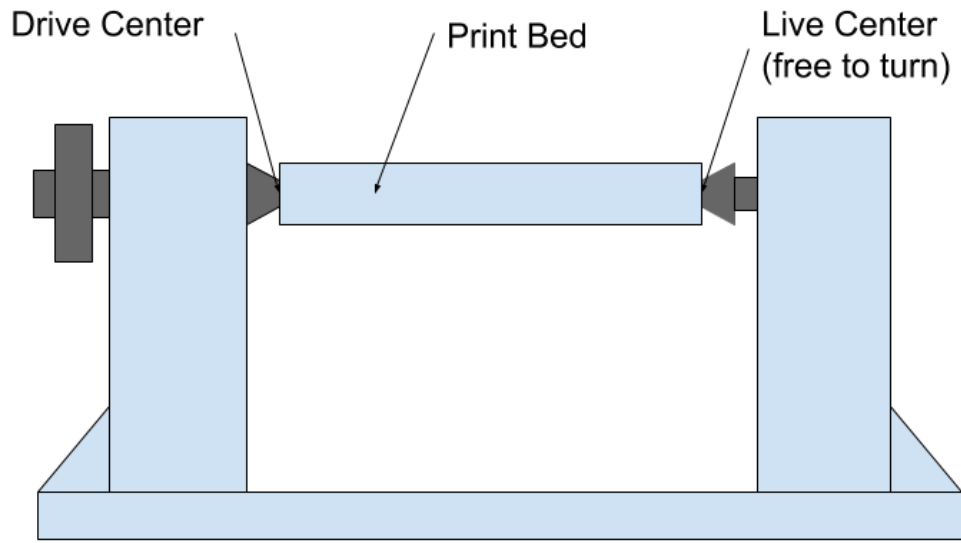


Figure 11: Turning between centers concept drawing

Some pressure between the centers and the print bed is required to produce the frictional force that holds the print bed in place. In our design, this pressure is generated by pressing

the print bed between the two ends by adjusting the free-end position.

The print bed is a cylindrical shaft. The cylinders require minor machining on the ends so that the centers can be pressed into the ends concentrically. The printer is currently operating with a lightweight aluminum precision linear shaft from Misumi. Should the research team wish to interchange the print bed for a different material at a later date, McMaster-Carr and Misumi offer precision cylinders in ceramic, borosilicate-glass, and steel with the option to have the ends machined so interchanging the print bed will be straightforward and relatively inexpensive. This setup can be seen in Figure 12.



Figure 12: CAD model of the turning between centers technique used in our final prototype.

The option to switch out the mandrel to a different material or size is convenient for the lab to test the best procedure to remove finished prints from the mandrel without damaging or compromising the print. Methods to reduce the difficulty of removal include a layer of uncured biomaterial, a water soluble film applied to the mandrel before printing, or lubricant in between the mandrel and the print. Alternatively the biomaterial may also have difficulty adhering to the mandrel in which case an adhesive layer such as hairspray or Kapton tape may be used. During testing Kapton tape was used on the aluminum mandrel and the print was firmly adhered. However, the print had to be cut off the mandrel.

A possible alternative to the single piece mandrel is the use of a tapered split-mandrel, to make the component easier to remove. It would be relatively simple to create such a

mechanism by machining identical tapers in a matched pair of mandrels. Part removal could also be made easier by only partially curing the first layer, or placing some type of a buffer material on the mandrel. Finally, the aluminum mandrel can be replaced with a different material, and the overall length of the mandrel can be decreased. The actual implementation of the rotational axis can be seen in Figure 13.



Figure 13: Mechanical design of the rotational assembly

### Alignment with the Axial axis

The alignment of the extrusion tip to the print bed is dependent on the alignment of the axial axis with the rotational axis. As the carrier of the extrusion system the axial axis must run parallel to the rotational axis which is a challenge due to the regular shifting of parts of the rotational axis when the mandrel is moved. Improper placement of the rotational axis is currently a major source of error.

The frame of the printer is partially responsible for ensuring the axial and rotational axes are parallel through having the mounting slots aligned but the actual mounting of the rotational axis can still result in misalignment. For now, the axial axis will be permanently mounted to the extrusions. A square was used to make sure the driven end of the print bed

was aligned properly with the axial axis.

To ensure correct mounting and placement of the floating end of the rotational bed, a square was used similar to the driven end. Permanent mounting of the floating end is not the ideal solution, because it means the bearing needs to be taken off before the print bed can be removed. It was difficult to find a better solution that was cost efficient and accurate. To assist in proper placement, visual markers have been placed on the frame to indicate the correct position and alignment of the bearings for the print bed.

The ideal solution for removing the print bed would include some kind of screw loaded guide or rail that the bearing is sitting on. This way the bearing can be pulled away from the print bed and allow it to be removed and inserted easily. As long as the guide or rail was mounted square to the axial axis, moving the bearing along the guide or rail will maintain a parallel position at all times. The screw would apply the horizontal force to the bearing that maintains the friction needed to hold the print bed in place.

## 2.3 Linear Actuators

The axial and radial axes are linear actuators where the axial axis carries the radial axis which carries the extrusion system. Options for precise linear actuation are outlined here to justify the choices for the respective axes. The most common types of linear actuators are belt drives, lead screws and ball screws.

### Belt Drive

Belt drives use a rubber timing belt to convert rotary motion into linear motion. Belt drives are well suited to high speed motion. They are inexpensive, and do not require the motor's shaft to be axially aligned with the axis. Also, belt drives are excellent for long travel applications. Unlike lead screws and ball screws, the cost of the belt drive does not increase in direct proportion to the drives axial length. Figure 14 shows an example timing belt drive used in the Zen Toolworks 3D printer.



Figure 14: Zen Toolworks 3D printer timing belt. Figure from [9].

However, belt drives do not function as a mechanical reduction, which means that they must be driven using a motor with a high angular resolution. Belt drives also exhibit mechanical backlash proportional to the stretch in the belt and the inertia of the load. Finally, belt drives used for positioning have a relatively short service life before they require adjustment.

### Lead Screws

Lead screws convert rotatory motion into linear motion by advancing one or more nuts along their threaded length. They have the advantage of being relatively precise compared to belt drives. They are particularly ideal for small step linear motion, because they function as a reduction allowing them to be directly driven by a standard resolution motor.

Lead screws can be integrated directly into the armature of a stepper motor as shown in Figure 15. This is ideal for use in small lightweight assemblies as a motor coupling is not needed.

The disadvantages of lead screws are that the friction between the nut and screw can be substantial, especially when driving high inertia loads. This friction leads to heat and wear in the lead screw's moving nut. High quality lead screws are machined out of stainless steel, and a softer material is used for the threads of the nut, such as plastic or brass. This way, the wear between components only damages the relatively inexpensive nut, the nut can



Figure 15: A stepper motor with a lead screw integrated directly into its armature. Figure from [10].

be periodically replaced in machines with tight accuracy requirements.

The primary source of backlash in a lead screw is mechanical slop between the nut and the threads. Thus, backlash increases over time as the nut wears against the screw. Lead screw backlash can be decreased by using two nuts in series, with a stiff spring in between to preload the nuts against the screw threads. Alternatively, backlash can be reduced significantly by using the lead screw in a vertical orientation, and using the mass of the carriage as a preload.

### Ball Screw

Ball screws are similar to lead screws. The difference is that instead of using a static coupling between the nut and the screw thread, they use a high precision system of recirculating balls through circular grooves in the ball screw as seen in Figure 16. These ball bearings are preloaded against the screw, which is why they have so little backlash.

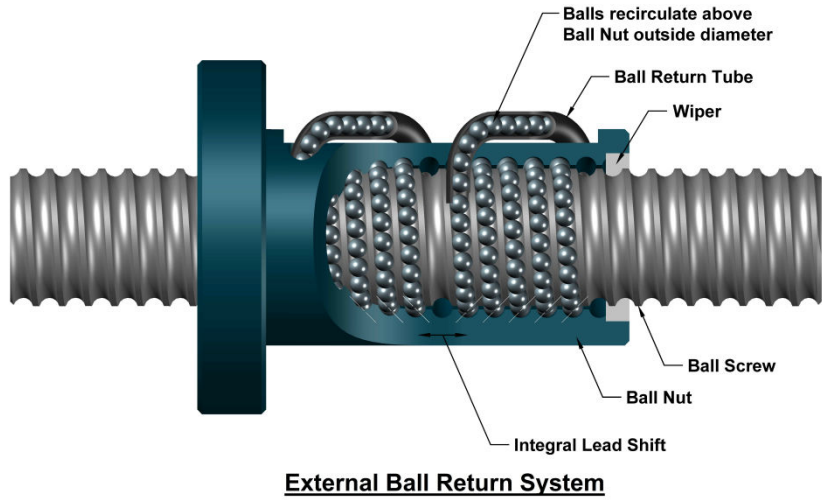


Figure 16: Cutaway view of a ballnut, illustrating the tight coupling between the ball bearings and the screw threads. Figure from [11].

The ball screw mechanism achieves higher efficiency than lead screws (80% or greater), and is not subject to the same problems with wear. Ball screws particularly excel in their backlash and full scale error specifications.

## 2.4 Axial Axis

The design was specified to have at least  $> 20\text{cm}$  of usable print length. The width of the gantry that will prevent some of the length of the actuator from being useful. With this constraint in mind a  $38\text{cm}$  actuator length was chosen and the printer has a usable length of  $28.5\text{cm}$  after taking into account the position of the limit switches.

The axial axis will have a full scale error less than the width of an extruded bead of material. The eventual goal of the lab is to reduce the width of extruded strand to less than 100 microns. Thus the full scale error of the axial axis must be less than 100 microns over the  $28.5\text{cm}$

This strict accuracy tolerance limits the linear actuator choices to a screw type. A ball screw was selected over a lead screw, because ball screws have high accuracy and efficiency. Also, ball screw setup has the least backlash of the available actuators in horizontal applica-

tions. We chose a ball screw with accuracy grade C7, which corresponds to a maximum error of  $\pm \frac{50\mu m}{300mm}$ , including the error introduced by the bearing supports [12]. This means there is 50 microns of error for every 300mm of usable actuator length. To meet the axial accuracy specifications, we chose to use an anti-backlash ballnut, which is specified to exhibit  $< 15\mu m$  backlash error.

The ends of ball screws are machined to fit into a fixed end and floating end supports. The fixed end supports the ball screw using angular contact bearings that lock onto the screw and provide both axial and rotational support. This fixed end can then be attached to a motor coupling and the motor. The floating end supports the shaft using a standard deep groove ball bearing which provide rotational support at the end opposite to the motor. An exploded view of the ball screw assembly is shown in Figure 17.

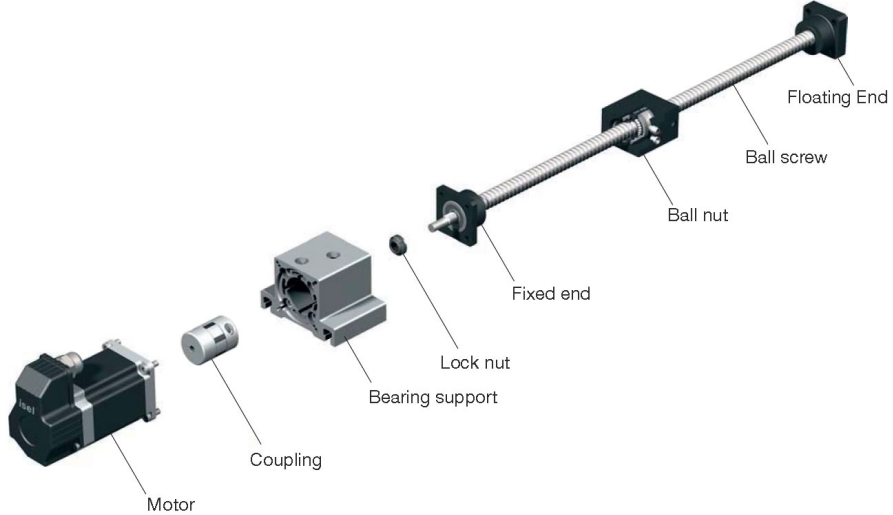


Figure 17: Ball screw assembly from ISEL Automation. Figure from [13].

The ball screw pitch was selected based on the desired linear travel corresponding to one motor step. Ball screws typically come in either 5mm or 10mm pitch. The travel distance is calculated using  $d = \frac{pitch}{steps\_rev}$ . The motor chosen for the axial axis has 200 steps per revolution so the possible travel distances are  $d = 25\mu m$  or  $d = 50\mu m$ . In this case the 5mm pitch with the  $d = 25\mu m$  travel distance is suitable to maintain the required axial resolution and while simultaneously achieving the desired speed for the axial axis.

To ensure linear motion and proper alignment of the carriage there will be linear mo-

tion rail mounted under the ball screw. The linear motion rail (Hiwin rails from Automation4Less) has a ball bearing gantry that will be mounted to the carriage that guides the carriage along the rail as the ball screw turns.

A CAD render of the axial axis is shown in Figure 18 and the real implementation of the axial axis is shown in Figure 19.

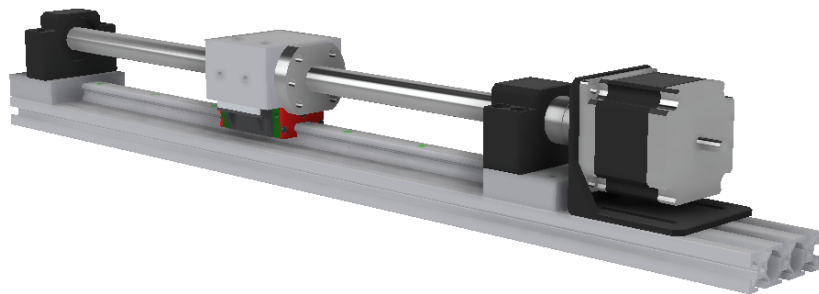


Figure 18: CAD model of ball screw assembly in our final prototype.



Figure 19: Mechanical design of the axial assembly

## 2.5 Radial Axis

The radial axis assembly is used to actuate the extrusion system radially from the rotational axis. In other words, the radial axis moves the extruder closer to or away from the print bed.

The radial axis needs to have a usable range of movement of greater than  $3cm$ . To account for the size of the extruder system, the screw was designed to be  $12cm$ . Due to the size of the linear guide and the positions of the limit switches, the final range of movement was  $5cm$ . The error budget of the radial axis is greater than the axial axis at  $150\mu m$  for the full scale error across the  $5cm$  length. However, the shorter length of the radial axis compared to the axial axis also makes the full scale error more achievable.

A lead screw is an acceptable linear motion actuator for the radial axis, because it will be mounted in a vertical orientation and the gravitational preload of the block holding the extrusion system will significantly reduce the backlash error. Originally we wanted a NEMA17 motor with an integrated precision lead screw and an anti-backlash nut from Lin Engineering (LE17LT) for the radial axis. However, the quote we received for one lead screw

indicated a cost that was outside of our budget and a lead time of seven weeks so other options were considered. Pololu offered a similar lead screw that was affordable with the only drawbacks being that there was no anti-backlash nut and we would have to cut the screw to size ourselves. Since there was the gravitational preload of the block holding the extrusion system, the nut that came with this lead screw was used.

To determine lead screw pitch a similar calculation as the ball screw pitch was performed. Lead screws have the same pitch options as ball screws. A  $8\text{mm}$  pitch lead screw was selected to achieve a suitable travel distance of  $d = 40\mu\text{m}$  with respect to a  $200 \frac{\text{steps}}{\text{rev}}$  motor. The lead screw was directly integrated into the motor to avoid the need for a motor coupling, and has a floating end at the base to stabilize the screw as seen in Figure 20.

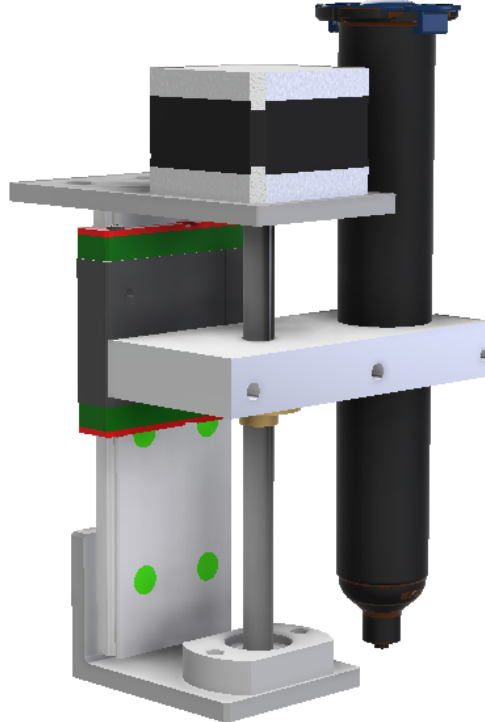


Figure 20: CAD model of the radial axis assembly in our final prototype.

Just like the axial axis, the radial axis uses a linear motion rail (Hiwin rails from Automation4Less) mounted behind it to guide the block on the lead screw. The block on the lead screw holds the extrusion system. The radial axis will use smaller linear motion rails

to support and guide the block seen in Figure 20.

The block that holds the syringe was custom machined. The original design of this block had four mounting holes into the linear guide. The final part was too heavy for the radial motor so we cut the block in half, leaving only two mounting locations into the linear guide. This block has a through hole for the lead screw and holes for the lead nut to attach to. Another through hole was made for the syringe to fit in.

The radial axis assembly is then mounted on a carriage that travels along the axial axis. The combination of movements in the axial and radial axes create the helix structure desired on the print bed. The real implementation of the radial axis mounted on this carriage can be seen in Figure 21.

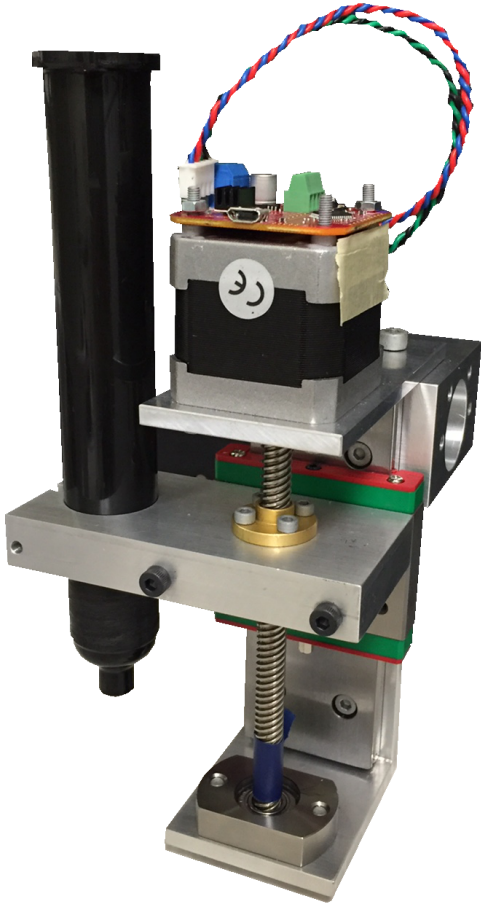


Figure 21: Mechanical design of the radial assembly

## 2.6 Motor Selection

### Stepper Motors vs Servo Motors

Originally the printer design used DC servo motors to control the printer's axes using PID closed loop control. A DC servo was the motor used throughout the low fidelity testing but the switch to stepper motors was made when it was discovered that small DC servo motors have substantially less low-speed torque than an equivalently sized stepper motor. This is

because stepper motors have many more poles compared than standard servo motors.

During the low fidelity print tests with the DC servo motor, issues arose with maintaining smooth low speed motion of the print bed. Switching to a small stepper motor for this application resolved the issue.

## Stepper Motor Application Notes

Stepper motors are designed to move repeatably in discrete steps, and are typically driven using open-loop controllers. Positional control is obtained by counting the steps that have been sent to the motor. Stepper motors are inexpensive as they are widely used in consumer electronics.

Stepper motors are available in typically available with either 200 or 400 counts per revolution, corresponding to 1.8 or 0.9 degree steps respectively. We opted to use 200 count motors on all axes in the design because the resolution can be controlled through the selection of pitch and gear reduction on the axes.

Stepper motors travel one angular step when a stepper motor driver sends a step pulse. In ideal conditions, they can be driven in a precise repeatable manner using an open-loop controller without positional feedback. This is the design used in low cost 3D printers, and entry level CNC mills.

This open loop control strategy is not sufficient for producing bone grafts for mechanical testing. For the lab purposes the motors need to have close loop control to account for mechanical disturbances that could compromise a print. The implementation of closed loop control with positional feedback is described in the controls section.

## 2.7 Motor Sizing

The most important specifications for selecting an appropriate motor for the printer are step size and torque rating. The step size determines the smallest increments that the motor can move in while the torque determines the maximum angular force force output the motor can achieve. The motor sizings were chosen based on the torque output, because all stepper motors have sufficient maximum speeds for our application.

The torque calculations are based on the required acceleration of the axis and the load torque. The acceleration torque is the torque required to start, stop, and change directions, while the load torque is the load the motor has to turn based on the inertia and friction that opposes movement in the axis.

The axial axis uses a horizontal ball screw as a motion actuator. Driving the ball screw will require a relatively low torque, because the ball screw has low friction and the weight of the carriage will be supported primarily by the linear guide rail. The other consideration for this axis is that the motor will be in constant motion so it is best to purchase a motor that is slightly over sized so the motor does not burn out from running near its maximum power output for an extended period of time. The calculation for the required torque can be found in Appendix A. The result for this calculation is  $T \approx 0.5Nm$  so a suitable stepper motor would be a NEMA-23 motor which has a holding torque rating of  $1.06Nm$ .

For the radial axis a vertical lead screw will be used for motion actuation which has higher friction compared to a ball screw, but the motor will be moving less weight, and will only move during infrequent layer changes. For the radial axis a Pololu NEMA-17 motor (with an integrated lead screw) with a holding torque of  $0.36Nm$  is used.

The rotational axis motor will be utilizing a timing belt reduction which will reduce the required torque of the motor. As the rotational axis will be running constantly a NEMA-23 motor is also used here. The belt calculations and the rotational motor torque equations can be found in Appendix A.

## 2.8 Frame

To maintain the accuracy requirements for all three axes, the printer's frame must be rigid and have a high moment of inertia, so that it does not wobble or vibrate while the axes are accelerating. The frame also had to ensure the axial and rotational axis could be mounted in exact parallel orientations to ensure proper alignment of the extrusion tip with the print bed.

The printer has many components that need to be mounted which made creating custom plates for mounting impractical due to continuing revisions and adjustments. Extruded aluminum has channels that can allow for placement of t-nuts anywhere which is convenient

for quick revisions and a variety of mounting needs. The use of extruded aluminum was initially discounted as it is typically made with low accuracy tolerances. Fortunately, custom extruded aluminum pieces with milled surfaces that met the accuracy tolerances required by the printer are available through Misumi so extruded aluminum was implemented as the horizontal components of the frame.

The vertical side plates are made of aluminum that was machined on a highly accurate three axis CNC mill. The side plates hold the aluminum extrusions in place. Rubber dampers are added as feet to reduce vibration from the motors.

The stiffness of the frame is important, because any frame deflection detracts from the machine's error budget. To ensure that the frame is sufficiently stiff, the moment of inertia and modulus of elasticity of the extrusions were computed using the calculator on 8020.net. The 80/20 calculator is based on a less rigid grade of billet aluminum than the actual manufacturer we used (MISUMI) so these numbers can be considered as the worst case.

The 80/20 calculator implements the standard beam deflection equation:

$$\frac{1}{\rho} = \frac{M}{EI}$$

Where  $\rho$  is the radius of curvature of the beam, M is the bending moment, E is the modulus of elasticity and I is the moment of inertia of the cross section about the neutral axis. The advantage of using the calculator over doing these calculations manually is that it estimates the E and I terms based on measurements made on the 80/20 product lineup.

Using an estimated center load of 2kg, and point supports on the ends of the beam. It was computed that the deflection of the center bottom rails will be  $< 1\mu m$  and the deflection of the top rail will be  $< 2\mu m$ . Thus, the contribution of frame deflection to the overall printer error budget will be negligible.

Analysis of the resonant frequencies of the frame was not carried out. Our physical testing has not yet revealed any problems with vibration. Our (unproven) assumption, is that using high frequency PID control for the motors as opposed to standard low cost stepper drivers essentially eliminates the motor vibration problems that plague low-cost CNC systems. If resonance of the frame ever does become a problem, then the frame can be

disassembled and voids in the extrusions can be filled with material such as lead (or a more expensive non-toxic alternative) to increase their weight.



Figure 22: CAD model of the frame assembly in our final prototype.

In the future the side plates could be braced with right angle brackets for increased rigidity. We drilled a tapped holes in the sideplates for the possibility of mounting brackets (MISUMI HBLFSNK5). A support plate could also be added to the back of the frame to support the aluminum extrusions and reduce bending but this was determined to be excessive as the extrusions are sufficiently rigid for the current purpose of the printer. The real implementation of the final assembly of the printer can be seen in Figure 23.

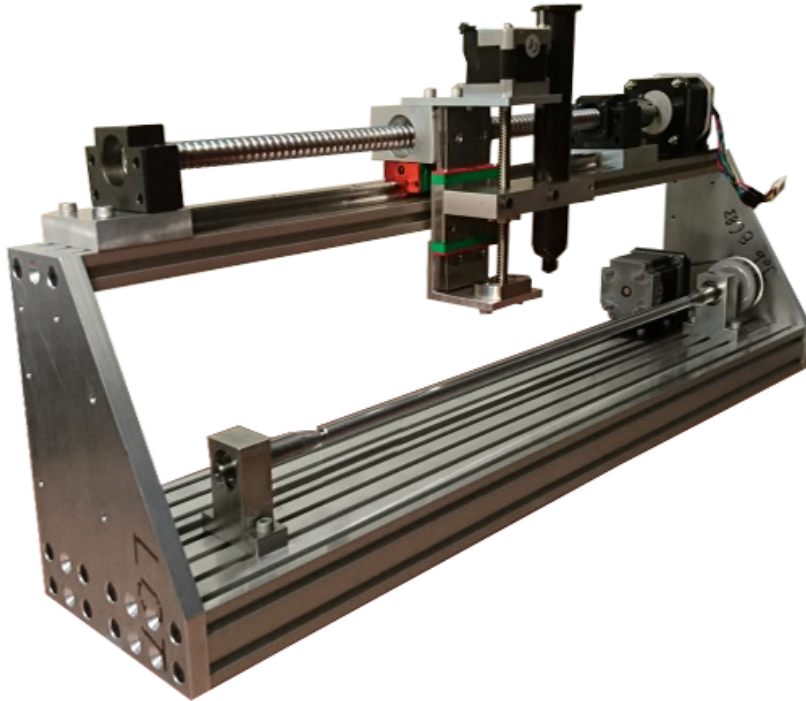


Figure 23: Mechanical design of the overall printer

## 2.9 A Note on Measurement Convention and Tooling

We used metric units of measure in the design and component selection process. Wherever possible, the nominal dimensions of our components were chosen to an integer number of millimeters. All of the actuators and motors are metric. We also used metric fasteners exclusively, so a set of four metric hex wrenches (M3, M4, M5, M6) are sufficient for installing or removing any component on the entire printer.

One unfortunate exception to this convention is the extrusion system. The extrusion system is designed in imperial units, because the extrusion system needed to be compatible with syringes and hoses produced by Nordson, and Nordson uses imperial system of measure. Also, it is essentially impossible to purchase small diameter, high pressure pneumatic fittings in metric sizes. Fortunately, only a single 1/2 inch wrench is required assemble the entire extrusion system.

Another less important exception to the metric convention is the electrical connectors.

All of the connectors used on the printer use imperial nominal dimensions. The standard connector pin pitch used throughout the entire printer is 0.1 inch. Imperial connectors were chosen, because we wanted to use off the shelf motor drivers, and the PCBs for those motor drivers were drawn in imperial units.

We highly recommend that future modifications to the printer use metric components, dimensions and hole sizes to avoid creating a confusing mess. Sticking to a convention also makes the machinists work easier when they build additional parts. The engineering machine shop has an excellent stock of metric tooling (though the student machine shop does not).

# 3

## Extrusion System

A pneumatic extrusion system has been designed for a  $90\text{psi}$  maximum pressure. A pneumatic system was chosen based on its ability to control pressure on the ink almost instantaneously. This removes any chance of over extrusion. Over extrusion is often the result of a pressure build up in the extruder, and it can be problematic when the extrusion head has to stop and change directions when depositing the ink. A displacement-type extruder was not chosen because it does not have the same dynamic response as pneumatic extruders - displacement-type extruders often deposit excess ink because of their inability to exhaust pressure build up. A schematic of the conceived system is shown in Figure 24.

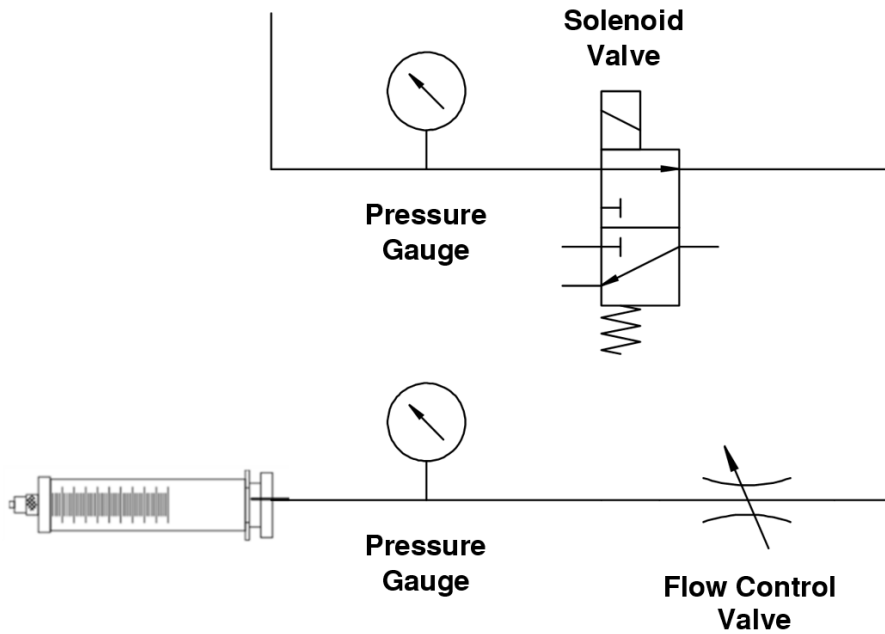


Figure 24: Schematic diagram of pneumatic extrusion system.

Figure 24 shows the current extrusion system design for a  $90\text{psi}$  maximum pressure input. There are two pressure gauges, a flow control valve, a 3 way solenoid valve, and a 55cc UV-blocking syringe. The first pressure gauge displays the pressure being output by the source,

and the second pressure gauge displays the pressure which has been adjusted by the flow control valve. The solenoid allows for air to flow when actuated, and stop air flow and exhaust pressure build up simultaneously when turned off. It was required that the system could connect to the input which is a serrated nozzle approximately 1/4" OD, and connect to the output syringe which has a 5/32" OD connecting hose. It was also required that each component could withstand over 100*psi* of pressure as a safety consideration. Hose clamps were added to each end of the tubing to avoid any weak points that could result in the air escaping the system.

Size and weight were a significant considerations in the design. A large extrusion head could prove to be problematic in the overall printer design. A heavy extrusion system would make the design of the axial and radial axis more difficult, because the actuators would have to support and accelerate a greater inertia.

The syringe chosen is a 55cc plastic luer-lock syringe which is relatively light compared to alternatives. The syringe is completely opaque to block any ambient light which can cause unwanted reactions with the UV curing agent in the biomaterial. Smaller components were selected where possible in the overall design to improve compactness and create a cleaner interface between the printer and extrusion system. The distance from the printer to the pressure source was addressed by procuring an adequate amount of tubing to meet any length requirements.

# 4

## Controls Design Summary

The control system for the printer has three major components. In order of usage, they are:

1. The toolpath generator that creates the G-code toolpath corresponding to the desired part. In 3D printing, these tools are called slicers.
2. The controller that interprets the G-code and sends power to the printers actuators.
3. The firmware that runs on the controller, and controls the motion of the axis in real time.

In the controls design process, we have investigated and designed these components.

Figure 25 below shows a high level system diagram for control system.

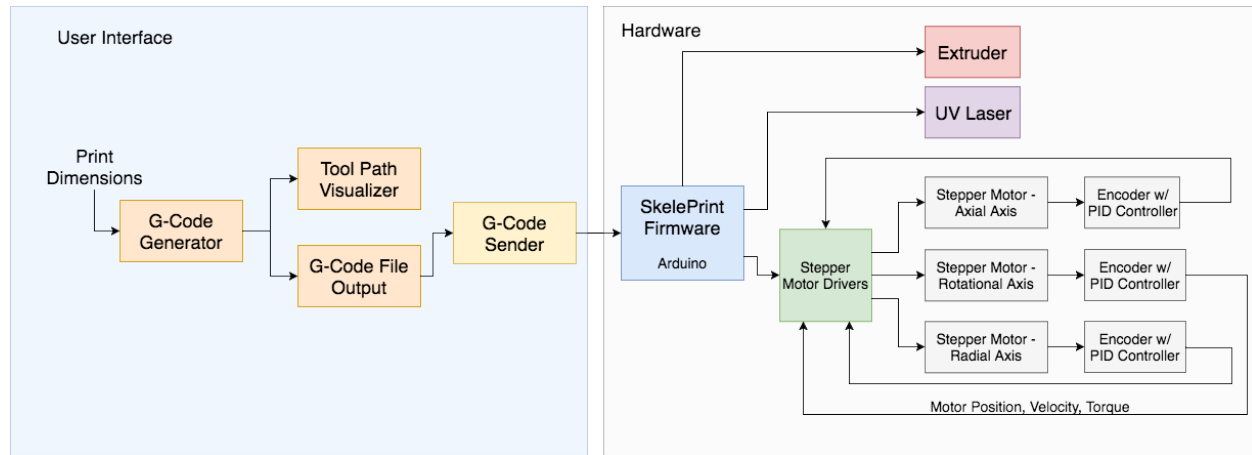


Figure 25: Controls system diagram.

### 4.1 Review of Open-Source CNC Firmware Packages

There are several open-source CNC control packages suitable for use with 3-axis robots. Some of these packages are summarized below.

## **RAMPS**

RAMPS is the defacto standard for open source 3D printers. RAMPS was created for the rep-rap 3D printer project. It runs on an Arduino Mega micro-controller.

RAMPS is highly optimized for the control of Cartesian 3D printers. This means that there is a substantial amount of source code that pertains only to optimizing movements of the x-y gantry.

## **Mach3**

Mach3 is the standard package used to control commercial 3 axis CNC machines. It runs on windows, and is optimized for controlling open-loop CNC mills. Mach3 requires the computer that runs it to have a parallel port, which is problematic. It is a massive project, and somewhat difficult to customize.

## **GRBL**

GRBL is a highly optimized 3 axis CNC control package that runs on an Arduino Uno. GRBL is the simplest full featured CNC control package in terms of code complexity. GRBL runs on a low cost Arduino Uno and can reliable maintain control loop frequency of  $30KHz$ . Closed loop control can be achieved with GRBL by using closed loop stepper motor drivers.

GRBL has the smallest amount of source code of any of the listed packages. GRBL includes routines for optimizing movement continuity and acceleration planning, but it does not have the complicated x-y gantry optimization routines found in Mach3 and RAMPS.

## **4.2 Choice of CNC Software Package**

After reviewing RAMPS, Mach3 and GRBL, our team chose GRBL to be the basis firmware for our additive lathe. Compared to the other projects, GRBL is more mature and much better documented. Also, there are several examples in the GRBL user groups in which users have used GRBL to control small CNC lathes, and their examples will be invaluable while we make our implementation.

GRBL is also a sound choice, because it has been incorporated into a wide variety of commercial packages, which means that many companies have a vested interest in maintaining the code base and documentation. Should the printer require firmware programming, the GRBL project and support forums should be active for several more years.

The most popular use of GRBL is in various models of ShapeOko mills by Carbide 3D. The ShapeOko Nomad has a similar design for the axial axis (x-axis) and the radial (z-axis) to our implementation, as seen in Figure ???. Since, the production level implementation of GRBL for the ShapeOko mills is open source and well documented, GRBL is the natural choice of base firmware for our project as it allows the project to build on top of a well defined and tested code base. This also minimizes the amount of duplicated work required. Figure 26 below shows the firmware assembly.

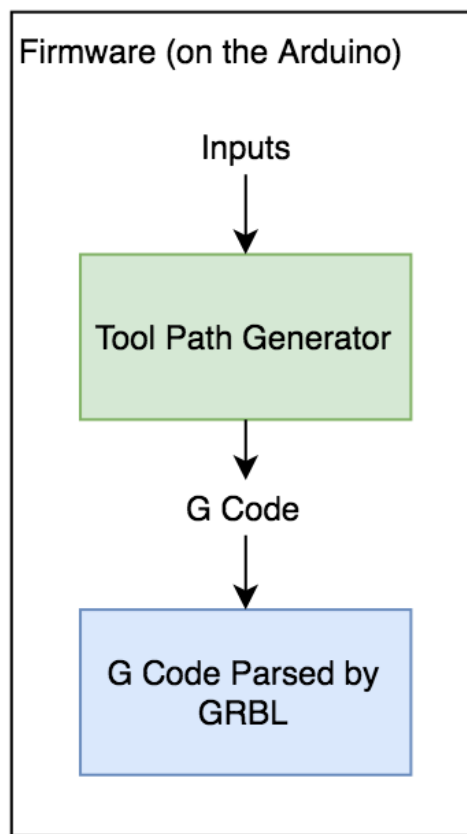


Figure 26: Controls system diagram.

### 4.3 Closed Loop Control

Closed loop control of stepper motors can be achieved by driving them with a standard brushless DC motor driver and using an optical encoder to track their angular position. This configuration is most accurate, but has the disadvantage of requiring much more sophisticated drive circuitry and a more involved controller tuning process.

A simpler model of positional closed loop control was implemented using the Mechaduino motion control platform. The platform consists of a Arduino Zero compatible microcontroller which houses a Dual Full-Bridge DMOS PWM motor driver and a 14-Bit on-axis magnetic rotary encoder. The encoder relies on a diametric magnet which is placed on the motor shaft to convert rotary movement into digital signals.

A diametric magnet was placed on the shaft of each motor before mounting the Mechaduino PCBs. Base firmware for each microcontroller was installed in order to process encoder data.

Each motor was then calibrated by stepping through a full rotation of the motor. The encoder values were used to generate a large lookup table of the calibrated angle at each encoder count. This allows the motor to move to the correctly calibrated angle for any given step.

The core firmware for the Mechaduino contains an implementation of a PID controller. Each axis however requires tuning as changes in inertia have a significant impact on the plant function.

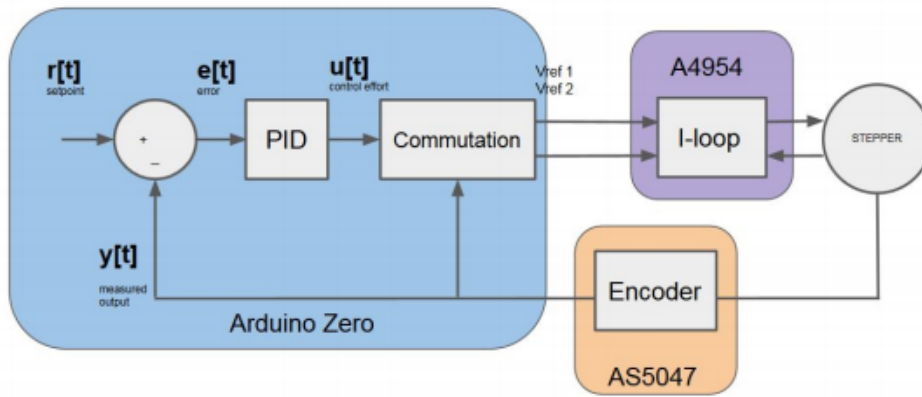


Figure 27: Mechaduino controller block diagram

## **Controller System Specifications**

After consulting with lab instructor Chris McClellan, the team chose the following specifications for controller response.

1. Zero steady-state error for step input
2. Minimize system rise time

Steady-state error is defined as the difference between the input and the output of the system as time goes to infinity. Zero steady state error is a key specification as any error in the system response would greatly affect the precision of the printer. Rise time refers to the time required for the response to rise from 5% to 95% of it's final value. This specification aims to minimize the overall system response time. Overshoot specifications were discussed but not included as the mechanical reductions of the actuators minimizes the effect of overshoot.

## **PID Controller Tuning**

In the interest of time, a plant function was not modelled for each axis and tuning was done using a strategic trial and error method until system specifications were met. The step size for each axis was initially selected by identifying the minimum movement required by each axis. Once the controller was tuned to meet the requirements, larger step responses were recorded to validate the overall system response and controller tuning.

The intelligent tuning began by setting the gain of the proportional, derivative and integral term to zero. The proportional term was increased until the system responded with steady oscillations. The derivative gain was then steadily increased until the system was critically damped. The steps above were repeated until the system a desirable rise time. The integral term was then added to remove any steady state error and the proportional and derivative terms were adjusted to improve response.

The step input size was selected by determining the smallest step size required by each motor during operation. After the controller specifications were met, the step input was increased to larger step inputs to ensure consistent system behaviour.

The radial axis and axial axis were tuned with a step input of 0.1 mm and the rotational axis was tuned with a step input of 1 rotation.

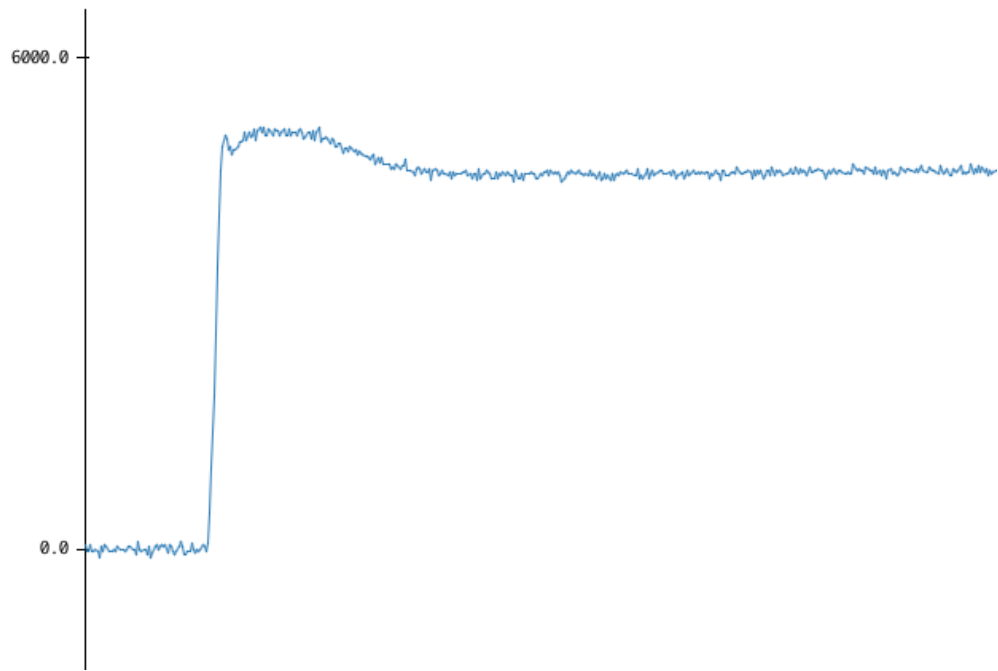


Figure 28: System response of radial axis

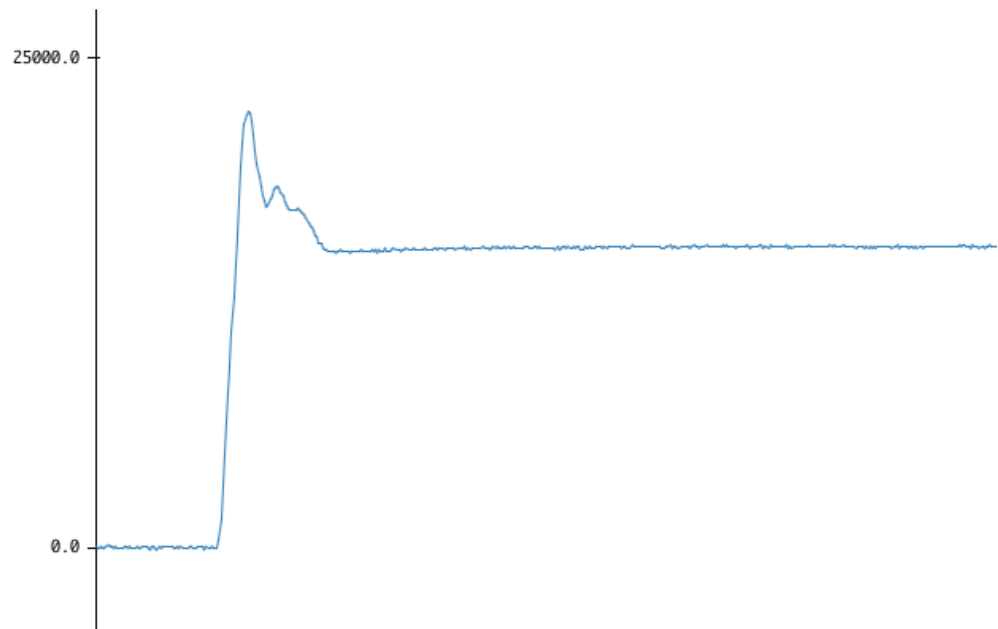


Figure 29: System response of axial axis

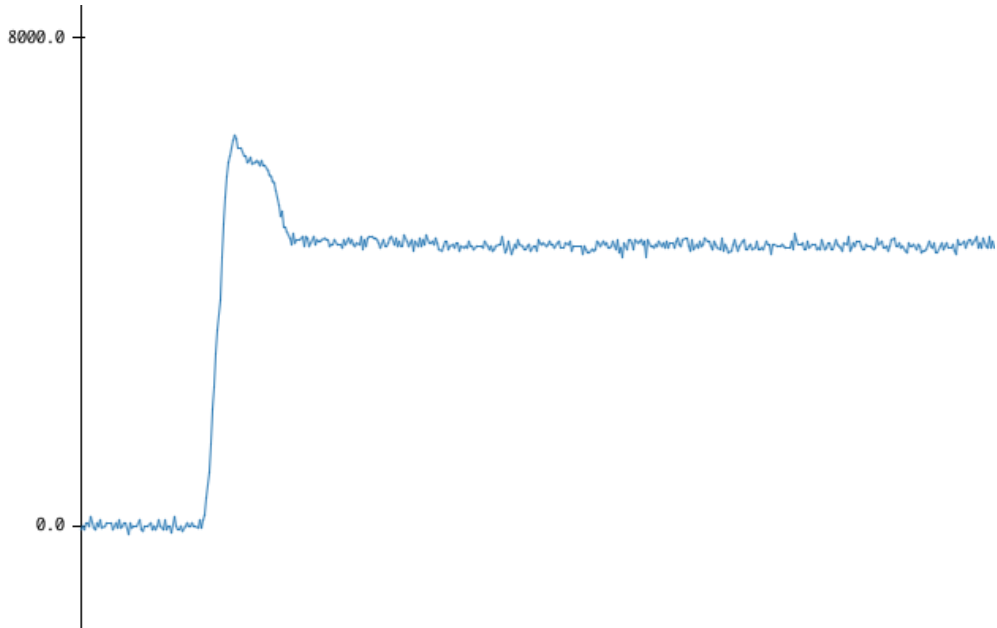


Figure 30: System response of rotational axis

### Quantifying Encoder Noise

The tuning process shed light on irreducible encoder noise in the system. The noise was quantified to ensure that noise did not have a significant impact on the overall system response. Encoder values were output for each axis to identify the maximum angular measurement error caused by the noise. This angular value was then divided by each axis's respective mechanical reduction ratio to determine the actual positioning error caused by encoder noise. The maximum noise resulted in a difference of 0.00481 mm in the radial axis, 0.00458 mm in the axial axis, and 0.00034 mm in the rotational axis. The mechanical reduction on each axis minimizes the impact of the encoder noise. Thus, the encoder noise is not a significant source of positioning error.

## 4.4 Extruder Controller

Control of the extrusion is relatively simple. When the solenoid valve is energized, it allows air to flow from the high pressure line to the extrusion syringe. When the solenoid is de-energized, it opens the extrusion syringe to atmosphere, releasing the remaining pressure.

The pressure from the syringe has to be vented promptly to avoid run-on. The run on

behaviour of Professor Willett's previous extruder design was demonstrated during the low fidelity prototype testing.

The solenoid coil is rated for a continuous DC voltage of 12V, and at 12V it draws 0.3A. The power consumption at 12V is  $P = VI = 3.6W$ . It is not desirable to have the solenoid valve continuously draw 3.6W, because the solenoid coil will self heat which could shorten its operating life [14].

To reduce the solenoid operating current, the solenoid should be driven with a voltage controlled driver, that produces a voltage waveform similar to the one displayed in Figure 31. An initial current surge is required to actuate the valve. After that point, the solenoid requires significantly less current to hold the valve open [15].

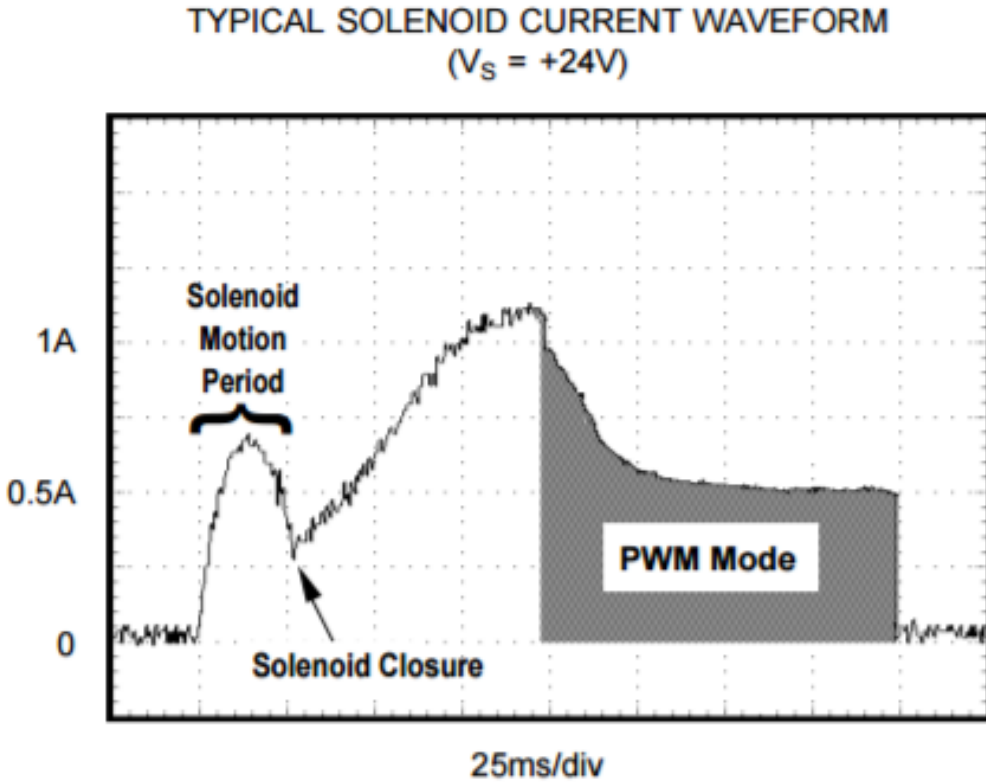


Figure 31: Typical solenoid current draw when powered by a PWM driver. Taken from the Texas Instruments DRV101 Datasheet. Figure from [15].

For ease of configuration, it was desirable that the solenoid controller use only one 5V digital IO line from the microprocessor. It was also required to run on 12V, to be compatible

with the power supply.

Based on these requirements, the solenoid driver DRV101 was selected. The reference design shown below was used as the starting point for implementing the solenoid driver. DRV101 produces the voltage waveform shown in Figure 32. The values of  $C_d$  determines the period at which the solenoid voltage is held high, and the value of  $R_{PWM}$  sets the driver's duty cycle during the hold period [15].

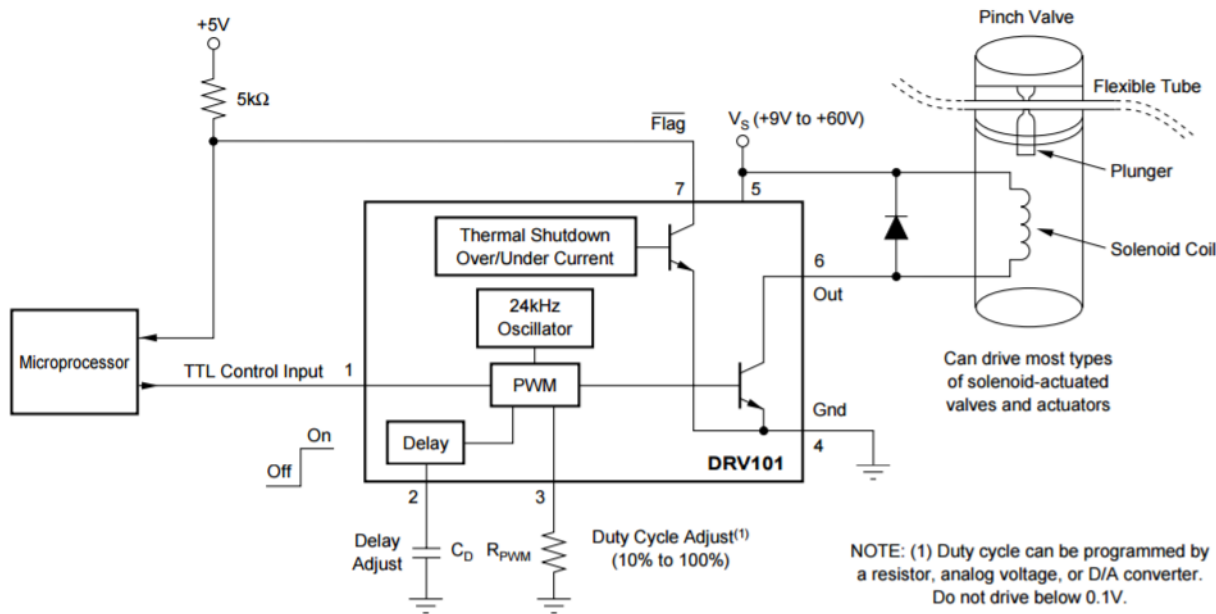


Figure 32: Texas Instruments reference design for a solenoid controller.

The value of  $C_d$  was set at  $0.1\mu F$ , to achieve a high voltage period of  $100ms$ , based on the solenoid valves actuation period at its maximum pressure rating of  $120psi$  [16]. A  $1k\Omega$  variable resistor was used in place of  $R_{PWM}$ , because the manufacturer datasheet for the solenoid does not specify the hold current value. Using the variable resistor we can tune the hold current manually.

The complete circuit implementation is shown in Figure 33.

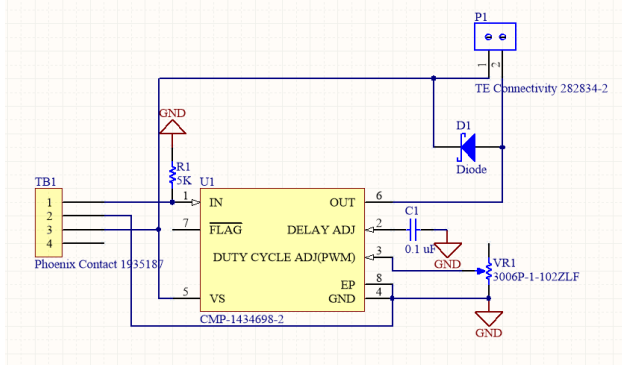


Figure 33: Solenoid controller schematic.

This circuit was manufactured on a PCB. The PCB layout is shown in Figure 34.

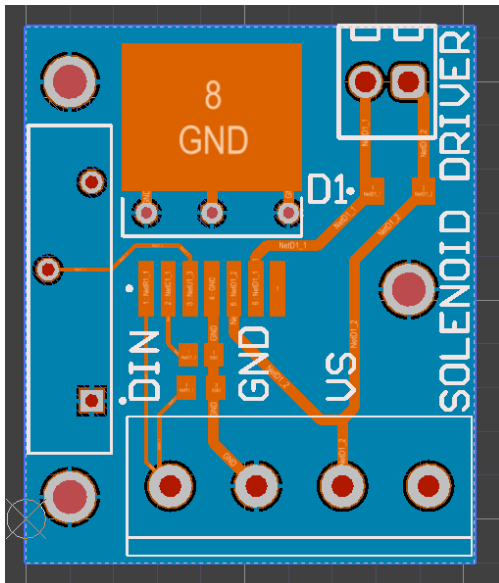


Figure 34: PCB Layout for the Solenoid Driver.

This circuit was constructed worked for over one thousand solenoid actuations, but it ultimately ended up shorting out and being scrapped. This fault was most likely caused by an assembly error that caused one of the coil snubber diodes to be poorly connected. The printer is wired using a much simpler solenoid driver, which was constructed based on this tutorial:

<http://playground.arduino.cc/Learning/SolenoidTutorial>

This solenoid driver is inferior, because it does not minimize the power consumption of the solenoid. However, this problem is minimized because the solenoid is mounted on the aluminum frame of the printer which is an excellent heat sink.

## 4.5 Tool Path Generator

A key user requirement of the project was to ensure the ability to develop helical structure at various angles in order to test the properties of the microstructure. The implementation of the rotating print bed requires a novel toolpath generation approach. The team created the SkelePrint Tool Path Generator which generates the G Code commands for the control of each axis of movement, the extrusion system, and the high powered UV laser.

### Core Algorithm

The algorithm accepts a set of parameters which are used to calculate and timing the motion of the motors, the start and end of the biomaterial extrusion, the activation of the UV laser. The following parameters are accepted as input:

1. Axial Length - The axial length (mm) is equal to the total length of the print and used to determine the total axial distance needed to travel.
2. Printbed Diameter - The printbed diameter (mm) is equal to the diameter of the mandrel.
3. Final Print Diameter - The final print diameter (mm) is equal to the final diameter of the print including the diameter of the printbed. Based on the value provided for the final print diameter the algorithm checks how many layers to print using the following logic:

```
layers = ((final_diameter - printbed_diameter)*0.5)/(filament_width_og * smear_factor)

if (layers < 1):
    layers = 1.0

if (layers % (filament_width_og*smear_factor) != 0):
    layers = math.floor(layers)
```

4. Filament Width - The filament width (mm) is equal to the inner diameter of the needle tip used.
5. Helix Angle - The helix angle (degrees) is angle of the helix on each layer. This value is used to determine how many start points are required for each layer. It is often not possible to print at the exact angle you specified as the the number of start point must be a whole number. The algorithm takes the value provided for the helix angle and adjusts it slightly to ensure the number of start point is a whole number. A helix angle of 0 degrees means that layers will consist of a single helix printed as close together as possible. A helix angle of 90 degrees means that layers will consist of many (almost) straight lines and have many start points.
6. Feed Rate - The feed rate (mm/min) is equal to the speed of movement based on flow rate of the extrusion system. The algorithm uses the entered feed rate to calculate the tangential velocity. The tangential velocity is recalculated at each layer as the diameter has been changed for each layer.
7. Layer Height - The layer height % is used to calculate the smear factor. At 100% the layer height is equal to the filament width. If layer height % is less than 100% then the radial axis only moves up some percentage of the filament width which means you are smearing the ink.

The core algorithm for the tool path generator focuses on calculating the movement required in the axial direction for every rotation of the rotational axis. This relationship determines the helix angle and thus the composite microstructure. Appendix A contains a detailed overview of the algorithm, as well as links to the source code.

## User Interface Design

An intuitive interface was designed and developed to accept user defined parameters and generate G Code commands. As the client identified a need for a cross-platform interface, the SkelePrint Tool Path Generator was developed in Python and hosted on the Python

Package Index allowing users to install the package with a single line of code on any Internet connected computer.

The user interface was designed specifically for the members of the biomaterials lab and relies on isometric diagrams to provide useful context on correctly defining parameters.

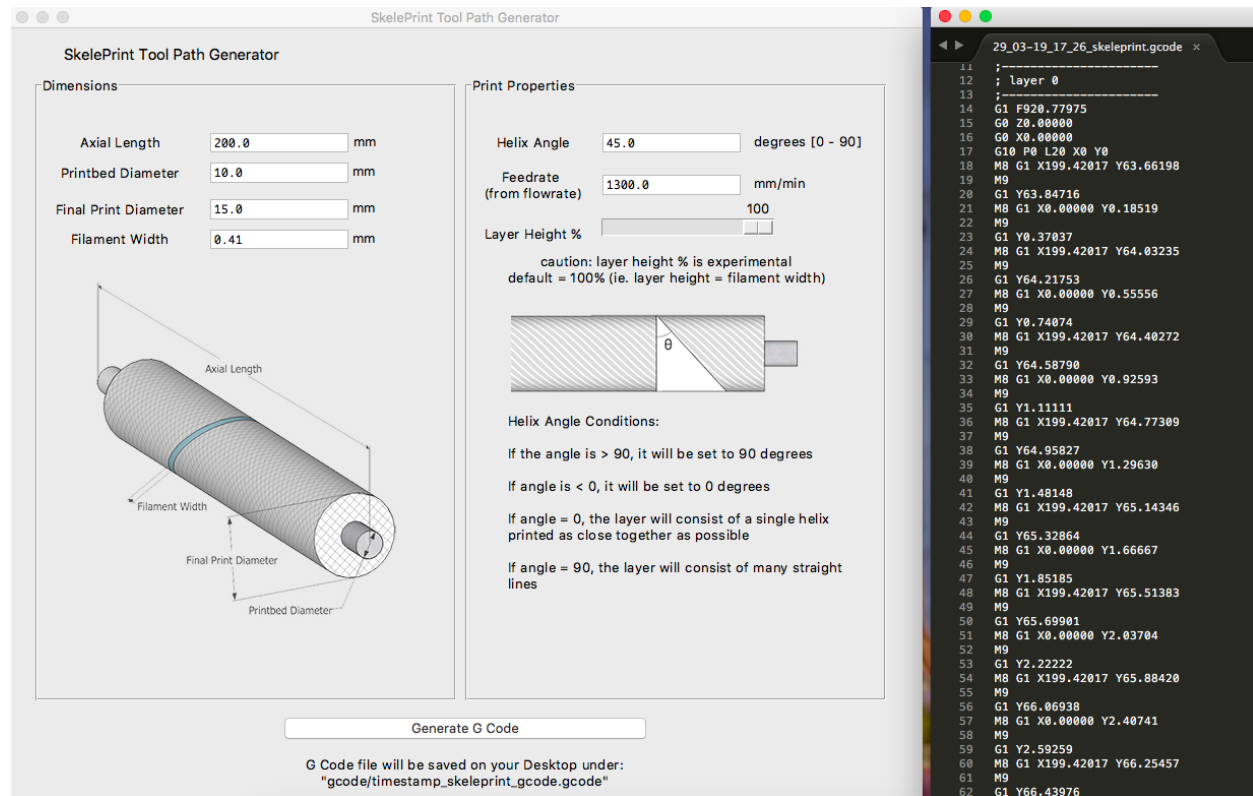


Figure 35: Graphical user interface for SkelePrint Tool Path Generator and generated G Code file.

The result is a G Code file containing the commands to produce the defined print.

## Tool Path Visualizer

Traditional 3D printing software allows users to visualize the component being printed to gain an understanding of what their printed component will look like once complete. 3D printing visualization software will often display a summary of the desired print including information on orientation, scale, dimensions, and print time of the component.

An interface was developed in MATLAB to help the user visualize the component they wish to create on the printer. This was done by coding an animated parametric helix that

is constructed in real-time to allow for the user to validate the print pattern. The helix's structure is based on the user's input parameters (e.g. filament width, print diameter, helix angle) so they have an idea of what their resulting printed component will look like. In addition, a plot of the overlapping filaments in consecutive layers is constructed to give the user a detailed overview of the microstructure that will be fabricated given their input parameters. Pictured below are the figures output by the MATLAB code.

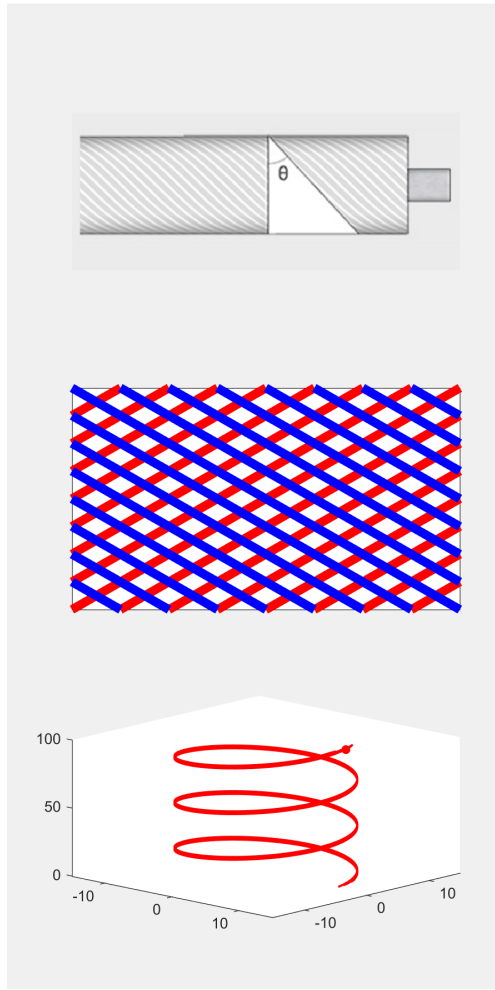


Figure 36: Plots produced by MATLAB visualization code.

The top plot reminds the user of where the helix angle is calculated. The middle plot shows the overlapping structure of consecutive print layers. The bottom plot visualizes the path that the printer takes to construct the component in near real-time. The MATLAB code also has the capability of outputting other parameter values to the user which have

been calculated by the the core algorithm, as described previously.

This visualization also serves as a means for validation of generated G Code identifying the expected behaviour of the SkelePrint 3D printer.

# 5

## Preliminary Experimentation Summary

### 5.1 Additive Lathe Prototype I

At the beginning of the project, the largest technical risk was behaviour of ink in printing. In particular, it was not clear whether or not the biomaterial would adhere to the mandrel or itself sufficiently well to print high layer-count parts. It was also not known whether it would be preferable to extrude round beads of the biomaterial, or place the extrusion head close to the print and smear the ink onto the mandrel in flat arcs.

To test each of these problems, we opted to make a low-fidelity prototype which had sufficient functionality to repeatably test the biomaterial's behaviour in printing. The prototype was constructed by placing a rotating mandrel inside a standard 3-axis Cartesian 3D printer. This set up can be seen in Figure 37. Our team opted to print using PLA filament as opposed to the actual biomaterial for the first round of testing to preserve supplies. PLA was chosen over ABS filament because we had no way of heating our print bed, which is necessary for ABS.

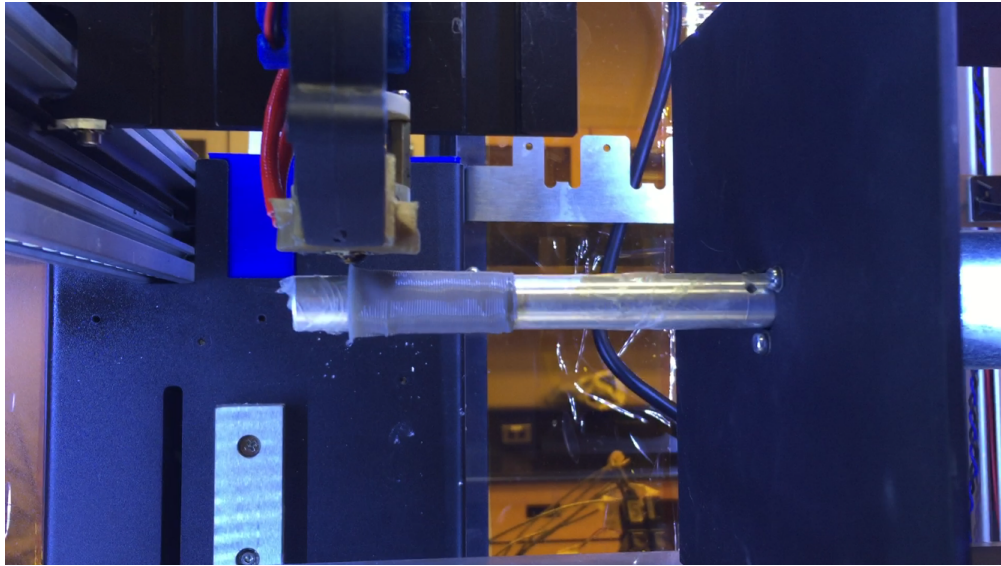


Figure 37: Additive Lathe Prototype 1 setup.

First, the mandrel was cut from half inch stock aluminum. It was press fit onto a DC motor that already had a control system integrated into it using a Maxon MR, 3-channel optical encoder and a 4x encoder counter. Applying a constant voltage was used to make the mandrel spin at a constant velocity.

Then, the mandrel and motor were mounted inside a HYREL 3-axis Cartesian 3D printer. The team first tested printing along the mandrel by just moving the extruder along the direction of the mandrel creating a line. Next, we printed a ring by only spinning the mandrel without moving the extruder. Next the team tried printing helices. This happened over many iterations with changes being made to the speed of rotation of the mandrel, speed of movement of the extruder in the axial axis, and flow rate of the PLA filament after each iteration.

## 5.2 Additive Lathe Prototype I Testing Results

Over the course of two lab sessions our team learned how to print helices on our low fidelity prototype with the best prints being four centimeters long and six layers high.

Figure 38 shows the progression of printing in the first lab session. After printing just a straight line along the mandrel and printing a ring around the mandrel, the rest of the time was spent printing helices of various shapes and sizes. The goal of the first lab session was to find the right printer movement speeds and optimal flow rate to print tight helices where each new ring would sit directly next to the last one. Moving from the left it can be seen how the helices become both more precise and tighter. The second last print can be seen as a solid cylinder where each consecutive ring in the helix touches the last one.

Figure 39 shows the four prints from printing session two. On the left is the first print from the day, using similar parameters to where we left off from day one. Moving to the next print, the speed of the extruder movements in the axial direction was reduced which brought the helices closer together.

Now at the middle right print, the extruder speed in the axial direction was further reduced which brought the helix pitch to the point where it was touching itself after one full revolution. This makes the print look like it is one continuous piece of material. However, since the movement of the mandrel and extruder were not synchronized and we were guessing



Figure 38: Results of first lab session with Additive Lathe Prototype 1.



Figure 39: Results of second lab session with Additive Lathe Prototype 1.

the parameter values, the helix pitch was actually a fraction smaller than one diameter width of material. This meant the material started printing on top of itself instead of the mandrel creating some wavy surfaces.

We wanted to remove the wavy surface errors so we increased the extruder speed again

which prevented the helix from printing on top of itself. The most right print uses this print speed and was allowed to print four more layers than the previous prints. Printing more layers removes some of the errors in extrusion, as seen by how straight the edges are on this print compared to the other three prints.

After completing testing using PLA plastic, we wanted to try printing with the actual biomaterial using our prototype. The process for printing is the same, with the exception that we needed the displacement extruder shown in Figure 3 to deposit the biomaterial onto our mandrel. Since the biomaterial does not solidify right after being deposited like plastic would, we were able to smear the ink as it was printing and get thin layer heights. The results of the print can be seen in Figure 40.



Figure 40: Result of first print using the biomaterial instead of plastic. Image taken as soon as print completed.

However, when the biomaterial dried it began to shrink as the water was removed from the material which initiated crack propagation. By the time the print had completed drying, it had almost fully fallen off the mandrel. The dried print can be seen in Figure 41.

This severe cracking should not happen in future revisions of the biomaterial because it is supposed to have much less water content. Also, this version of the ink did not have a UV curing agent. We believe that using the UV laser to cure the biomaterial at the time of deposition would reduce the probability of cracking.

Overall we are happy with the results of the first biomaterial print. The helices were printed in a clean fashion and we were able to achieve a good resolution for the size of extrusion tip we were using. Further experimentation with the biomaterial will wait until there is a new revision of the biomaterial ready for testing.



Figure 41: Result of first print using the biomaterial instead of plastic. Image taken as after print finished drying.

### 5.3 Controls Testing Apparatus

To test the firmware and software design, the team decided to build a small scale prototype which would allow testing of the axial, radial, and rotational axes. The prototype was built using LEGO parts which allowed the team to build and refine the prototype as needed. Connected to the LEGO were three NEMA-17, 200-step motors to control the movement the axes. The system diagram for the LEGO prototype is shown in Figure 42.

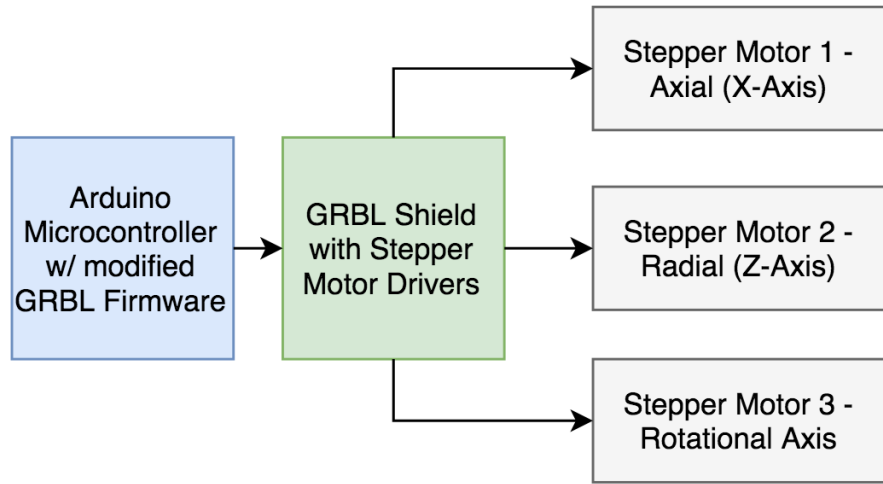


Figure 42: System diagram of LEGO prototype.

The extruder system was simulated using a pen cartridge which “prints” a helix on the rotational axis which was wrapped with masking tape allowing the pen ink to be deposited on the simulated mandrel. The LEGO prototype setup can be seen in Figure 43.

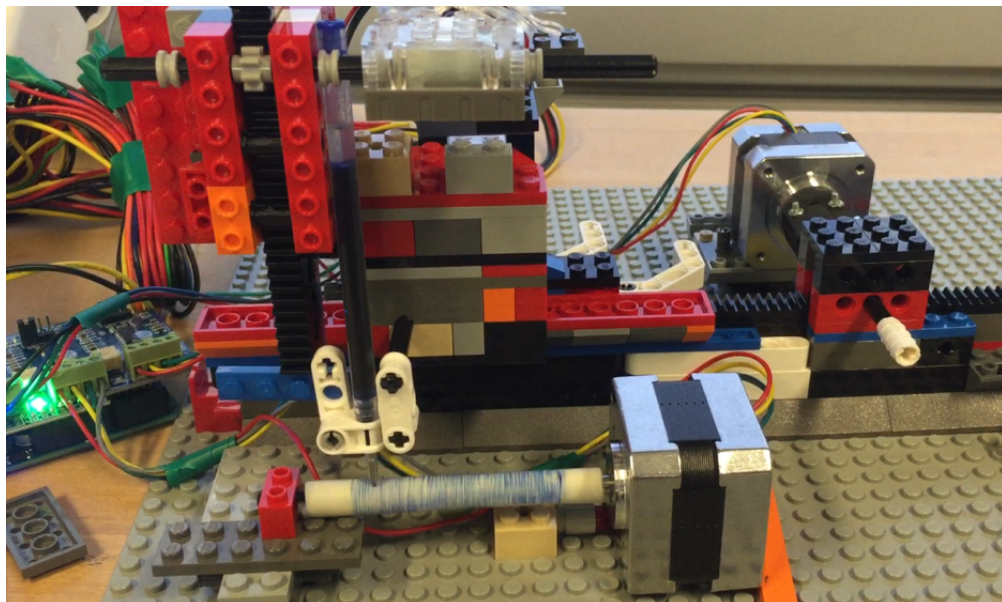


Figure 43: Controls testing LEGO prototype.

This prototype facilitated the testing and refinement of the GRBL firmware which helped

define the algorithm shown in Appendix A. The simulation of the extrusion system using the pen cartridge then validated the algorithm by allowing the group to visualize the helical layers and the expected composite structure. This test apparatus also ushered the refinement of the firmware to allow for an unbounded rotational axis. There were many important learnings from this test about hardware integration as well. For example, the group was able to identify the amount of current required to power each of the stepper motors in order to generate the required torque. This test also identified many issues and possible risks such as the overheating of motors, and positioning of wires. These insights helped refine the design specifications and develop risk mitigation plans.

## 5.4 Extrusion Testing Apparatus

The extrusion system was assembled according to Figure 24 and tested using multiple iterations of the biomaterial.

This initial test resulted in a number of problems which ultimately lead to the decision to replace the pressure regulator with a flow control valve, as seen in Figure 24. The regulator did not function well since the system's low flow rate puts the regulator in the "seat load drop" or "lockup" region of a pressure vs. flow plot seen in Figure 44.

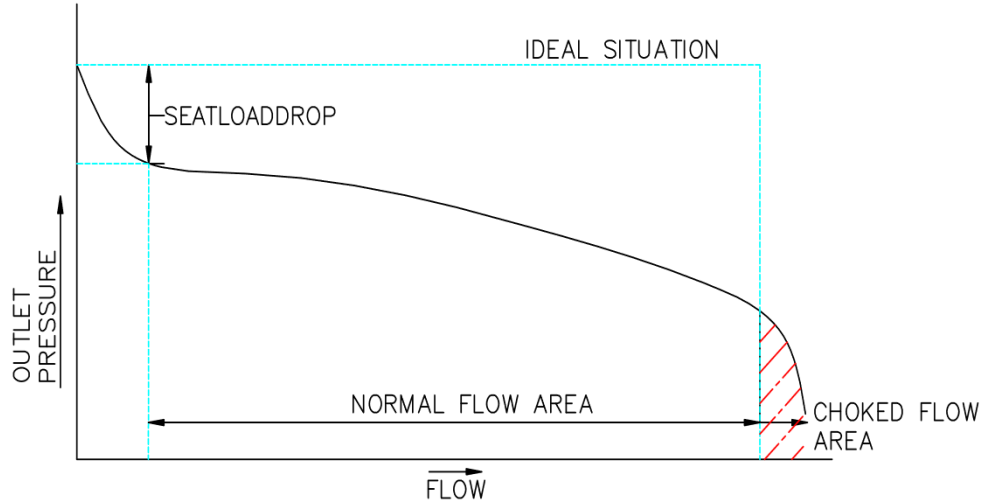


Figure 44: Typical regulator outlet pressure vs. flow curve. Figure from [17].

*Seat load drop* is the region of the curve where an increase in flow rate results in a

significant decrease in output pressure. Operating in this region is not ideal for our extrusion system.

Another apparent issue at this low pressure is the slow extrusion speed of the ink biomaterial, which inhibits a pressure differential initiated by the regulator. If there is  $20\text{psi}$  on either side of the regulator, and the regulator is then engaged, a  $0\text{psi}$  pressure differential will remain since the flow of ink out of the syringe is so slow. This was solved by swapping the pressure regulator with a flow control valve.

A second extrusion test was performed using high pressure air nozzle. This test was much more successful. Pressure was tested between  $70 - 90\text{psi}$  which resulted in consistent extrusion of the loaded ink through the syringe. The ink used was also dry and thick, much more than current iterations of the ink biomaterial, which suggests that the  $70 - 90\text{psi}$  range is much higher than we will need during our actual printing. A video of said extrusion test can be found in Appendix A.

Two new versions of the ink biomaterial created in the Willett lab, and they were tested unsuccessfully. One ink caused excessive clogging in the needle tip, even at gauge sizes up to  $0.8\text{mm}$ . Microparticles were collecting at the nozzle tip and halting the flow within seconds of applying pressure to the syringe. Another ink produced was sticky and difficult to handle which led unsuccessful prints.

Finally, a suitable ink was settled on. Extrusion tests were successful and numerous test components were produced. Below is an example of a print our team completed using our printer and the pneumatic extrusion system.

The ink in figure 45 flowed well, cured quickly, and allowed for numerous test prints to be completed. The extrusion system accurately controlled the pressure to allow for an appropriate flow rate of the ink through the nozzle tip.

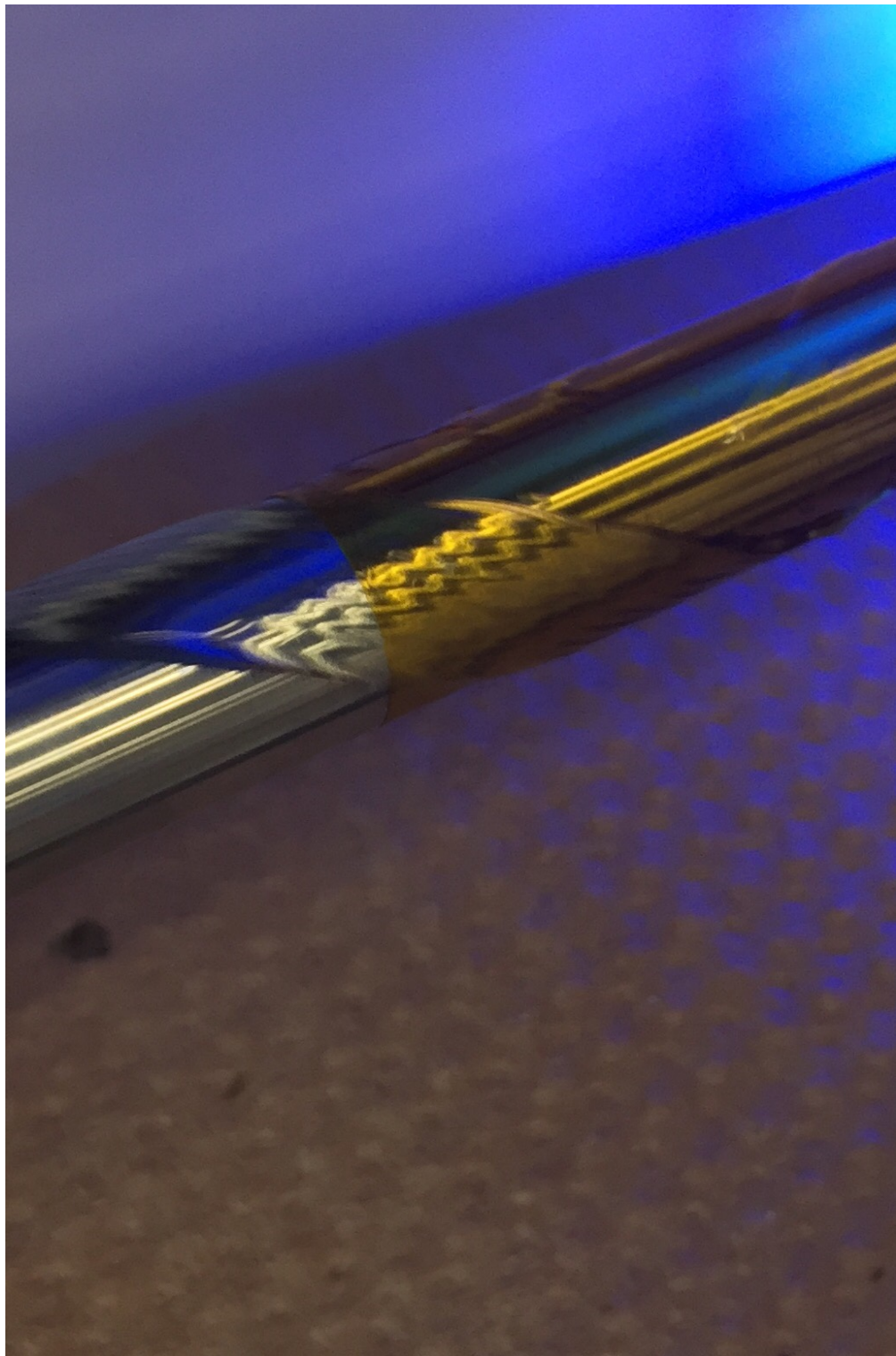


Figure 45: Example of a test print completed using a new iteration of the Willett Lab ink.

# 6

## Design Verification Summary

Since the start of the project, the SkelePrint team followed a simple methodology for defining specifications: “Don’t specify what you can’t verify.” Although the design specifications seen in Section 1.3 were generated based on the client’s needs, the specifications were also defined in a manner that can be easily verified.

As this project consists of many components, the design verification process involved engineering analysis, prototyping, and testing of the various sub-assemblies.

### 6.1 Mathematical Modelling and Analysis

Thus far, the actuators and moving components of the printer have been verified by consulting reference material on machine design, and by creating first principles dynamics models.

In particular, geometric models were developed to determine the resolution and absolute accuracy of the printer based on the actuators and motors selected. These are described in the Mechanical Design section and Appendix A. These models show that the printer will achieve its accuracy specifications.

Additionally, the motor sizings were verified by creating dynamics models based on the required print speed and the known physical properties of the printer’s moving components. These models are somewhat imprecise, because they neglect factors such as static friction, bearing friction and the effects of lubricant degradation. These effects were accommodated by simply multiplying the torque requirements by a factor of safety of two, and up-sizing the stepper motors accordingly.

The core algorithm for the SkelePrint Tool Path Generator was modelled mathematically using MATLAB to validate the helical properties of the print and the behaviour of axes. This mathematical model was then animated to serve as the tool path visualizer for users.

## 6.2 Prototyping and Testing

Initially, our prototyping effort has been restricted to creating low fidelity bone graft prototypes using a modified Cartesian 3D printer. These tests allowed us to verify our specifications for the extrusion system. Testing using the preliminary prototypes allowed for rapid iteration of final prototype design and validated assumptions.

The additive lathe prototype discussed in Section 5.1 identified many issues with the original frame design, and shed light on the challenge of print removal from the mandrel. The test provided insight into the precision requirements and the need for extrusion homogeneity which refined the design of the pneumatic extrusion system. This test also identified issues and risks within the firmware of the Hyrel 30M printer which were used to develop risk mitigation plans for the controls software. The inconsistencies in the prints from this test also identified the need for higher precision parts in the mechanical setup as well the need for closed-loop control of the printer for retroactive error correction. The inconsistencies in the hardware and software integration of the Hyrel 30M printer also led the team to develop a small-scale hardware prototype for firmware testing. The team understood that validation of the software was a function of its integration with the printer hardware, and thus decided to build a small-scale LEGO printer prototype.

Although the team had analyzed and developed the algorithm for printing the composite helical microstructure, it was difficult to validate the algorithm without the hardware. The additive lathe prototype showed the team that many unforeseen issues can be identified from a simple test. The use of the LEGO prototype allowed the team to not only validate the algorithm, it allowed for rapid iteration and testing of the modified GRBL firmware. This test also helped define some of the maintenance and calibration specifications as the team noticed a need for repeated calibration. The LEGO prototype helped the team visualize and validate the hardware limitations and output requirements.

Once the final prototype had been assembled, the team was able to validate the helical printing concept and test printing with the biomaterial. Initial tests with the biomaterial were not successful because the ink was not homogeneous enough to have an even flow through the nozzle. This led to clogging and uneven curing. Instead, the team used a

soybean oil with a UV curing agent in place of the biomaterial. This ink had a viscosity of thick honey which was much easier to control and the UV curing agent meant we could solidify the ink once it was on the print bed.

### 6.3 Verification of Design Specifications

The key specifications outlined in Section 1.3 were also verified through these methods.

#### Precision and Error Budget

Precision with respect to the full scale error and resolution specifications are addressed through an error budget.

The allocated error budget is a deterministic method to predict repeatable and non-repeatable errors. When error sources are identified they can be accounted for and sometimes reduced or controlled. Our error budget focuses on repeatable errors from mechanical aspects of the printer.

The basis of error budgets is that the total error in each direction (full scale error) is the sum of the individual components. As it is unlikely that all errors will occur simultaneously as well as in the same sign direction direct summing the values is not an accurate representation of constant error. The commonly accepted way to find the total error is using a vector norm where  $\rho$  varies dependent on the optimism of the estimate. Typically  $\rho = 1$  for a conservative estimate,  $\rho = 2$  for an optimistic estimate, or  $\rho = \sqrt{2}$  for a commonly used estimate in between [18].

$$e = \left[ \sum_{i=1}^n |e_i|^\rho \right]^{(1/\rho)}$$

	Axial	Radial	Rotational
Motor vibration	10	10	10
Linear motion actuation	50	35	N/A
Nut backlash	15	15	N/A
Motor coupling	2	N/A	N/A
Belt slip	N/A	N/A	10
Misalignment of centers	N/A	N/A	75
Specification	150	100	100
Sum	77	60	95
Vector norm	60.04	46.00	81.04

Figure 46: Full scale error budget in  $\mu m$ .

The printer error budget is calculated in microns,  $\mu m$ , and uses the value  $\rho = \sqrt{2}$  in the vector norm calculation. The expected errors in the chart are drawn from part specifications and also include estimations for the motor vibration and misalignment. The error totals per axis are within the desired specifications.

Some sources of error were not included in the budget as their magnitude was likely negligible comparable to the main sources of error. This may include bearing misalignment, the impact of temperature on the materials, non-straightness of motion actuation, and many other possible small errors.

Currently it is unlikely that the limiting factor on the accuracy of printing is due to mechanical error and can more likely be attributed to the variability of the flow and extrusion of the ink. If at some point in the future the mechanical error in the printer needs to be more specifically quantified the use of parametric error mapping can be employed through a series of one dimensional tests intended to identify systemic errors. These tests are also often called volumetric error mapping and focus on measuring and recording positional and angular errors with the goal of physically correcting or compensating for them. The Precision Controls Lab at uWaterloo graciously offered their equipment for this purpose but more pressing priorities to getting the printer functional took precedence.

The resolution accuracy specifications were addressed in the selection of motion actuators

and motors in their respective sections have a lower variability of error compared to the full scale error calculations.

While accuracy specifications played an important part in the design of the printer and selection of mechanisms it is not the key functional specification to the success of the project. Error reduction techniques like using elastic averaging (connecting two objects through multiple contact points to create a highly constrained connection, as seen in the motor coupling, the ball nut in contact with the ball screw, and angular-contact thrust bearings) as well symmetry principles in the mechanisms helps the printer reduce the magnitude of mechanical errors.

## Closed Loop Control

The implementation of positional closed loop control of all three axis was done through the implementation of the Mechaduino motion control platform. Through analysis of the system response the team was able to verify the successful implementation of PID controllers and its application for positional error correction. Manual testing was also done to validate the requirement of positional error correction.

## Safety

To ensure that the printer met all safety specifications, the team enlisted the help of Chris McClellan who verified the printer's power supply and wiring. The power supply meets the safety rating of Underwriter Labs (UL) certification. Wires used to send power to the printer were all high tensile strength, flexible cables with CSA approval. Strain relief for wires was implemented with cable clamps and zip-ties to minimize the risk of disconnected wires.

The client has agreed to meet the University of Waterloo lab safety requirements when operating the UV Laser along with the printer. This includes building an enclosure that provides UV protection around the printer or providing safety glasses for the users of the printer.

## Design Project Management Summary

todo[inline] Review of changes to the design project plan with justifications for changes made and/or proposed

The project plan was affected by the possible budget available to us. At the beginning of the project our team was given \$1,000 from Professor Willett's research lab for the project. Since then, though, we applied for and were awarded \$4,000 in extra funding from the Engineer of the Future Trust and \$5,000 from the Baylis Medical Capstone Design Award. This brought our total funding to \$10,000. Having the additional funds changed allowed us to build a more precise and better quality high fidelity prototype.

Our plan for the second semester of the project involved having the final prototype assembled by reading week so that we could come back from the break with momentum and get started on testing. Unfortunately there were quite a few parts back ordered or ordered incorrectly so we were still waiting on key parts when reading week began. By the time we returned from the break we were able to assemble the final prototype and begin our testing and validation.

Our schedule and work breakdown structure are detailed in Appendix B. Work completion percentages have been added to reflect our current progress. At the end of this term, we have completely finished all scoped work to be done on the project. There are still some errors to be fixed in the software of the printer, but the current state of the printer allows our client to begin testing of the biomaterial. At the time of submitting this report, we have completed all deliverables for GENE 404 with the exception of Teamwork Assessment 4 which will be completed after our panel exam. The SYDE team members have also submitted all deliverables towards SYDE 462.

# 8

## Next Steps

### 8.1 Mechanical Design

There are a few parts that need to be redesigned to improve the functionality of the printer. The hole for the syringe in the block on the radial axis is too tight. The hole was toleranced incorrectly when sending it to the machine shop, and due to the notch in the block we were unable to re-machine it. This block should be machined again with proper tolerances such that the syringe has no issues with insertion or removal. Another solution would be to find a new way of mounting the syringe to the block, rather than having it be one mechanism.

A new solution to aligning the print bed with the axial axis needs to be designed. Currently we are just using a square to align the bearings on either end of the rotational axis. The floating end of the rotational axis needs to be disassembled each time the print bed is to be removed. Designing a method that maintains a parallel print bed and axial axis while not needing to disassemble the rotational axis is desired.

The belt that connects the two pulleys in the rotational axis transmission system is a little loose. A shorter belt could be ordered to increase the tension in the system. Alternatively, the slots on the motor mounting bracket could be milled out to increase the separation between the rotational axis motor and the print bed.

Since we have not used the true biomaterial in any of our testing, we do not know how easily the parts can be removed. The soybean based ink had to be cut off using a razor because it adhered to the mandrel quite well. This is obviously not ideal, but printing the biomaterial on Kapton tape or saran wrap should improve the process.

### 8.2 Electronics Design

During our testing, we may have damaged the Mechaduino for the axial axis. We were able to remove the issue without affecting the performance of the board. It is highly recommended that the lab place an order for new Mechaduino PCBs as they are often back ordered.

## **8.3 Control System Design**

The controls system is one of the best designed and robust aspects of the printer. Modifications to the mechanical assembly require re-tuning of PID controller in order to ensure smooth operation of the printer. Currently the maximum acceleration for each of the axes is set conservatively. Testing should be conducted to identify maximum rates of acceleration.

## **8.4 Software Design**

The current algorithm is limited to producing tool paths for cylindrical geometries as complex geometries were considered out of scope for this project. Next steps include developing a slicer which can generate G Code for non-cylindrical geometries. We began working on modifying an existing open-source slicer software to determine changes in the radius and generate G Code for printing a section of a human femur from a CAT Scan.

The slicer was broken down in an effort to understand which components of the code could be modified to construct a slicer for cylindrical geometry in the future. This information can be found in Appendix A.

## **8.5 Extrusion System Design**

The flow control valve should be replaced with an appropriate pressure regulator. The flow control valve currently has the capability of precisely changing the pressure in the system. However, if there is a blockage in the syringe tip, this will result in a pressure build up throughout the entire system. This is not desirable, since a pressure build in the syringe can cause the ink to violently extrude and ruin the component being printed on the mandrel. Alternatively, a pressure regulator will maintain a constant pressure throughout the system. This would avoid any of the said problems if there is a blockage in the syringe.

## **8.6 Biomaterial Properties Testing**

Future use of the printer will consist of printing structures using the next iteration of the biomaterial and testing the mechanical properties. The lab will continue to improve the

biomaterial to a state where it can be extruded in a continuous manner. Once extrusion is working properly, the lab will experiment with the parameters in the user interface (ie. angle, flow rate, resolution) to create the strongest print possible.

## Appendix A: Engineering Data

The system level diagram of this design contains three main components: mechanical, extrusion, and controls. Mechanical describes the three axes of movement of the printer, extrusion describes the method of extruding the ink onto the print bed, and controls describes the hardware and firmware required to run the printer. A system level diagram is shown in Figure 47

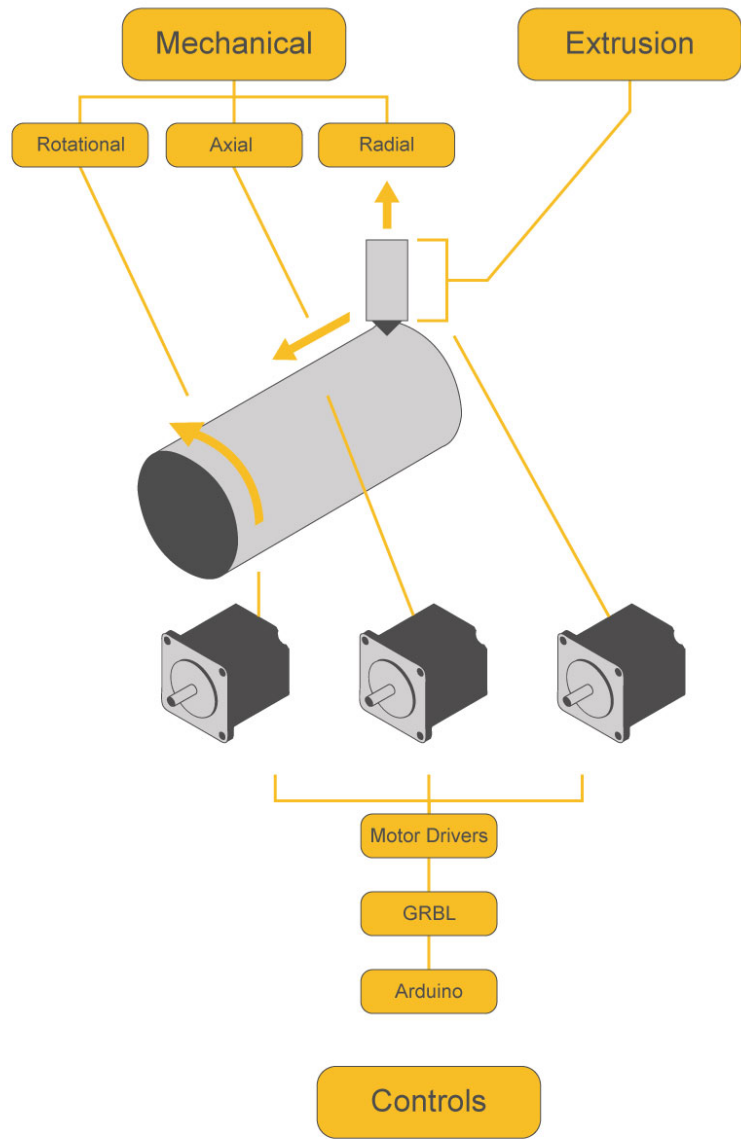


Figure 47: System level diagram of our printer design.

## Design Specifications

Our team's detailed design specification can be found on the following four pages. This specification clearly details the team's key specifications, the target we are aiming to achieve for each one, and how we plan to verify each specification.

The document is divided into functional requirements detailing the actions the printer must perform, non-functional requirements detailing desired qualities we want our printer to have, and constraint requirements that describe boundary conditions on our problem space.

**Title:** Skeleprint Bone Graft 3D Printer

**Number:** SP-004

**Revision Level:** A

**Originator:** Alex Upenieks, Isaac Hunter, Josh Bradshaw, Kyla Gardner, Matt Jones, Shubh Jagani

Date: Nov 24, 2016

Intended application: This printer is intended for use in Professor Thomas Willett's laboratory, which is a clean, climate controlled environment. The design must be safe and usable by lab technicians, who may choose to leave it running overnight unsupervised.

No	Characteristic	Relation	Value	Units	Verification Method	Comments
	<b>Real Need</b>					
-	Deposit Biocompatible Material					
-	Control Bone Graft Microstructure					
	<b>Functional Requirements</b>					
1	Usable Print Volume Length (absolute minimum is 1.5x the diameter of the bone graft [6x1.5=9cm])	>	20	cm	Analysis	Adult human femur length (maximum possible graft size)
2	Usable Print Volume Radius	>	3	cm	Analysis	Adult human femur radius (maximum possible graft size)
3	Extrusion Bead Diameter	<	170	microns	Analysis	Required by client
4	Extrusion Homogeneity (consistency of bead cross sectional diameter)	+/-	10%	Of bead diameter	Analysis	Required by client
5	Print Bed Diameter	<	1.5	cm	Measurement	Specified by client
6	Print Speed	>	4	mm/s	Test	Based on extruder's minimum speed (may be subject to revision)

7	Maximum Print weight	=	1	kg		Based on density of bone
8	Radial Resolution (layer height)	<	25	microns	Analysis	
9	Radial Full Scale Error	<	150	microns	Analysis	
10	Axial Resolution	<	25	microns	Analysis	
11	Axial Full Scale Error	<	100	microns	Analysis	
12	Rotation Resolution	<	100	microns of arc length	Analysis	At maximum radius of 35mm
13	Rotational Full Scale Error	<	200	Microns of arc length	Analysis	
14	Extrusion Capacity	>	60	cm^3	Measurement	
15	Rotational Steady State Error of the Motors	=	0	Step counts	Analysis	Printer should detect and rotational errors immediately after a step. No step loss.
	<b>Non-functional Requirements</b>					
16	Power	=	120	VAC	Test	
17	Capable of producing freeform structures				Analysis	Required by client
18	Service Period	>	250	hr	Analysis	Hours of printing between required servicing in which the printer meets its accuracy requirements.
19	Reliability	>	24	hr	Test	Hours of continuous printing. (Required by client)
20	Maintainability/Serviceability				Analysis	

21	Easy to setup	<	30	min	User Testing	
22	Long life	>	2	years	Analysis	The design must be made fault tolerant and maintainable so that the printer can not destroy itself by crashing.
23	Mechanically safe to set up				Analysis	No exposed pinch hazards, positive shut-off on any heating elements. Proper protection for any pressure vessels.
24	Material		Hydroxyapatite-based biomaterial			
25	Surface Finish		Smooth		Client inspection	
26	Quiet Operation	<	60dB			Scientists will have to work in the same room.
	<b>Constraint Requirements</b>					
27	Safe Operation				Analysis	
28	Human Machine Interface				Demonstrate	
29	Cost	<	\$10000		Analysis	
30	Reasonably Compact	<	50cm x 50cm x 50cm			Must not consume too much valuable lab bench space.
31	Quiet Operation	<	60dB			Scientists will have to work in the same room.

32	Electrically safe in electrical and mechanical failure conditions					Electrical insulation and isolation in compliance with Underwriters Laboratories standards for similar appliances.
33	Does not damage print when mandrel is removed				Test	
34	Prints cylindrical structures composed of helices				Analysis	
35	Compatible with the current generation of ink produced by Thomas Willett's biomaterials lab				Analysis	
36	UV Laser enclosure must comply to ANSI Z136				Analysis	UV opaque enclosure, auto shutoff door

## Motor Sizing Calculations

For the horizontal ball screw:

$$T_{bs} = T_a + T_l = I_G \times \alpha + \left( \frac{FP_B}{2\pi\eta} + \frac{\mu_o F_o P_B}{2\pi} \right) \frac{1}{i} \quad (2)$$

For  $T_a = M = I_G \times \alpha$  where  $I$  is the moment of inertia and  $\alpha$  is angular acceleration. Angular acceleration is selected as  $\alpha = 100 \frac{rad}{s^2}$  based on the value determined by the Imperial College of London as an appropriate magnitude [8]. The calculation for moment of inertia  $I$  is estimated by adding the components of the assembly as approximate moments of inertia, such as equating a gantry to a rectangle and a ball screw to a cylinder. This assembly is similar to that of the Imperial College group so  $I_G = 4.97 \times 10^{-3} kg * m^2 \approx 0.5 kg * m^2$  [8].

$$T_a = 0.005 kg * m^2 * 100 \frac{rad}{s^2} = 0.5 Nm$$

$$T_l = \left( \frac{FP_B}{2\pi\eta} + \frac{\mu_o F_o P_B}{2\pi} \right) \frac{1}{i}$$

Where the force  $F$  is comprised of external forces and friction  $F = F_E + f$ . The ball screw will be horizontal so  $\theta = 0$ .

$$F = 0 + mg\mu \cos\theta = 0.75 kg \times 9.81 \frac{m^2}{s} \times 0.01 = 0.0735 N$$

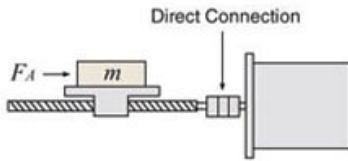


Figure 48: Ballscrew free body diagram from Oriental Motor [19]

Other variables for calculating the load torque include  $\eta$ , the efficiency,  $\eta = 0.80$ ,  $P_B$  is the lead on the ball screw,  $P_B = 0.01 m$ ,  $i$  is the gear ratio,  $i = 1$ ,  $\mu = 0.01$  is the coefficient of friction and  $\mu_o = 0.1$  is the static coefficient of friction that must be overcome to start

movement, as stated in the Hiwin ballscrews technical information index. [20]

$$T_l = \left[ \frac{0.0735(0.01)}{2\pi(0.80)} + \frac{0.1(\frac{1}{3})0.0735(0.01)}{2\pi} \right] \frac{1}{1} = 1.499 \times 10^{-3} Nm$$

Summing the results of  $T_a$  and  $T_l$  gives

$$T = 0.5Nm + 1.499 \times 10^{-4} \approx 0.5Nm.$$

This indicates a motor with a rating of  $0.5Nm$  will be suitable for the ball screw application. It can be noted that due to the high efficiency and low coefficient of friction of the ball screw the load torque is low.

The radial axis has a similar calculation, the main differences are a lower moment of inertia and that the screw will bear the weight of the extrusion system,  $m \approx 0.75kg$ , and the efficiency of a lead screw is lower at  $\eta = 0.4$ . As a result  $F = F_E + f = mg + mg\mu\sin\theta = 0.75kg \times 9.81\frac{m^2}{s} \times (1 + 0.01) = 7.43N$ . Calculating the new  $T_a$  and  $T_l$ :

$$T_a = 0.001kg * m^2 * 100 \frac{rad}{s} = 0.1Nm$$

$$T_l = \left[ \frac{7.43(0.01)}{2\pi(0.4)} + \frac{0.1(\frac{1}{3})7.43(0.01)}{2\pi} \right] \frac{1}{1} = 26.89 \times 10^{-3} Nm$$

Summing the results of  $T_a$  and  $T_l$  gives

$$T = 0.1 + 0.0264 = 0.126Nm.$$

As a factor of safety a slightly bigger motor should be used but this axis does not run constantly so it does not need as large of a safety factor. Adding more weight to the extrusion system could be cause for a higher torque motor.

The rotational axis has primarily the same calculation as the ball screw, but is not driving a load so only the  $T_a$  component is needed. This gives  $T_{rot} = 0.5Nm$ . Due to the use of the belt drive the rotational motor will not need as large of a factor of safety as the axial axis.

## Print weight

The weight of a fully printed bone graft can be calculated using the density of the biomaterial and the expected volume of the print. Where the density  $\rho = 1680 \frac{kg}{m^3}$ ,  $R$  is the maximum print radius, and  $r$  is the mandrel radius.

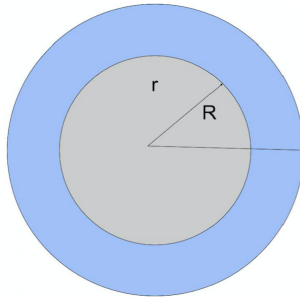


Figure 49: Print and mandrel radii

$$V_{print} = \pi(R - r)^2 h = \pi(0.03 - 0.0075)^2 0.25 = 3.976 \times 10^{-4} m^3$$

$$m_{print} = \rho V_{print} = 1680 \frac{kg}{m^3} \times 3.976 \times 10^{-4} m^3 = 0.668 kg$$

## Tool Path Generator Algorithm

In cylindrical layers, each layer is deposited as a helical coil, as illustrated in Figure 50. The coil can either be a single fluted coil, or a multi-fluted coil. The number of coil flutes is given by the parameter  $k$  as shown in Figure 51. The code refers to a flute as a start point.

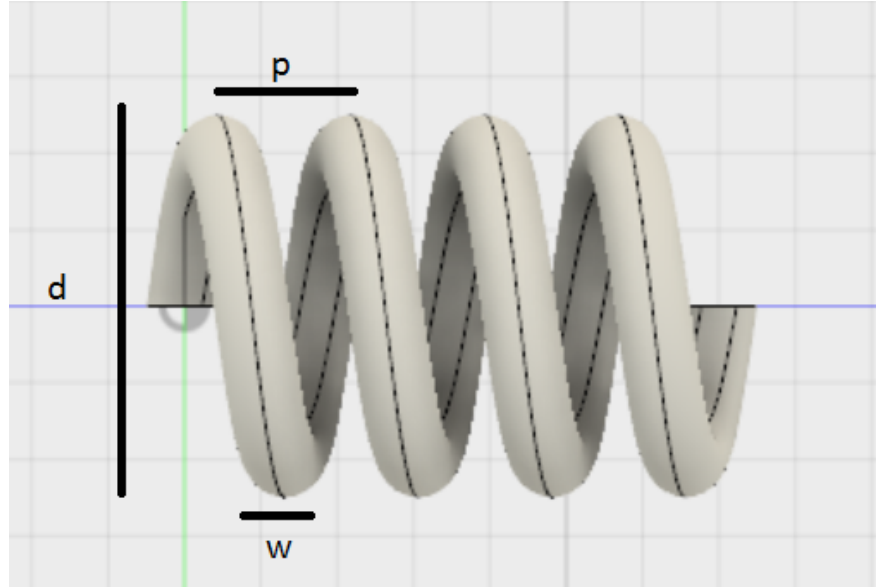


Figure 50: Pitch and diameter of the windings.

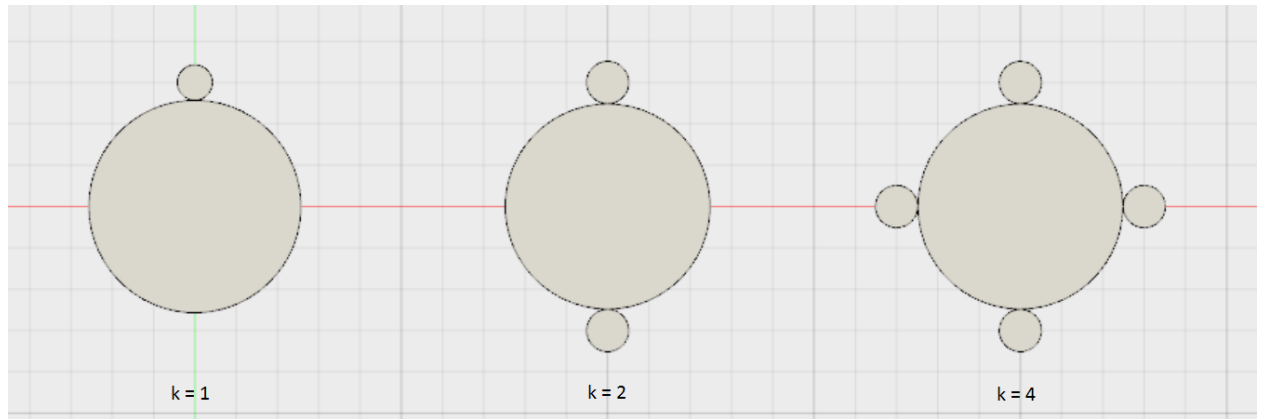


Figure 51: Start locations of multi-flute coils.

After the helix angle  $\theta$  has been set, the axial travel required per revolution ( $x_r$ ) is calculated by:

$$x_r = \pi d * \tan(\theta) \quad (3)$$

The filament width ( $w_{fo}$ ) is originally defined by user, and needs to be updated to represent the width of the filament based on the helix angle

$$w_f = \frac{w_{fo}}{\tan(\theta)} \quad (4)$$

$$n = \frac{x_r}{w_f} \quad (5)$$

Where  $d$  equals the layer diameter,  $w_f$  the updated filament width and  $n$  equals the number of start points. The axial travel per revolution is used to determine how many revolutions of the print bed are required in the traversal of the axial travel.

$$y = \frac{x_t}{x_r} \quad (6)$$

$x_t$  equals to total axial length of the print and  $y$  represents the number of rotations of the rotational axis. These values are used to generate the path for each flute or start point of the helix. The generated G Code now commands the rotational axis to complete  $y$  rotations in the same time as it take to travel  $x_t$  in the axial direction.

The key parameter is the helix angle. As layers increase the diameter is modified, which increases the number of start points in order to maintain the same helix angle at each subsequent layer. Thus, the helix pitch and angle depend on the number of start points in the cylindrical layer and the diameter of the layer. The coil angle will slightly decrease with each successive layer.

### Feed Rate and Tangential Velocity Calculations

The feed rate is equal to the speed of movement of all axes based on flow rate of the extrusion system. Having a precise feed rate is important because it is needed to be able to print the exact helix structure defined in the user interface. The feed rate can be calculated in the lab as follows:

$$\text{flowrate} = mL/s = cm^3/s$$

$$A_x = mm^2$$

Where  $A_x$  equals the cross sectional area of the nozzle.

$$s = \text{flowrate}/A_x = \text{mm/s} * 60 = \text{mm/min}$$

Where  $s$  equals the linear feed rate. When this value is input into the GUI the algorithm uses it to calculate the tangential velocity using the following algorithm:

$$\text{arclength} = (\pi * d) / \cos(\theta)$$

$$t = \text{arclength} / \text{feedrate}$$

$$w = (2 * \pi) / t$$

$$v_t = w * (d/2)$$

Where  $d$  is the diameter of the current layer,  $\theta$  is the angle being printed,  $t$  is time,  $w$  is the angular velocity, and  $v_t$  is the tangential velocity. This calculation sets the tangential velocity of the rotating print bed to match the flow rate of the biomaterial such that the biomaterial can adhere to the print bed nicely.

## Code

The complete repository for the SkelePrint Tool Path Generator can be found on GitHub.

The MATLAB code has been provided to the lab.

## Belt Length Calculation

The length of the pulley depends on the line tangent to both circles  $h$ , which can be determined by geometry.

$$h = \sqrt{c^2 - (r_1 - r_2)^2}$$

The angle  $\alpha$  can then be obtained using the right angled triangle:

$$\alpha = \cos^{-1}\left(\frac{r_1 - r_2}{c}\right)$$

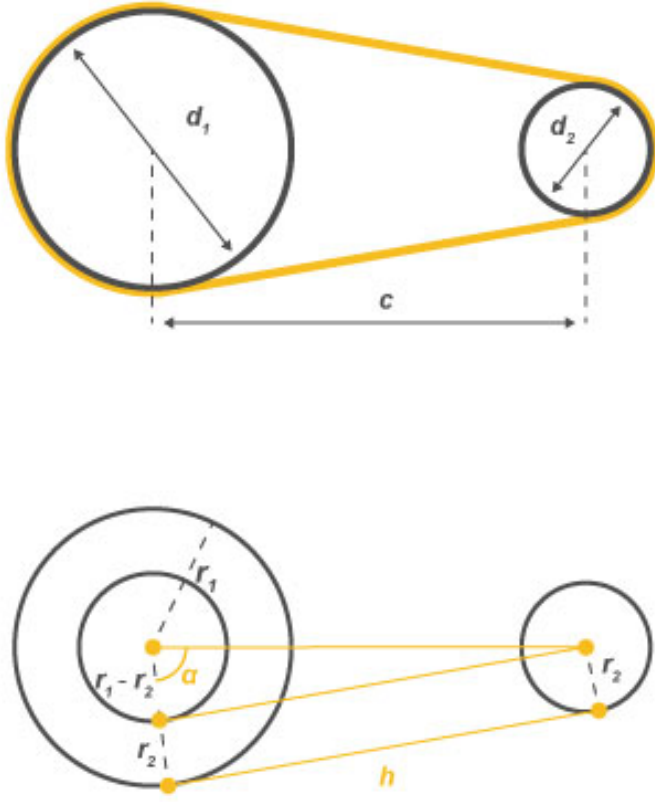


Figure 52: Schematic diagram of the pulley reduction assembly to measure required timing belt length.

The timing belt length  $l$  can be obtained by summing the length on the small pulley, the length on the large pulley and two times the distance between the pulleys  $h$ .

$$l = 2\alpha r_2 + 2(\pi - \alpha)r_1 + 2h$$

For our final prototype the pitch diameters of the two pulleys were  $d_1 = 45.84mm$  and  $d_2 = 16.55mm$  with a distance of  $c = 70mm$  between the two pulleys. Plugging this into the equations above we find that  $h = 68.46mm$  and  $\alpha = 1.36radians$ . This resulted in a final required length of  $l = 241.1mm$ .

This calculation was implemented as the MATLAB script shown in Figure 53 so that revisions to the rotational axis could quickly be verified to ensure that they would be compatible

with commercially available belt lengths.

```
r1 = 45.84/2; % P.D. of big pulley is 45.84 mm
r2 = 16.55/2; % P.D. of small pulley is 16.55 mm

x = 70;          % x distance between pulleys is 70 mm
y = 0.95;        % y distance between pulleys is 0.95 mm

c = sqrt(x^2 + y^2);

h = sqrt(c^2 - (r1 - r2)^2);

alpha = acos((r1 - r2)/c);

l = 2*alpha*r2 + 2*(pi-alpha)*r1 + 2*h;
```

Figure 53: Matlab code for calculating the required belt length based on the pulley radius, and the vertical and horizontal distance between the pulleys.

## Extruder Pressure Requirement Calculation

Matlab code based on the Herschel-Bulkley model was developed to predict the pressure required to extrude the biomaterial. The Herschel-Bulkley model is a rheological equation typically used in the food processing industry to predict the flow profile of colloidal fluids. [21]

$$\tau = \tau_o + k\dot{y}^n \quad (7)$$

$\tau$  is the stress applied to the fluid,  $\tau_y$  is the yield stress of the fluid,  $k$  is the consistency index of the fluid,  $\dot{y}$  is the shear rate of the fluid, and  $n$  is the flow index of the fluid.

Equation 7 can be combined with

$$\tau = \frac{r}{2} \frac{dP}{dL} \quad (8)$$

and

$$\tau_o = \frac{R_c}{2} \frac{dP}{dL} \quad (9)$$

to give:

$$\frac{r}{2} \frac{dP}{dL} = \frac{R_c}{2} \frac{dP}{dL} + k \frac{dv^n}{dr}. \quad (10)$$

Equation 10 can be integrated and rearranged to yield the velocity profile of a Herschel-Bulkley fluid travelling through a cylindrical tube. [22]

$$v(r) = -\frac{1}{2k} \frac{dP^{\frac{1}{n}}}{dL} \frac{n}{n+1} [(R - R_c)^{\frac{1}{n+1}} - (r - R_c)^{\frac{1}{n+1}}] \quad (11)$$

Where  $R_c$  is the plug flow radius,  $dP$  is the pressure differential,  $dL$  is the length of the tube. This equation for the velocity profile can easily be plotted in Matlab.

Furthermore, the volumetric flow rate of the ink can be evaluated by integrating over the plug radius and the laminar shell. [22]

$$Q = \int_{R_c}^R v dv + \int_0^{R_c} v dv \quad (12)$$

Upon integration of equation 12, the following equation for volumetric flow rate is produced. [22]

$$Q = \frac{8\pi^{\frac{1}{n}}}{k} \left( \frac{L}{dP} \right)^3 \left( \frac{RdP}{2dL} - \tau_o \right)^{1+\frac{1}{n}} \left[ \frac{\left( \frac{RdP}{2dL} - \tau_o \right)^2}{3 + \frac{1}{n}} + \frac{2\tau_o \left( \frac{RdP}{2dL} - \tau_o \right)}{2 + \frac{1}{n}} + \frac{\tau_o^2}{1 + \frac{1}{n}} \right] \quad (13)$$

If input pressure is unknown, the Matlab "fzero" function can be used with equation 21 to determine  $dP$  for a specified volumetric flow rate.

## Slic3r Software Breakdown

To tackle the problem of printing non-cylindrical geometries the team analyzed a popular open source 3D slicer, Slic3r.

The source code for Slic3r was analysed so individuals in the future will have an easier time modifying it for non-cylindrical geometry.

**polypartition:** This file takes a cross section of the 3D CAD file, and constructs triangles in the cross sectional area. This is called "triangulation" which means that triangles are used to determine the distances and relative positions of points spread over a particular area. Users looking to develop a new slicer for cylindrical geometry should start with modifying this file. Recommendations include:

- Testing points in an arbitrary line from origin. The origin would be center of the mandrel placement.
- For each point call TPPLPartition:IsInside(). This returns a Boolean value for an individual point indicating whether this point is in a specified triangle.
- Users looking to modify this code should develop a simple bisection algorithm which will take the center point of the cross section and a point outside the cross section.
- Points in the outer circumference of an arbitrary circle should be checked to see if they are inside or outside a triangle using the TPPLPartition:IsInside() file.
- Once a critical point has been found that signifies a point is outside the cross section of the object (i.e. outside a triangle inside the cross section), this distance should be saved.
- This distance denotes the diameter of a perfect cylinder that could fit in an irregularly sized bone.
- This method can be built upon to 3D print irregular geometries in the future.

## Video Demonstrations

A YouTube video demonstrating our pneumatic extrusion technique can be found at the following URL: <https://www.youtube.com/watch?v=b1FNGlH-Jkg>. A thumbnail of the video can be seen in Figure 54.

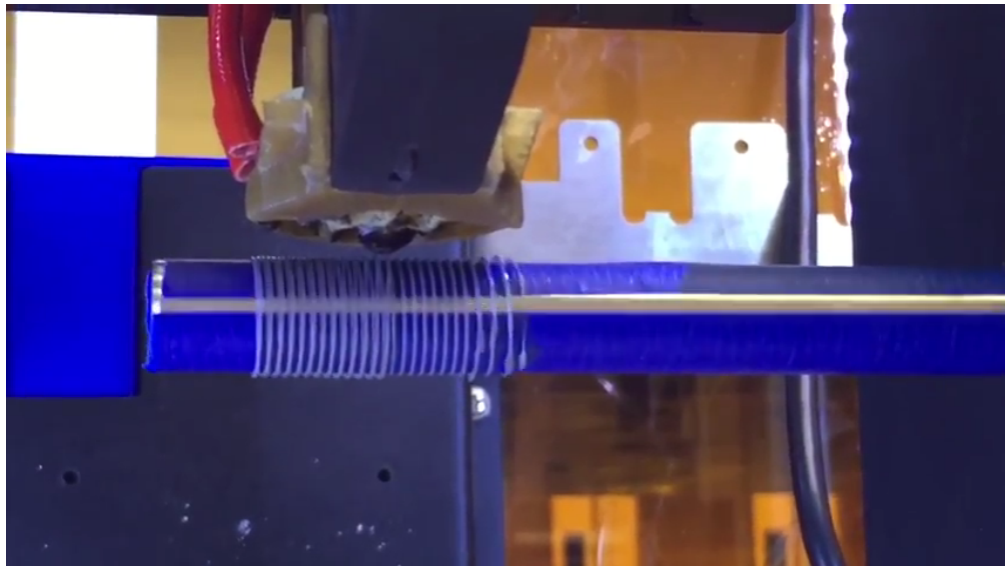


Figure 54: YouTube Video of low fidelity prototype demonstration.

A YouTube video demonstrating our pneumatic extrusion technique can be found at the following URL: <https://www.youtube.com/watch?v=-qkTdwZNFFg>. A thumbnail of the video can be seen in Figure 55.



Figure 55: YouTube Video of extrusion demonstration.

A YouTube video demonstrating the final prototype of the SkelePrint 3D Printer printing biomaterial at a helix angle of 60 degrees while UV curing: <https://www.youtube.com/watch?v=xaBsvowsy>

A thumbnail of the video can be seen in Figure 56.



Figure 56: YouTube Video of final prototype demonstration.

# Appendix B: Project Management Data

## Project Schedule and Work Breakdown Structure

Figure 57 shows the planned work budget in blue in comparison with the actual work budget in red for the entire length of the project. Focusing on the second semester of the project, our contingency that was budgeted at the beginning of the project started after reading week as seen by the many weeks with few “planned work hours”. We wanted to front load the second semester as seen by weeks 15 - 20 that have many more hours worked than planned. Much of our testing and validation came after reading week, which is shown by four consecutive weeks of many worked hours during our contingency period.



Figure 57: Comparison chart for planned work hours (blue) vs actual work hours (red) across the entire project.

Overall, we scoped out approximately 785 hours of work for the team but we recorded approximately 1223 actual hours worked. We likely worked more hours than the number recorded, as it is difficult to track the exact number of hours when the priority of our project is so high. Even though we had to put in a lot of hours during our contingency time, we

were able to complete the project to a degree that satisfied our client.

An updated project schedule and work breakdown structure is shown on the following two pages.

Schedule and WBS													13 51 42 48						
			Week		PRE	1	2	3	4	5	6	7	8	9	10	11	12	13 51 42 48	
						13	23	12	89	49		16	37	49	25	13	49	13 51 42 48	
						42	42	42	42	42		42	42	42	42	42	42	13 51 42 48	
						105	32	79	43	95	45	15	42	10	23	15	39	70	13 51 42 48
<b>Design Project Objective (Total Scope)</b>	785		Hours	% Work Complete	Person	Finish Date													
Need Analysis	40	<b>100</b>																	
Research	24	100					30	12	12										
Real need	1	100										1							
Functional analysis	6	100						15					6						
Generate design specification	5	100											5						
Revise	4	100											4						
<b>Project Planning</b>	32	<b>100</b>																	
Lessons-learned	2	100											2						
Project objective	1	100											1						
WBS	8	100											8						
Schedule	7	100											7						
Resource assignments	7	100											7						
Risk register	7	100											7						
<b>Conceptual/Preliminary Design Phase</b>	112	<b>100</b>						20					10	18	12				
Generate ideas	40	100																	
Develop ideas	24	100						10											
Evaluate and Select	42	100																	
Revise	6	100													24	30	6		
<b>Embodiment Design Phase</b>	84	<b>100</b>																	
Generate embodiments	42	100																	
Verification by analysis	42	100																	
<b>Procure, Build and Test</b>	238	<b>100</b>																	
Procure parts	40	100																	
Build	60	100																	
Initial testing	48	100																	
Verification by test	90	100																	
<b>Data and Documentation</b>	100	<b>100</b>																	
Final Report	60	100																	
Body	60	100																	
Drawings	0	100																	
Other Appendices	0	100																	
Presentation	40	100																	
<b>Grants</b>	65	<b>100</b>																	
Engineer of the Future Trust	10	<b>100</b>					9/28/2016					10							
Baylis Medical	55	100					10/3/2016	10					25	30					
<b>Class Deliverables</b>	114																		
GENE 403	46	<b>100</b>																	
Design Project Proposal	16	100					9/30/2016	20	10	6									
Teamwork Assessment 1	3	100					10/14/2016												
Design Project Review 1	12	100					10/28/2016												
Design Project Review 2	12	100					11/18/2016												
Teamwork Assessment 2	3	100					11/25/2016												
GENE 404	42	<b>100</b>																	
Design Project Review 3	12	100					1/13/2017												
Design Project Review 4	12	100					2/3/2017												
Design Project Review 5	12	100					2/24/2017												
Teamwork Assessment 3	3	100					2/10/2017												
Teamwork Assessment 4	3	100					3/24/2017												
SYDE 461	26	<b>100</b>																	
Accountability Log 1	8	100					10/28/2016	1	1	1	1	1	1	1	1	1	1		
Accountability Log 2	5	100					12/5/2016												
SYDE 462		<b>100</b>																	
Accountability Log 3	7	100					2/17/2017												
Accountability Log 4	6	100					4/3/2017												



## Organizational Structure and Roles

The organizational structure of the student team, instructional team, advisors, and client can be seen in Figure 58.

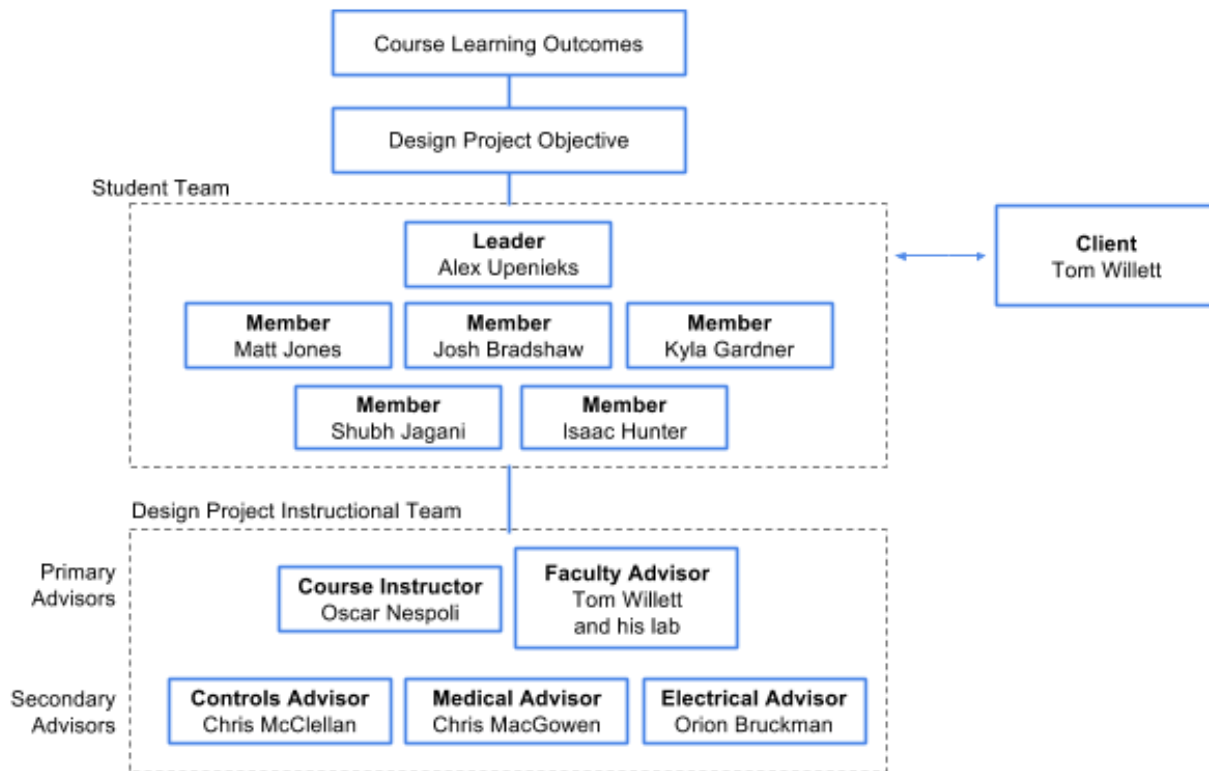


Figure 58: Organizational chart of Team SkelePrint.

The roles of individual team members are summarized below. These roles are not all encompassing, but rather who will lead their respective areas.

### **Shubh Jagani (SYDE) - 20470615 - ssjagani@uwaterloo.ca**

Shubh's role in the project included firmware design and development. His work also included the design of the tool path generator. He worked closely with Josh Bradshaw to ensure seamless integration between hardware and software.

### **Matt Jones (SYDE) - 20474981 - matt.jones@uwaterloo.ca**

Matt's role in the project included controls hardware testing and design of the frame supporting the printer. He created CAD models and drawings to visualize the different design concepts. He also monitored the project management techniques the team applied to

the project.

**Kyla Gardner (SYDE) - 20490354 - k2gardne@uwaterloo.ca**

Kyla's role included the mechanical and controls systems design of the printer axes. She also performed mathematical modelling to optimize the strength and physical capabilities of printed pieces through structural modification.

**Josh Bradshaw (SYDE) - 20479758 - jabradsh@uwaterloo.ca**

Josh's primary role in the project was the development of the printers electronics and controls hardware. This included the main logic board, the motors, positional feedback systems and the fault detection systems. He also worked closely with Shubh Jagani, and Kyla Gardner on the controls and mechanical systems respectively.

**Isaac Hunter (SYDE) - 20480938 - ichunter@uwaterloo.ca**

Isaac's primary role in the project was the mechanical design and development of the printer. He is responsible for the development of a low fidelity prototype and contributing to the CAD model. He also creates promotional and branding material.

**Alex Upenieks (CHEM) - 20487426 - ajsupeni@uwaterloo.ca**

Alex's role included working on the ink biomaterial and its interface with the printer. This included creating new inks for testing, working on the ink extrusion mechanism, and using programs such as Comsol and MATLAB to model the ink's behaviour in the device.

## Risk Register

The risk register for our projects outlining the risks, their probability and impact, our proposed mitigation and planned contingency are shown on the following three pages.

Risk	Probability	Impact	Mitigation	Contingency
Biomaterial under revision	medium	high	Design the printer to be compatible with inks with various viscosities and densities.	Printer can be verified using plastic materials.
Laser causes eye damage or burns to the end user	low	high	Designing the printer to provide laser protection compliant with ANSI Z136. (UV opaque encasing, auto shutoff door)  For redundant protection, all operators will be required to wear protective goggles and lab coat, in accordance with UW policy.	Most of the printer's functionality can be tested without operating the laser.
Printer motion causes it to collide with the operator	low	low	The printer will be designed to turn itself off when the door is open.	Print speeds will be low, so any impact between the printer and the operator would not result in injury.
Printer becomes electrified with mains voltage, and electrocutes the operator	low	high	The power supply will be compliant with UL standards. The printer's frame will be electrically grounded to ensure that it cannot become energized.	The printer will be on a GFI protected circuit, which will cut power if someone electrocutes themselves.
Printer crashes while operating unattended and damages itself	medium	medium	The printer's firmware includes checking to prevent basic collisions, such as the printer colliding with its end stops.	The motor drivers will all have stall detection, so that the printer will apply a very limited amount of torque in a crash situation.  The fine pitch on the ball screw and lead screws mean that the axial and radial axis will not move at a high speed even in a malfunction situation.
UV emissions laser causes degradation of printer components	low	low	UV light degrades plastic components, so no plastic components are used within the printer's body.	UV emissions should not harm the parts we have chosen for the printer.

Mandrel removal process damages the print	low	high	The mandrel will be made of a material that is unlikely to stick to the ink during curing.	The research team can retrofit the printer with a split mandrel or use a water soluble film on the mandrel.
Over/under extrusion	low	low	Using a pneumatic extruder should minimize the occurrence of this. Smearing ink over multiple layers will reduce the effects of mis-extrusion.	Minimizing the layer height will reduce the effect of mis-extrusion over each layer.
Printer catches fire while operating unattended	low	high	The printer be use a fused UL compliant power supply. Additionally, the motors will all have overtemperature shutoffs.	The printer will be made of non-combustible material.
The printer fails to meet its accuracy specifications after prolonged use	high	low	A maintenance schedule for the printer will be developed.	Manual inspection of the printer should be performed on a regular basis.
Abrasive biomaterial particles infiltrate and damage the printer's moving parts	medium	high	A cleaning and lubrication plan for the printer will be developed.	If damage is caught in time, it could be addressed by simply replacing the lead screw nut and ballnut and relubricating the assemblies.
Extrusion inaccuracies create errors beyond the printer's accuracy specification	high	high	The extrusion system was completed first, so that it can be tested.	The printer could potentially be retrofitted to use a more precise extrusion controller, such as those produced by Nordstrom, although they are much more expensive.
Particles remain in ink and prevent homogeneity of extrusion	med	med	Ultrasonic mixing should reduce the chance of this happening, allowing a strong microstructure to form.	Until Professor Willett's lab has figured out their best ink, we can test with their current generation of biomaterial.
Ink is not isovolumetric, and the parts shrink during curing	high	high	Professor Willett's research team is attempting to develop an ink that does not have this problem.	It may be possible to accommodate for a small amount ink shrinkage through clever modification of the control system.

Limited extrusion material volume limits the size of feasible prints	high	low	Multiples syringes can be purchased and interchanged during printing.	Syringes can be prepared in parallel and interchanged during the print if absolutely necessary.
--	------	-----	---	---

## **Project Budget and Current Expenses**

The project budget is shown on the next page. The budget was created after the team received funding at the start of the project. The original budget shows the planned expenses for the mechanical, controls, and extrusion systems, as well as remaining funds. The project expenses as of April 1, 2017 is shown following the budget. As of April 1, 2017 the project is 1,392.09 Canadian Dollars under budget. The most under-budget subsystem is the extrusion system. This is because we did not think it was necessary to purchase everything be budgeted for, like an air compressor. Also, the extrusion system has been the last subsystem to be completed so some expenses may still come in under that area. Our mechanical subsystem was also cheaper than we budgeted, and this was mainly due to parts being cheaper than we expected. Finally our main subsystem that is over budget is the miscellaneous area. We did not budget for this because at the start of the project we did not anticipate the need to print a poster or for us to be charged duty fees. Thankfully our overall project was much more under budget than these extra expenses.

# SkelePrint Budget

	Quantity	Value	Total
<b>Revenue</b>			
Funding from Professor Willet's Lab	1	1,000.00	1,000.00
Baylis	1	5,000.00	5,000.00
Engineers of the Future	1	4,000.00	4,000.00
		<b>Total</b>	<b>10,000.00</b>
<b>Expenses</b>			
<b>Mechanical System</b>			
Precise Linear Actuators	2	300.00	600.00
Linear Guide Rails and Linear Bearings	4	150.00	600.00
High Resolution Stepper Motors	3	80.00	240.00
Frame	1	550	550.00
Print Bed and Rotary Mounts	2	250	500.00
Misc Mechanical Components	1	500.00	500.00
Machining	1	1000	1,000.00
		<b>Subtotal</b>	<b>3,990.00</b>
<b>Control System</b>			
PCB Manufacturing	5	100	500.00
Position sensors (limit switches or otherwise)	3	10	30.00
High Precision Optical Rotary Encoders	3	70	210.00
		<b>Subtotal</b>	<b>740.00</b>
<b>Extrusion System</b>			
Precise Pneumatic Actuator	1	350.00	350.00
Pressure monitoring (sensor and feedback)	1	200.00	200.00
High Pressure Luer Lock syringes	5	30.00	150.00
Syringe switching system	1	300.00	300.00
Air compressor	1	200.00	200.00
		<b>Subtotal</b>	<b>1,200.00</b>
		<b>Total Revenue</b>	10,000.00
		<b>Total Expenses</b>	5,930.00
		<b>Surplus/(Deficit)</b>	4,070.00

# SkelePrint Expense Report

As of: April 1, 2017

## Mechanical System

Ball screw assembly and linear rails	Automation 4 Less	859.96
Fasteners and accessories	McMaster Carr	739.01
Frame assembly and aluminum plates	Misumi	1377.71
Lead screw	Pololu Corp	169.73
Aluminum components	UW Machine Shop	155.00
Mechanical accessories	Home Hardware	27.09
	<b>Total</b>	<b>3328.50</b>
	<b>Budgeted</b>	<b>3990.00</b>
	<b>Surplus / (Deficit)</b>	<b>661.50</b>

## Control System

Electronic components	Digi Key	211.60
Power supply	NCIX	144.08
Electronic accessories	Orion Electronics	22.87
Mechaduinos	Tropical Lab	212.19
Stepper motors	Stepper Online	158.15
	<b>Total</b>	<b>748.89</b>
	<b>Budgeted</b>	<b>740.00</b>
	<b>Surplus / (Deficit)</b>	<b>(8.89)</b>

## Extrusion System

Syringe extruder	Nordson EFD	117.46
	<b>Total</b>	<b>117.46</b>
	<b>Budgeted</b>	<b>1200.00</b>
	<b>Surplus / (Deficit)</b>	<b>1,082.54</b>

## Miscellaneous

Duty charges	FedEx	248.94
Symposia poster printing	FedEx Print Shop	94.12
	<b>Total</b>	<b>343.06</b>
	<b>Budgeted</b>	<b>0.00</b>
	<b>Surplus / (Deficit)</b>	<b>(343.06)</b>

<b>Total</b>	<b>4537.91</b>
<b>Budgeted</b>	<b>5930.00</b>
<b>Surplus / (Deficit)</b>	<b>1392.09</b>

## **Bill of Materials**

The bill of materials for our printer is shown over the next few pages. It shows the part name, part number, quantity, and where the part was purchased or machined from. This bill of materials will be useful in replacing parts of the printer after time.

The bill of materials does not include the fasteners for the printer. A separate document with the screws and nuts is included after the bill of materials. Screws that are the same across multiple assemblies of the printer are colour coded the same. All components found in the fasteners spreadsheet were purchased from McMaster Carr.

## SkelePrint Bill of Materials

Part Name	Part #	Quantity	From
<b>Axial Axis</b>			
Motor Mounting Bracket	NEMA23-MB	1	Automation4Less
Motor	NEMA23	1	OMC stepper
Motor Coupling	DR1-C-25x30-10x6.35	1	Automation4Less
Ball Screw	RM1610-0450-0300-FS	1	Automation4Less
Ball Screw Nut	RM1610-0450-0300-FS	1	Automation4Less
Ball Screw Mount	BK12	1	Automation4Less
Ball Screw Mount	BF12	1	Automation4Less
Ball Screw Mount Plate	KPLAY15-A50-B60-X10-Y10-F21-G40-V13-S7-W46-N5-MA6	2	Misumi
Linear Rail	EGR15Rxxxx	1	Automation4Less
Linear Rail Carriage	EGR15Rxxxx	1	Automation4Less
Carriage Block	Custom Made from Aluminum	1	UW Machine Shop
Cable carrier	4516Txx	1	McMaster Carr
<b>Radial Axis</b>			
Linear Rail	MGWR15RxxxxH	1	Automation4Less
Linear Rail Carriage	MGWR15RxxxxH	1	Automation4Less
Lead Screw	2690	1	Pololu Robotics & Electronics
Lead Screw Nut	2690	1	Pololu Robotics & Electronics
Motor	2690	1	Pololu Robotics & Electronics
Lead Screw End	SBGTN608ZZ_2_14	1	Misumi
Motor Mounting Plate	KPLAU5-A96-B50-X15-Y12_5-F56-G25-S25-Q31-R31-N6-NA4-D22	1	Misumi
L Bracket	KPAAF5-A60-B40-L50-X9_5-Y46-F13_5-G27-V23-S31-N5-MA4	1	Misumi
Syringe Holder	Custom Made from Aluminum	1	UW Machine Shop
<b>Rotational Axis</b>			
Center Mounts	BGMWS6900ZZ-40	2	Misumi
Driven Center	SFTG15-50-F40-P10-J24-M4	1	Misumi
Floating Center	SFTG15-50-F20-P10-J24-M4	1	Misumi
Mandrel	SSPJW10-380-M6-N6	1	Misumi
Pulley - Large	GPA72MR2090-A-H10	1	Misumi
Pulley - Small	GPA26MR2090-A-H6.35	1	Misumi
Motor Mounting Bracket	NEMA23-MB	1	Automation4Less
Motor	NEMA23	1	OMC stepper
Timing Belt	GBN242MR2-090	1	Misumi
<b>Frame</b>			
Left Side Plate	Custom Made from Aluminum	1	Misumi
Right Side Plate	Custom Made from Aluminum	1	Misumi
Bottom Front Extrusion	HFSP5-8040-550	1	Misumi
Top Extrusion	HFSP5-6020-600	1	Misumi
Bottom Back Extrusion	HFSP5-6040-600	1	Misumi
Rubber Foot	9540K781	8	McMaster Carr
<b>Controls</b>			
Mechaduino Motor Controller	Mechaduino	3	Tropical Labs
Limit Switches	Z4737-ND	4	DigiKey
EVGA SuperNova Power Supply	220-GS-0650-V1	1	NCIX

ORDERED?	ASSEMBLY	STYLE	THREAD (M)	LENGTH (mm)	QUANTITY (min)	PART #	NOTES
	2/6/2017						
y	Sideplates to extrusions	COUNTERSUNK FLAT	M5	20	20		
y	Axial axis rail to T-nuts (E rail)	SOCKET CAP	M3	10	24		
y	Axial axis carriage to ballnut block	SOCKET CAP	M3	10	4		ORDER M3 T-nuts from MISUMI
y	Motor mount to Tnuts	SOCKET CAP	M4	6	4		ORDER new linear bearing from MISUMI
y	Motor mount to NEMA 23 motor	SOCKET CAP	M4	16	4		Need M4 nuts (#92497A250)
y	Mounting radial rail to ballnut block	SOCKET CAP	M4	8	2		
y	Motor plate to ball nut block	SOCKET CAP	M5	10	2		
y	Ball nut to ball nut block	SOCKET CAP	M5	14	4		
y	L bracket to radial rail	SOCKET CAP	M4	16	2		ALSO BUY CORRESPONDING HEX NUTS #92497A250
y	Radial bearing to L bracket	SOCKET CAP	M5	14	2		
y	Motor plate to NEMA-17 motor	SOCKET CAP	M3	8	4		
y	Ball screw bracket to extrusion	SOCKET CAP	M5	20			
n	Ball screw fixed end and floating end brackets	SOCKET CAP	M6	40			
y	PCB to MECHADUINO	SOCKET CAP	M3	4	8		
y	Rotational axis bearings to extrusion	SOCKET CAP	M5	14	4		
	02/07/17						
y	NEW radial axis bearing	SOCKET CAP	M5	14	2		
y	NEW axial axis carriage to ballnut block	SOCKET CAP	M5	16	4		have 17mm between socket head and end of screw hole
y	Lead nut screws	SOCKET CAP	M3	16	4		
y	Syringe holder to radial carriage	SOCKET CAP	M4	50	4		
y	Loctite					1810A315	
y	Cable Carrier						
y	Angle Braces					5537T81	
y	Wire 4 strand						
y	pneumatic muffler						
						2 4450K2	

# Appendix C: Knowledge Application

Calculating required motor torque:

$$T_{bs} = T_a + T_l = I_G \times \alpha + \left( \frac{FP_B}{2\pi\eta} + \frac{\mu_o F_o P_B}{2\pi} \right) \frac{1}{i} \quad (14)$$

Calculating the total amount of external forces and friction on the ball screw:

$$F = 0 + mg\mu\cos\theta \quad (15)$$

Calculating the expected volume of a print:

$$V_{print} = \pi(R - r)^2 h \quad (16)$$

Calculating the expected mass of a print:

$$m_{print} = \rho V_{print} \quad (17)$$

Calculating the axial width of the coil, as a function of the extrusion width  $w_e$ :

$$w = \frac{w_e}{\cos(\theta)} \quad (18)$$

Calculating the timing belt length:

$$l = 2ar + 2(\pi - \alpha)R + 2h \quad (19)$$

Calculating the velocity profile of a Herschel-Bulkley fluid travelling through a cylindrical tube:

$$v(r) = -\frac{1}{2k} \frac{dP^{\frac{1}{n}}}{dL} \frac{n}{n+1} [(R - R_c)^{\frac{1}{n+1}} - (r - R_c)^{\frac{1}{n+1}}] \quad (20)$$

Calculating the pressure requirement to extrude a Herschel-Bulkley fluid through a cylindrical tube:

$$Q = \frac{8\pi^{\frac{1}{n}}}{k} \left( \frac{L}{dP} \right)^3 \left( \frac{RdP}{2dL} - \tau_o \right)^{1+\frac{1}{n}} \left[ \frac{\left( \frac{RdP}{2dL} - \tau_o \right)^2}{3 + \frac{1}{n}} + \frac{2\tau_o \left( \frac{RdP}{2dL} - \tau_o \right)}{2 + \frac{1}{n}} + \frac{\tau_o^2}{1 + \frac{1}{n}} \right] \quad (21)$$

# Appendix D: Troubleshooting

## Known Problems with the Printer

We have chosen to give an honest accounting of every problem that exists in our delivered printer, because this will be useful for future refinement and troubleshooting. While this section is relatively long, we ask the evaluators to remember that the scope of this project was quite large, and that most of these problems are relatively minor.

### Mechanical Problems

Some of the printer's edges are still quite sharp. We did our best to take all of the sharp edges down, but we were limited in how much we could do because we had already assembled the printer when we noticed the problem. This can easily be resolved using a small whetstone or file, just ensure that you take precautions to avoid getting any abrasive dust in the printer's moving parts. The ideal way to do this would be to completely disassemble the machine, deburr it and reassemble it. Alternatively, all of the moving ports could be sealed with sandwich wrap, tape and rubber bands during the filing and cleaning process.

At the moment the plate that holds the syringe in place is misaligned with the rotational axis, and the hole that holds the syringe is too tight. Revising this part and having an improved version machined would be an excellent task for a co-op student. The machine shop will charge \$40 including labor to remake that part.

One easy way to revise the part would be to simply cut off the section that holds the screw, tap a couple of holes in the remaining block and design a new syringe holder that can screw into that block. For revisions to the existing part, get in touch with Grahme from the engineering machine shop, who made the part in the first place.

Another problem is that the axial axis linear bearing carriage does not fit the axial axis block in an ideal manner. The axial axis carriage originally came with hardened steel threaded holes for mounting, but we opted to clearance drill those out using a combination of tungsten carbide drills and endmills. Unfortunately, there is not enough clearnace for the screw heads on one side of the linear bearing carriage, so we can only insert 2 of the

four fasteners at the moment. This is not a major problem, but it does slightly degrade the stiffness and accuracy of the printer.

This could be fixed by revising the axial axis ballnut block so that the fasteners pass into the carriage from above, and purchasing a new linear bearing carriage from Automation4Less (EGW 15SC). This fix was too time consuming for our team to complete during our term.

Finally, the belt that drives the radial axis cannot be tensioned quite enough to achieve the maximum backlash specification that we designed the printer for. This can be fixed by ordering a shorter belt from MISUMI (the current belt is part GBN242MR2-090).

Alternatively, the slots on the motor mounting bracket could be milled out by the engineering machine shop so that the motor can be placed slightly farther away from the rotational axis. See the belt length calculation section to help you make an informed decision on this issue. Adding a spring tensioner to the belt drive is not an acceptable solution, because it will increase the backlash of the axis beyond its specification.

## Firmware Problems

There are currently no known firmware faults in the machine, but we had to debug many problems during the leadup to symposium that there are certainly a few issues remaining. The controls system troubleshooting section for more information.

## Electrical Problems

The mechatuino for the axial axis was damaged during a pneumatics test. The 5V rail was shorted after the test, testing with a 3.5 digit multimeter isolated the short to being in the power status LED MOSFET. We removed that part and the board has appeared to be stable ever since, but there is no way to fully test the encoder and microcontroller. We suggest purchasing additional mechatuinios from Tropical Labs while this part is still available.

There is a lot of capacitance on the 5V line of the printer, and sometimes the 5V rail takes enough time to stabilize (100-500ms) after a cold power up that the mechatuinios fail to boot properly. This problem is tricky to debug, because the printer typically needs to sit unused for 3-4 days for this problem to become apparent.

The easiest way to solve this issue would be to add a relay or logic level mosfet circuit (it

would need to have  $R_{gs} < 10\Omega$  for a 5V gate to drain voltage) between the power supply and the mechaduino 5V line. The power supply provides a 5V TTL *PWRGOOD* signal when its outputs have fully stabilized. This *PWRGOOD* signal could be used to trigger the relay or mosfet. Searching the internet for soft latching power switch circuits should provide plenty of inspiration.

## General Warnings and Advice

When working with the printer, at all times be cognisant of the fact that it is a prototype. Many parts of the machine are somewhat fragile, and they must be handled with care. For example, most of the custom parts on the printer are constructed with aluminum blocks fastened together with steel screws. If you aren't careful while inserting and removing the fasteners you can easily cross-thread the aluminum threads or strip them entirely. Use no more than finger tension on any fastener that goes into aluminum.

Likewise, do not ever pull hard to tug on any component of the printer. If you get the syringe stuck in the block, you may have to partially disassemble the radial axis to get it out before a new syringe holder solution is designed. If you try to force it, its likely that you will rip the radial axis off of the machine by tearing the screws out of the axial axis mounting block.

Similarly, there are several electronic components of the printer that are held in place with two part epoxy. These parts include the mechanduino PCBs that sit on the ends of the motors, and the solenoid driver. Be careful not to hit these circuit boards while moving the printer or you will find yourself with a tedious sanding and re-gluing job.

Finally, with the exception of a few crimp connections in the power supply wiring, all of the wires are connected with screw terminals. It is important that the strain on these wires is taken up by cable ties, or else they will easily pull out of their connections. Once loose, the wires will almost inevitably short to something, potentially destroying large portions of the electrical system.

## **Electrical Troubleshooting**

Anytime you perform maintenance on the electrical system, you should use a multimeter to check your connections before you power the system up. At the least, put the multimeter on the resistance test (Ohms) mode and check to ensure that the ground rail is not shorted to either the 12V or 5V rails. The easiest place to check these connections are not shorted is on the mechatronics, because they are connected to both 12V and 5V.

## **Firmware Troubleshooting**

To reflash the Arduino that runs the GRBL firmware package, or the mechatronics, you will need the latest version of the Arduino IDE. This is available at:

<https://www.arduino.cc/en/main/software>.

The process for reflashing boards is documented well on the Arduino website. We have provided you with all of the applicable firmware packages. If a board fails to reflash, try pressing the reset button on the board just before you press upload. This can take several tries to get right.

## **Controls System Troubleshooting**

### **Problems with the Mechatron Motor Drivers**

During our build process, the mechatronics caused us the most trouble by far. We spent many hours getting them aligned, tuned and debugged to our satisfaction. The mechatronics are not as robust as we hoped they were. When troubleshooting them, always keep the possibility that circuit board may have been damaged in mind. You can purchase replacements from tropical labs. There are also several variants on this circuit board available from other manufacturers. Some general links for mechatron troubleshooting are available here:

The full firmware for the mechatron boards is available at:

<https://github.com/jcchurch13/Mechatron-Firmware>.

The hardware schematics and PCB layouts for the PCB layouts are available at:

<https://github.com/jcchurch13/Mechatron-Hardware>.

The manual is available here:

<https://cdn.hackaday.io/files/11224480207616/MechaduinoManual.pdf>.

Note that the green LED on the axial axis mechaduino doesn't work. The MOSFET that drives that LED was destroyed during a failed test, and we had to desolder it to salvage the board. We are unsure whether the failure that destroyed the MOSFET degraded the stability or longevity of the other components, but this board has been running quite happily for many hours.

### **One or more axis is unresponsive upon startup**

Begin by doing basic electrical troubleshooting. Check that the 12V and 5V rails are not shorted. Check that the controls wiring is firmly connected at both ends. Check the arduino ground cable to ensure that it is firmly connected. Also check that the motor cable is firmly connected, and that there are no broken strands in the cabling.

Next, try pressing the reset switch on the mechaduino. Occasionally the mechaduinos will fail to start when the power supply is turned on. We did not get to fully work out the cause of this problem, but we believe that it may be related to the high levels of capacitance on the 5V rail causing power supply instability during the boot period.

If resetting the board doesn't work, connect it to a PC and reflash it with the appropriate firmware. Open the serial monitor and check if the mechaduino is responsive. If the mechaduino is not responsive at this point then there is likely an electrical failure, and the mechaduino may need to be replaced. If it is responsive, try running it in open loop mode by sending the 's' command several times to verify that it can drive the motor, and that the motor windings are intact.

### **Motors turn erratically, missing their setpoint**

There are several possible root causes for this problem. First check that the mechaduino is firmly fastened on the motor and that the encoder chip is aligned with the magnet. Next, recalibrate the motor using the procedure described in the mechaduino manual. The calibration procedure allows the mechaduino to correct for misalignment between the encoder and the magnet, and even the slightest movement of the PCB will generally be cause for

recalibration. If these procedures are not enough to fix the problem, reflash the Mechaduino with the appropriate firmware for that particular axis (we provided you with these files). If neither of those procedures were enough to fix the axis, you may need to tune the controller.

### **Motors make a rattling noise or vibrate violently, but stay in one place**

First follow the same troubleshooting as outlined for ‘Motors turn erratically, missing their setpoint’. If the motors are still rattling and missing their setpoint, then the controller may require tuning.

Tuning should not have to be carried out often, so be sure to rule out more basic issues like loading the wrong firmware or mechaduino calibration before you start tuning. Before tuning the controller, disconnect the motor and manually actuate the axis over its full range of motion. Feel for any sticky spots, or mechanical binding. Lubricate or adjust the axis as required before doing any tuning. Once the axis is in perfect mechanical condition, tune it using the procedure outlined in the Mechaduino manual.

### **Motors jerk upon startup**

This is not actually a problem unless the motors are moving more than one full rotation, or hitting an end-stop. The mechaduinos do this because they have absolute position encoders, and they want to self-align themselves upon start-up. If the motors do jerk into an endstop upon startup, power down the machine, disconnect the Arduino from your computer and manually move the axis into its center position. Now power up the machine and try again, starting with the homing procedure.

## **Mechanism Troubleshooting**

The mechanisms of the printer are precise and must be aligned carefully to avoid binding. The lead screw and ball screw should always be lubricated with light machine oil.

If you disassemble the axial or radial axis, you must be careful during reassembly. The radial axis is particularly susceptible to being misaligned if you assemble it poorly. While assembling it, put all of the screws in place loosely, and tighten them all simultaneously in

small increments while manually actuating the screw over its full throw to ensure that it isn't binding.

You should be able to turn both the radial axis lead screw and the ball screw with your fingers. If that isn't the case, then the axis is misaligned and it will wear out, and its lifespan will be reduced by approximately 100x.

If you remove either of the linear bearings from their rails, there is a possibility that the ball bearings may fall out, and the expensive bearing block will be destroyed. Remove the bearings by following the procedure outlined in the HIWIN linear rail manual. You will find the plastic bearing inserts in the same box as the extra screws.

## Wiring Diagrams

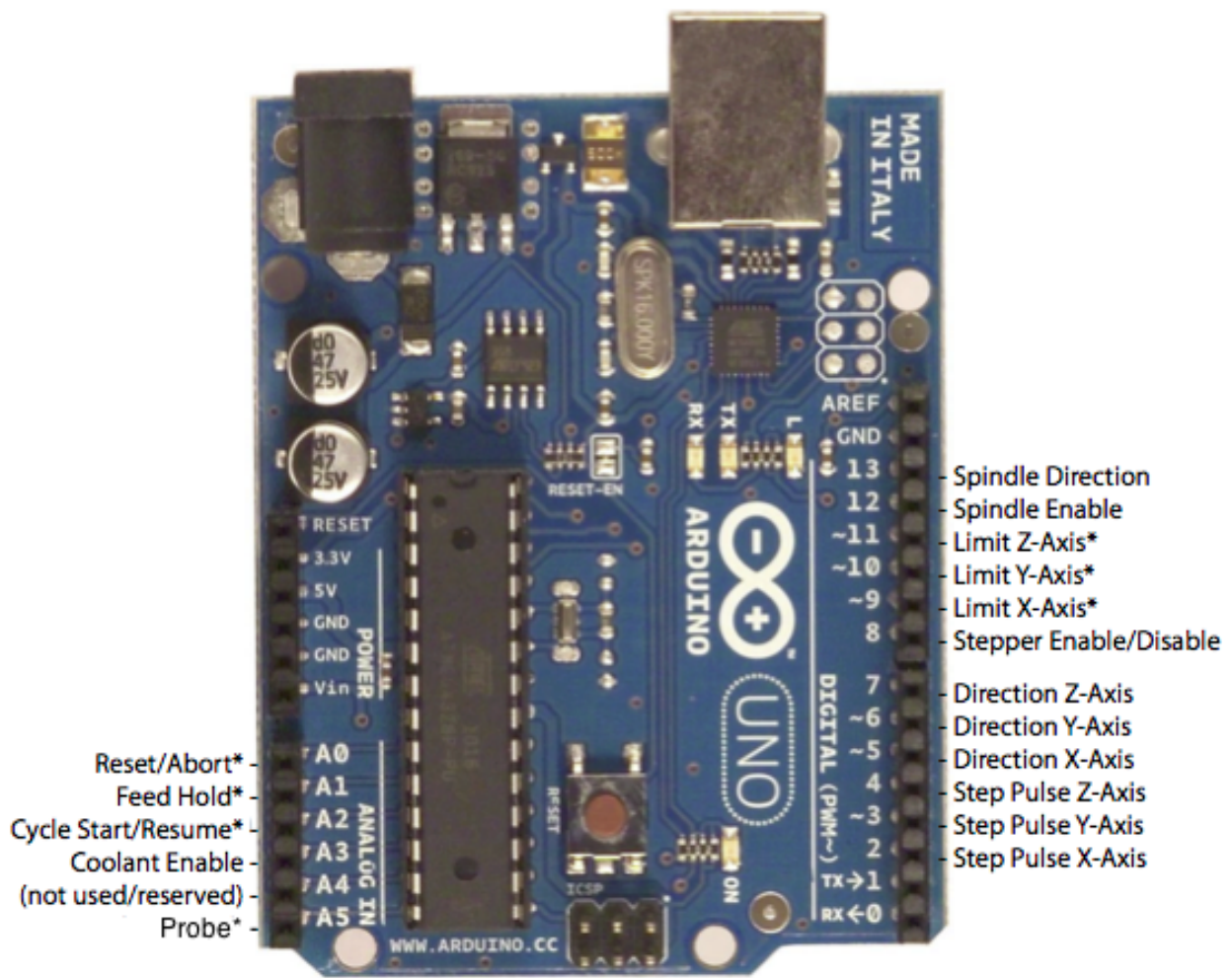
See the electrical troubleshooting section for all applicable warnings about wiring and rewiring the printer. The wiring diagrams that we used to connect the Arduino and the Mechaduinos are shown below.

The wiring diagram that we used to connect the Arduino to the three mechaduinos, the solenoid driver and the laser is shown in Figure 59. Note that the GRBL pinout is subject to change in the new version of GRBL. The step and direction wire pairs to the the mechaduinos. Recall that the axial axis is the X axis, the rotational axis is the Y axis and the radial axis is the Z axis.

The coolant enable line drives the extrusion system, which uses active HIGH 5V TTL logic. The spindle enable line drives the laser, which uses active LOW logic and is triggered by a falling edge.

We also run a ground wire from the pin beside pin 13 to the power supply ground. This connection is crucial, without it the mechaduinos and the arduino will not have a common ground reference and they will not work. This is a key connection to check if the printer ever malfunctions.

An improvement that could be made to the wiring would be to run a wire from the stepper enable/disable to all of the mechaduino boards, and setup the correccsponding enable/disable interrupt in the mechaduino firmware. This would make the limit switches more effective, because they would disable the motor drivers directly.



\* - Indicates input pins. Held high with internal pull-up resistors.

Figure 59: GRBL Pinout Diagram

The limit switches are wired using the scheme shown in Figure 60. The resistors and wires are soldered into the circuit from below. The RC network is necessary to provide noise suppression. Before we put those in place, we had frequent false limit switch triggers.

It's important to note that there is only a single IO pin for both limit switches for each axis. This means that when GRBL hits a limit switch, it has no way of knowing which one has been hit on that axis and cannot back away automatically. This could be improved by making minor modifications to the GRBL firmware to use four pins for limit switches. Pins A1, A2, A3, A5, 12, and 10 are all available for this purpose.

The mechaduino board wiring is illustrated in Figure 61. The step and direction connec-

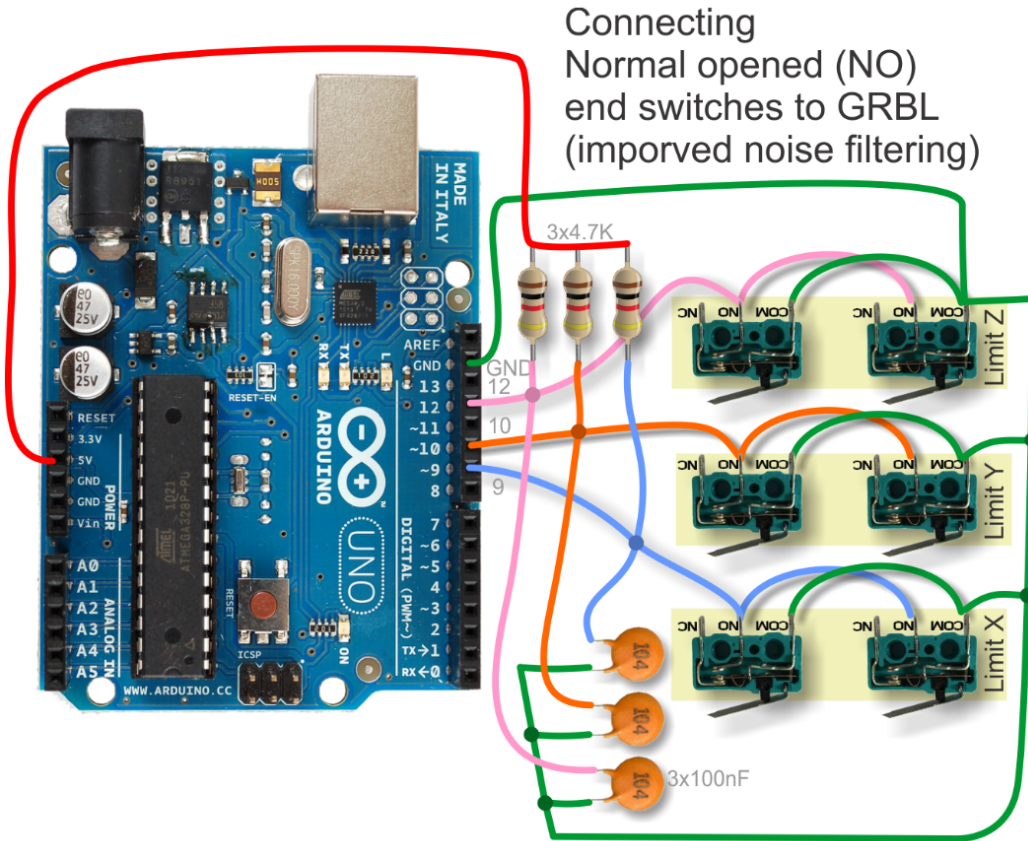


Figure 60: Mechaduino Wiring Diagram

tions come from the Arduino. The 12V, 5V and GND wires all come from the power supply. We opted to run two ground wires to each Mechaduino. This was not actually necessary, because the Mechaduino 12V rail is not electrically isolated from its 5V rail, but it does reduce the risk of the Mechaduino being destroyed if a ground wire comes loose.

We used high flex cable to deliver power to each Mechaduino. The BLACK and WHITE strands of that cable are both ground, the RED strand is +12V and the GREEN strand is +5V. Do not confuse the power wiring with the control and limit switch wiring, which unfortunately uses the same colours for different things. When in doubt get out your multimeter and do some connectivity checks.

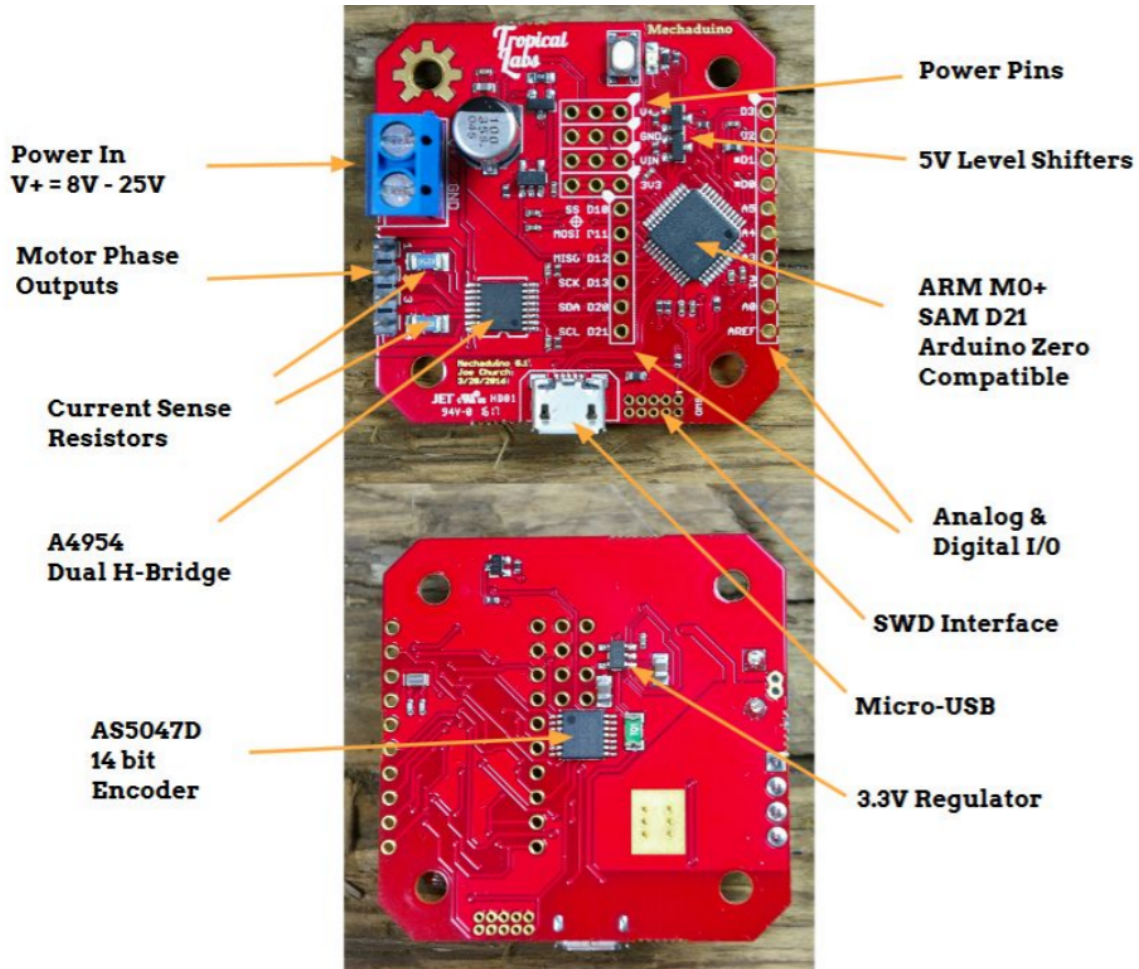


Figure 61: Mechaduino PCB Drawing.

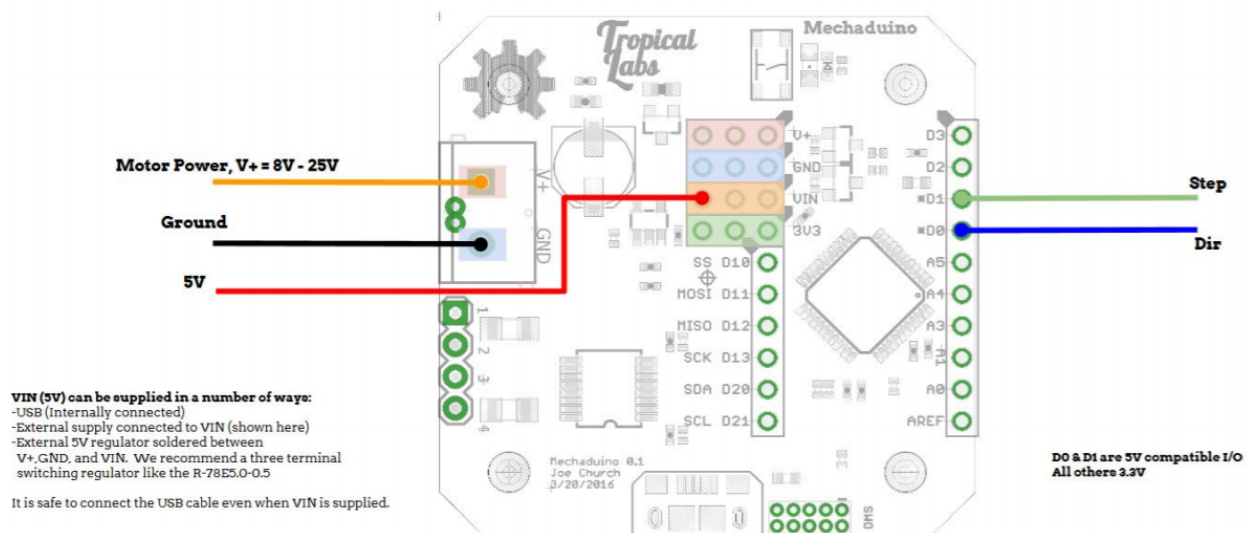


Figure 62: Mechaduino Wiring Diagram

# References

- [1] G. et al. TAYLOR. The free vascularized bone graft: A clinical extension of microvascular techniques. *Journal of Plastic Reconstructive Surgery*, 55(5):533–544, 1975.
- [2] Donald S. Bae M. Waters. Free vascularized fibula grafting: Principles, techniques, and applications in pediatric orthopaedics. *Children's Hospital*, 2006.
- [3] Joshua L. Simon et al. In vivo bone response to 3d periodic hydroxyapatite scaffolds assembled by direct ink writings. *Journal of Biometerials Research Part A*, 2006.
- [4] Section 9: Bone structure-function.  
<http://www.umich.edu/~bme332/ch9bone/bme332bone.htm>. Accessed: 2016-11-21.
- [5] Hyrel 3d sales webpage. Technical report, Hyrel 3D.
- [6] 3d printing industry: The free beginners guide. Technical report, 3D Printing Industry.
- [7] 5axismaker machine specs. <http://www.5axismaker.com/5axis/>. Accessed: 2016-11-23.
- [8] Erwan Rolland Youssef Ibrahim Alexandros Kenich, Matthieu Burnand-Galpin. Lathe type 3d printer. *Imperial College London Capstone Design Report*, 2013.
- [9] Zen toolworks flexible filament 3d printed timing belt.  
<https://www.youtube.com/watch?v=xgGvaA9S44E>. Accessed: 2016-11-23.
- [10] Linear actuator le11ls from lin engineering. <http://www.linengineering.com/products/stepper-motor-linear-actuators/le-linear-actuators/le11ls/>. Accessed: 2016-11-23.
- [11] How a ball screw works. Technical report, Barne Industries Inc.
- [12] Accuracy of the ball screw.  
[https://tech.thk.com/en/products/pdf/en\\_a15\\_011.pdf](https://tech.thk.com/en/products/pdf/en_a15_011.pdf). Accessed: 2016-11-20.

- [13] isel automation: Metric ball screws.  
<http://www.techno-isel.com/lmc/Products/BallScrewsMetric16.htm>. Accessed: 2016-11-23.
- [14] Paul Horowitz Winfield Hill. *The Art of Electronics 3rd Edition*. Cambridge University Press, 2015.
- [15] Drv101 - pwm solenoid / valve driver datasheet. Technical report, Texas Instruments.
- [16] Microking cross-reference guide to “xm” valve series. Technical report, Parker Pnumatics Division, 3 2007.
- [17] Glossary-of-terms. <http://www.swagelok.com/landingpages/EN/assets/pdf/Glossary-of-Terms.pdf>. Accessed: 2016-11-21.
- [18] Principles and techniques for designing precision machines. Technical report, Layton Carter Hale.
- [19] Basics of motion control. <http://www.orientalmotor.com/technology/articles/motor-sizing-calculations.html>. Accessed: 2016-11-24.
- [20] Ballscrews: Technical information. Technical report, Hiwin.
- [21] Evan Mitoulis. Flows of viscoplastic materials: Models and computations. 2007.
- [22] Martin J. Blunt Taha Sochi. Investigating shear-thinning fluids in porous media with yield stress using a herschel model. 2007.